AN ABSTRACT OF THE THESIS OF

Mark Onufer for the degree of Master of Science in Nuclear Engineering presented on December 11, 2013.

Title: An MCNP Benchmark Model of the Large Experimental ZPPR-19B Sodium Fast Reactor.

Abstract approved:_____

Andrew C. Klein

The International Handbook of Evaluated Reactor Physics Benchmark Experiments contains detailed descriptions of many different reactor facilities. A large portion of these experiments have not been fully modeled due to the unavailability of computational power at the time of the experiment's execution. With the advent of renewed interest in Sodium Fast Reactors, many of these experimental results are highly useful to benchmark current neutronic codes for these types of sodium systems.

This thesis is concerned with the modeling of the ZPPR-19B using MCNP. Great care was taken to rigorously document exactly how the facility was modeled. The neutron multiplication factor and reaction rate ratios resulting from the MCNP model were then compared with the measurements taken at the experimental facility in order to determine any bias in the MCNP model. These results are useful to reactor designers employing MCNP as a computational tool to design the next generation of nuclear reactors.

# An MCNP Benchmark Model of the Large Experimental ZPPR-19B Sodium Fast Reactor

by

Mark Onufer

A THESIS

Submitted to

Oregon State University

in partial fulfillment of

the requirements for the

degree of

Master of Science

Presented December 11, 2013

Commencement June 2014

Master of Science thesis of Mark Onufer presented on December 11, 2013

APPROVED:

Major Professor, representing Nuclear Engineering

Head of the Department of Nuclear Engineering and Radiation Health physics

Dean of the Graduate School

I understand that my thesis will become part of the permanent collection of Oregon State University libraries. My signature below authorizes release of my thesis to any reader upon request.

Mark Onufer, Author

# ACKNOWLEDGEMENTS

I would like to thank Dr. Andrew Klein, my major advisor, for his patience and helpful suggestions throughout the work on this Thesis. I would also like to thank all the professors of Nuclear Engineering at Oregon State, who have helped to vastly increase my understanding reactor physics. Thank you also to Jackson Harter who was always willing to provide technical support. Thank you to John Bess at INL for his assistance in finding ZPPR documentation and to Blair Briggs at INL for permission to use figures from the IRPhEP documentation

Additionally, I would like to thank TerraPower, LLC, for financial support of this work and Pavel Hejzlar and Zhiwen Xu from TerraPower, LLC for their intellectual guidance and advice.

Finally, I would like to thank my mother, father, family and friends, especially Megan for her patience and understanding.

# TABLE OF CONTENTS

Page

TABLE OF CONTENTS (Continued)

Page

# LIST OF FIGURES

# LIST OF FIGURES (Continued)

Figure Page

# LIST OF TABLES

Table Page

# LIST OF TABLES (Continued)

Table Page

An MCNP Benchmark Model of the Large Experimental ZPPR-19B Sodium Fast Reactor

# 1 INTRODUCTION

## 1.1 Primer on Fast Reactor Systems

The first implementation of a Fast Breeder Reactor (FBR) was a 2.5 liter reactor submerged in mercury called Clementine at Los Alamos National Laboratory which attained criticality in November of 1946. [1] Cooling a reactor using a liquid metal has significant advantages as well as disadvantages. Because there is little hydrogen in the system to thermalize neutrons, the energy spectrum of the reactor is shifted to having a larger fraction of fast neutrons. With this higher energy neutron spectrum, the number of neutrons emitted per absorption in Pu-239 is higher. Because of the higher number of neutrons per fission in Pu-239, the idea of breeding was developed since more neutrons would be available to convert U-238 into Pu-239 through neutron absorption. Thus, the primary motivation for fast reactors was to employ the U-238 resource, accounting for 99.27% of all naturally occurring uranium, which would increase the uranium resource by two orders of magnitude. [2] The second major advantage of this type of system is the possibility for significant reduction in transuranic waste. Transuranic waste accounts for most of the longer lived nuclear waste. If fast reactors were implemented they could burn much of the transuranic waste from thermal reactors and reduce the required storage time of nuclear waste from tens of thousands of years to a few hundred years. [3] The disadvantages of this type of system are that many liquid metals are highly chemically reactive and there are proliferation concerns with more extensive use of Pu-239 in reactors.

Because of these advantages, initially, researching and experimentation with Liquid Metal Fast Breeder Reactors (LMFBR) was spearheaded by the United States. The Experimental Breeder Reactor 1 (EBR-1), located at the National Reactor Testing Station in Idaho and operated by Argonne National Laboratory, employed Na-K, a room temperature eutectic alloy, as the coolant. This reactor is also typically cited as the first reactor to generate usable amounts of electricity, lighting four light bulbs on December

15, 1951 and increasing the output to 100 kW electric the following day. [4] The EBR II was the next significant implementation of fast reactor technology, using sodium as coolant with a pool type design. In this pool design all of the fuel, fuel handling equipment and many other reactor systems were submerged in sodium. The EBR-II was used for electricity production, fuel and structural material irradiation, instrumentation testing and implementation, and ultimately in a demonstration of passive reactor safety. In those tests the reactor was used to simulate the loss of coolant flow and the loss of heat removal through the primary system. In addition to the EBR facilities, the United States has also implemented fast reactor technology at the many facilities such as the Fast Flux Test Facility (FFTF), the Southwest Experimental Fast Oxide Reactor (SEFOR) and Fermi 1. Unfortunately, due to safety and proliferation concerns as well as questions regarding economic benefit, since its shutdown, EBR-II was the last major experimental demonstration of fast breeder reactors in the United States. [5]

**1.2 The ZPPR Facility**

In addition to these large power production facilities, many low power critical facilities were also used to study the neutronic properties of reactors, such as neutron multiplication factor and reaction rates of different nuclear reactions. Of primary concern for this thesis was the Zero Power Plutonium Reactor (ZPPR), later renamed the Zero Power Physics Reactor. This testing facility was a large split-table critical facility organized into a lattice of square matrix tubes. In each of these matrix tubes was a drawer which contained many different plates of different reactor material such as plutonium, uranium and steel and coolant. Drawers could be pulled out of the matrix tube and the plates within the drawers could be rearranged to simulate different reactor designs. The makeup of an experimental core at this facility was approximately the same size and contained the same masses of materials as the design it was meant to model. Only on the scale of inches, a scale similar to the mean free path of a fast neutron, was the facility significantly different from the design it was meant to model. Because the facility was very low power, cooling was not a significant concern and an insignificant amount of fission products were produced, thus materials could be used for

future experiments. Reuse of materials coupled with the relatively short time required to assemble a core vastly reduced the cost of testing new reactor designs for key neutronic behavior. Because of the extreme precision of the facility, these cores have been used to benchmark computer codes useful for reactor design and safety analysis. The ZPPR operated between 1969 and 1990 and contained twenty-one different assemblies. Over the past two decades, computing power has increased substantially and many of these cores have not been modeled fully with neutronic codes due to the unavailability of the code or computing power computing power at the time. Figure 1 shows a photograph of the facility. The scientist in the photograph is looking at one face of the core and is pulling out and examining a drawer. The other face of the core is behind him and when the core halves are brought together the reactor approaches criticality. [4] [6]

Figure 1: Photograph of the ZPPR Facility [7]

### 1.3 Current LMFBR Development

Recently there has been a renewed interest in Sodium Fast Reactors (SFR). This type of reactor was chosen as one of the six most promising designs based on the Generation IV study of the future of nuclear power. [8] TerraPower, LLC is developing a prototype SFR that can be used to produce electricity by 2023. The pool type design proposed by TerraPower has many advantages. Because the coolant is at atmospheric pressure, a LOCA (Loss of Coolant Accident) is not credible. Due to the pool type design of the system, the molten sodium provides an extremely large thermal mass to prevent core meltdown. Unmitigated, the decay heat will not cause coolant boiling for at least twenty-five hours which is significantly longer than the similar time for the current generation of light water reactors. In addition, the design is completely passively safe through the use of multiple redundant Direct Reactor Auxiliary Cooling Systems (DRACS) which are used to remove decay heat in the event that the Intermediate Heat Transport System is unavailable. Each of the DRACS operates with Na-K, a room temperature liquid metal, and contains two heat exchangers, one in the primary coolant pool above the core and one placed in an air stack to dissipate heat to the naturally flowing ambient air. Finally, the Zr-$H_20$ reaction which caused the explosion at Fukushima is not possible since there is no hydrogen in the system. [9] SFR designs are not without drawbacks however, the main of which is sodium's inherent chemical reactivity. Sodium oxidizes quickly and thus can be prone to fires in air and reacts violently with water. Thus, special care must be taken to avoid sodium contact with the atmosphere. Inert gasses such as Argon are typically used for this purpose.

### 1.4 Objectives

The current neutronic tools being used by TerraPower to design their reactor are MCNP and DIF3D. [9] The primary goal of this thesis is to contribute to the body of work being done to confirm that MCNP is a reasonable tool for this future reactor design. As such, a critical facility will be selected and modeled as closely as possible. Different neutronic properties such as the neutron multiplication factor ($k_{eff}$) and reaction rates of different nuclear materials will be compared to the actual results of the

facility to determine how useful of a tool MCNP is for this type of design and how accurately MCNP can predict the neutronic behavior of SFRs. In addition, any discrepancies or bias in the computer model will attempt to be accounted for.

**1.5 Document Overview**

This thesis is organized into the following sections:

Chapter 1: Introduction - This section contains overviews of fast reactor development, the ZPPR facility, the design of TerraPower and the goals of this thesis.

Chapter 2: Literature Review- Important core physics of fast reactors, the Monte Carlo method, the Verification and Validation process and the attempt to model the ZPPR-15 facility are contained in this section.

Chapter 3: Materials and Methods - A detailed description of the ZPPR-19B facility, which was modeled in MCNP for the first time as part of the work for this thesis, along with any assumptions in the MCNP model are catalogued here.

Chapter 4: Results and Discussion - The process used to verify the ZPPR-19B facility was modeled correctly along the results of the MCNP model are disused in this section. These results are compared to the core parameters measured at the ZPPR-19B facility.

Chapter 5 Conclusion - Concluding remarks along with possibilities for future work are discussed in this section.

Appendices and References are presented at the end of this document.

## 2 LITERATURE REVIEW

### 2.1 Core Physics Prominent in Sodium Fast Reactors

Since sodium fast reactors operate on a much higher neutron energy spectrum than typical thermal reactors it is important to review the core physics of these systems to give a better understanding of the effects of each material within the system. Tables 1 and 2 show the values of the average number of neutrons produced per fission and the number of neutrons produced per neutron absorption for fissile and fertile materials in a typical fast neutron spectrum. These values are referred to as ν and η respectively, and are not equal because when capture reactions occur in these isotopes no neutrons are produced. These data help to illustrate fuel choices in liquid metal fast breeder reactors.

| Fissile Isotopes | | | |
|---|---|---|---|
| | Pu-239 | Pu-241 | U-235 |
| ν | 2.96 | 3.04 | 2.50 |
| η | 2.40 | 2.73 | 2.01 |

Table 1: Typical ν and η in Fast Neutron Spectrum for Fissile Isotopes (adapted from [10])

| Fertile Isotopes | | |
|---|---|---|
| | Pu-240 | U-238 |
| Fission Threshold (MeV) | 0.60 | 1.4 |
| ν | 3.17 | 2.70 |
| η | 1.69 | 0.518 |

Table 2: Typical ν and η in Fast Neutron Spectrum for Fertile Isotopes (adapted from [10])

The goal of a fast breeder reactor is to generate more fuel than it consumes and to reduce actinide waste such as plutonium. To accomplish the task of breeding fuel, absorption within a fuel material needs to produce at least two neutrons, one for generating the next fission to continue the chain reaction and one to convert a fertile isotope into a fissile isotope.

From an inspection of Table 1, it is clear that U-235 would be extremely hard to engineer as the primary fuel for a fast breeder reactor. Each fuel-absorption, on average, only produces slightly above two neutrons, one of which is needed to continue

the chain reaction while the other is needed to breed more fuel. This means that the system would be required to have extremely low levels of leakage and non-fuel absorption to actually breed more fuel than it uses. For this reason it is likely impossible for any conceivable system using only U-235 as fuel. U-235 can be used as a conversion system that will create some fissile material, but ultimately cannot be used for breeding.

The primary breeding mechanism in fast reactors is the conversion of U-238 into Pu-239. This occurs from a neutron absorption in U-238 followed by two successive beta decays. In addition, it is also possible that fast neutrons above the 1.4 MeV threshold will cause fission in U-238 producing, on average, 2.7 neutrons. This reaction is less likely than conversion as observed by the low η value. In the event that Pu-239 absorbs a neutron without a fission occurring, it is converted into fertile Pu-240 which can then be converted into fissile Pu-241. Pu-240 absorption can also result in immediate fission producing 3.17 neutrons.

Exploring the significance of the η values of these isotopes can yield insight into their effects on the criticality of the system. U-238 with an η value of less than 1 will typically reduce the $k_{eff}$ of a system if it is located near the reactor fuel. While U-238 does occasionally fission to produce more neutrons, had the neutron been absorbed in the fuel, many more neutrons would have been produced. The exception to this is if the uranium is in a location where the neutron is highly likely to leak out of the system. In this context, an absorption in depleted uranium will produce more neutrons than if the neutron had simply leaked out and escaped the system. This is part of the reason that fast reactors typically have a blanket of depleted uranium surrounding the system since neutrons near the edge of the reactor have a much higher probability of leaking.

Pu-240 produces fewer neutrons per absorption than Pu-239 or Pu-241 and is always located at the same location as these other isotopes. Thus, $k_{eff}$ would be higher if the Pu-240 was replaced with Pu-239 or Pu-241, but it does produce more than one neutron per absorption so it does not act as a neutron sink.

**2.2 MCNP Overview**

MCNP was the primary tool of interest for this benchmark study. Since the reactor being designed by TerraPower has no moderator, the energy spectrum of neutrons in the system will be relatively high compared to that of a typical light water reactor. To be useful to TerraPower, any facility selected for this benchmark would need to have a fast spectrum. MCNP is the primary neutron transport computer code being used by TerraPower to design their reactor, thus it was selected to model the system to be benchmarked.

For criticality problems, MCNP operates through assuming an initial source distribution which can be as simple as a source point at the center fuel element of a reactor, or a source distribution from a previous, similar problem through the use of an SRCTP file. Neutrons are isotropically "birthed" for the initial source distribution and tracked through the geometry. This tracking is conducted through using the macroscopic total cross section of the material in the cell the neutron currently resides to calculate the probability that the neutron will reach the end of the cell without interaction. Once this probability is calculated, a random number is sampled to determine how far the neutron passes through the cell or if it reaches the end of the cell. If it reaches the end of the cell this process is repeated for the next cell. Any time a collision occurs, another random number is sampled to determine if the interaction is an elastic scatter, absorption or fission or some other type of interaction. If an absorption or fission occurs that neutron is no longer tracked and another is birthed from a random location based upon the source distribution. Neutrons can also exit the system through leaving the boundary of the model, typically where the neutron importance is set to zero and then the neutron is no longer tracked. This type of computer code operates in "cycles" and between each cycle a new fission source distribution is calculated based upon past fission absorptions. The source distribution often takes a fair amount of cycles to converge so the user must enter a certain number of cycles to not include within the statistical analysis of the solution.

An MCNP model is built in the form of text files called input decks. These input files have three parts, the cell card, the surface card, and the data card. The cell card is

the first to appear and it contains the three dimensional geometry of the core being modeled. Each cell has an associated identification number followed by a material number corresponding to a certain set of isotopes for the material in that region. Finally, there is a list of surfaces that bound the cell. Because surfaces have two sides, surfaces listed with a negative sign are "inside" the surface when dealing with curved surfaces such as cylinders or spheres or in a "negative" sense to that surface when dealing with planes. The surface card simply defines the surfaces needed to bound cells. The data card contains isotopic breakdowns of the materials within the system, as well any tallies that can be used to calculate reaction rates and neutron fluxes. In addition, the data card defines what type of problem is being run, for example a K-code calculation for criticality determination with the number of neutrons per cycle and the number of cycles being run.

It should be noted that, while MCNP can track the path of a large number of neutrons for a given problem geometry to reduce statistical uncertainty, the results obtained by MCNP are only as good as the nuclear data libraries used. These libraries give values for neutron cross section as a function of energy, but neutron cross sections have not been measured for every conceivable energy since neutron energy is essentially a continuous variable. Therefore, some interpolation must occur. Interpolation can be problematic in resonance regions where a specific neutron cross section can change rapidly with energy. For this thesis the 70c library was primarily used since the 60c library is known to be error prone when applied to fast reactors and the 50c library does not contain delayed neutron cross sections.

MCNP is a non-deterministic code, meaning that it employs the use of random numbers to sample probability density functions in order to determine the path and life of a neutron. Because it is non-deterministic, users may get different results for the same problem. This can be remedied through the use of a pseudo-random number generator with a consistent initial seed that will guarantee the stream of random numbers will be the same for each run. Even so, the results calculated by an MCNP model are always presented with an associated standard deviation since any results obtained were found through sampling random numbers. Assuming the stream of

values output by MCNP are a typical normal distribution, which should be the case if the code has converged, one can expect the standard deviation to be reduced by a factor of two if the number of active cycles is increased by a factor of four. This illustrates the tradeoff between precision and computation cost of a Monte Carlo method based calculation. Throughout this work, every attempt was made to balance obtaining statistically significant results with computational time. [11], [12], [13], [14]

**2.3 Verification and Validation Process**

Within the domain of computational methods, verification can be thought of as attempting to discern if the computational method being employed is actually solving the right problem and if its implementation is correct. MCNP has been well verified in that it actually solves the neutron transport equation and most importantly for this study it has also been well verified for eigenvalue problems.

Validation determines whether the model gives accurate results to the problem in question. In this case the problem in question is the modeling of a large sodium fast reactor. Thus, this work is on the validation side of the spectrum. [15]

If the context of the word “model” is shifted from MCNP itself to the actual input deck model of the a reactor which MCNP operates on, there is also some verification work being done. The input deck needs to be verified to ensure that the model of the reactor is actually as close as possible to the experimental facility being modeled, especial with respect to the geometry and material properties.

Thus, it is necessary to verify that the experimental facility is being modeled correctly within MCNP in order to validate whether MCNP itself gives accurate results for this system. If there is little certainty that the facility is modeled correctly, then any validation or bias reported is not meaningful.

**2.4 ZPPR-15B**

The initial facility that TerraPower was highly interested in modeling was the ZPPR-15. This facility was advantageous because it contained little oxygen, similar to TerraPower’s reactor design. In contrast, many of the other ZPPR assemblies contained

$Fe_2O_3$ and $U_3O_8$ to simulate a mixed oxide fuel design. While the plutonium and enriched uranium used in the facility were typically in metallic form, the presence of these oxides provided similar isotopic concentrations of oxygen near the fuel in order to simulate MOX fuel. Thus these assemblies were typically characterized as "MOX Assemblies" even though they contained metallic fuel. Because fast neutrons tend to have a larger mean free path this was a reasonable approximation to examine the effects of oxygen on the system.

Ultimately, after a thorough review of the publicly available description of the ZPPR-15, it was determined that there was not enough information available to build an accurate model of the system. Explicitly, the drawer master, describing individual drawer layout, and the "hot constants memos," describing plate composition within the drawer were unavailable. An effort was made to contact some of the researchers at Argonne National Laboratory, but they conveyed that these documents were never intended for external distribution. [16],[17],[18],[19],[20],[21],[22],[23]

One important note is that results were available for an MCNP-5 benchmark of the ZPPR-15B and these showed that ENDF VII libraries under-predict $k_{eff}$ by about 203 pcm. [16] A core with similar composition could be expected to under-predict $k_{eff}$.

## 3 MATERIALS AND METHODS

### 3.1 JUPITER Program Overview

The Japanese-United States Program of Integral Tests and Experimental Researches (JUPITER) program was a collaborative endeavor to study FBR physics. In all, there were a total of twenty one cores assembled, 9 of which are available in the International Handbook of Evaluated Reactor Physics Benchmark Experiments (IRPhE). Various sizes and designs of FBR cores were studied as part of the JUPITER program. Many different, important, reactor physics parameters were measured. Figure 2 shows an outline of the cores considered within the JUPITER program.

| Series of Program | Core Image | Core Type | Assembly No. |
|---|---|---|---|
| JUPITER-I | 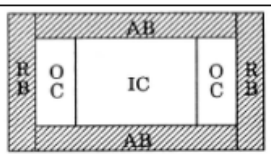 | 600 – 800 MWe class, Two-zone homogeneous core | ZPPR-9<br>ZPPR-10A<br>ZPPR-10B<br>ZPPR-10C<br>ZPPR-10D<br>ZPPR-10D/1<br>ZPPR-10D/2 |
| JUPITER-II | 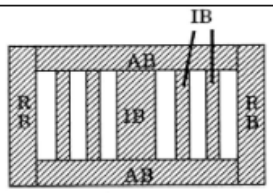 | 600 MWe class, Radial heterogeneous core | ZPPR-13A<br>ZPPR-13B/1<br>ZPPR-13B/2<br>ZPPR-13B/3<br>ZPPR-13B/4<br>ZPPR-13C |
| JUPITER-III | 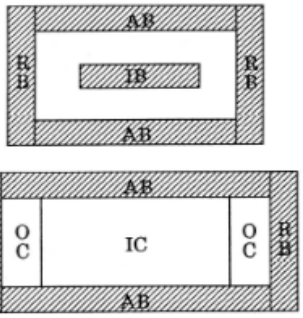 | 650 MWe class, Axially heterogeneous core<br>1000MWe class, Two-zone homogeneous core | ZPPR-17A<br>ZPPR-17B<br>ZPPR-17C<br>ZPPR-18A<br>ZPPR-18B<br>ZPPR-18C |
| JUPITER-Io | 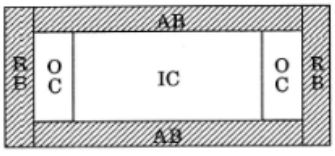 | 1000MWe class, Two-zone homogeneous core | ZPPR-19A<br>ZPPR-19B |

(Symbol) IC: Inner Core, OC: Outer Core,
AB: Axial Blanket, RB: Radial Blanket, IB: Inner Blanket

Figure 2: Outline of JUPITER Program [7]

In the JUPITER I and II set of experiments, Pu-U-Mo fuel was exclusively used, while in the JUPITER III and Io experiments, enriched uranium was added due to the

larger size of these cores and a limited inventory of Pu-U-Mo fuel available at the ZPPR facility. The inner core typically contained a lattice of single column fuel, while the outer core contained a mixture of single and double column fuel, thus increasing the average fuel density within this region. The Blanket regions contained depleted uranium which could fission through interaction with fast neutrons or be converted into fissile Pu-239 through neutron absorption. Because the facility was extremely low power, insignificant amounts of U-238 were bred into Pu-239, but it was important for the core to contain U-238 so that the physics of a core with large concentration of this isotope could be studied. While not shown in Figure 2, these cores typically had stainless steel axial and radial reflectors surrounding the system.

The nine cores that were presented in the IRPhE were reviewed for determining the selection of the most applicable core to the needs of TerraPower. These cores were:

- ZPPR-9
- ZPPR-10 A, B and C
- ZPPR 13 A
- ZPPR-17 A
- ZPPR-18 A, and C

Some of the significant similarities of these FBR cores were that they all contained Pu-U-Mo fuel as well as sodium or sodium carbonate. In addition to material properties, the method of cataloging the core layout was important for the purposes of model development. If the core was not described in a desirable manner (such as an spreadsheet document) and had to be manually transcribed into an MCNP deck, there would be a larger opportunity for error in this transfer since for many for these cores there were upwards of 5,000 lattice elements and about 100 types of materials. For these reasons the method in which the data were recorded was also important in facility selection. Fortunately, the core map, which showed the arrangement of drawers within the lattice, and Drawer Master, which showed the arrangement of material plates within a drawer, were both presented in attached Excel files for all of these cores.

**3.2 Selection Criteria**

For the selection of the appropriate facility to model, the differences between each of the facilities were catalogued and analyzed. These properties are shown in the selection matrix in Table 3. The selection criteria included are:

- Enriched Uranium: Did the system contain enriched Uranium?
- Plate Composition: Was plate material data included and was it presented in the form of a spreadsheet file?
- Benchmark Data: Was the benchmark data expressed in an Excel spreadsheet?
- Number of MCNP 5 Input Decks: Did the Benchmark already have an MCNP model and how many input decks did it have?
- Lattice Size: How large was the lattice of the core?
- Estimated Number of Universes: This property is the estimated number of universes for an MCNP input deck. It is a good measure of the complexity of the core and amount of effort required to build the MCNP model as well as the predicted length of the input deck since the cell card is likely the largest card in this type of problem. This was estimated by counting the number of unique drawers in the drawer master and multiplying by two since the other half of the core will have different drawer orientation.
- Types of Benchmarking: Contains a list of acceptable benchmarks meaning the type of experimental data taken at the facility that had low enough uncertainty to be compared to a model of the facility. These include measurements such as Criticality and Reaction Rate Ratio.

| | Enriched Uranium | Plate Composition | Benchmark Data | # of MCNP 5 Input Decks | Lattice Size | Est. # Universes | Types of Benchmarking |
|---|---|---|---|---|---|---|---|
| ZPPR-9 | no | poor/no Excel | no Excel | 11 | 57x57 | 140 | CR, RRR, CRW, SVR, SDRW, RRD |
| ZPPR-10 A | no | yes | yes with sensitivity coefficients | 11 | 61x58 | 220 | CR, RRR, CRW, SVR, RRD |
| ZPPR-10 B | no | yes | yes | none | 61x59 | 280 | CR, RRR, CRW, SVR, RRD |
| ZPPR-10 C | no | yes | yes | none | 71x65 | 260 | CR, RRR, CRW, RRD |
| ZPPR-13 A | no | yes | yes | 12 | 68x68 | 230 | CR, RRR, CRW, SVR, SDRW,RRD |
| ZPPR-17 A | no | yes | yes | none | 64x64 | 180 | CR, RRR, CRW, SVR, RRD |
| ZPPR-18 A | outer core metallic* | yes | yes | none | 77x75 | 150 | CR, RRR, CRW, RRD |
| ZPPR-18 C | outer core metallic* | yes | yes | none | 77x75 | 180 | CR, RRR, RRD |
| ZPPR-19 B | outer core metallic* | yes | yes | none | 77x75 | 160 | CR, RRR, CRW, RRD, SVR measured but too large uncertainties to benchmark |

*Enriched Uranium is contained in the outer core due to the large size of the core and not enough Pu in ZPPR inventory

| | |
|---|---|
| CR | Criticality |
| RRR | Reaction Rate Ratio |
| CRW | Control Rod Worth |
| SVR | Sodium Void Reactivity |
| SDRW | Sample Doppler Reactivity Worth |
| RRD | Reaction Rate Distribution |

Table 3: ZPPR Selection Matrix

### 3.3 Facility Selection

Since the ZPPR 9, 10A and 13A cores all have had MCNP input decks previously created, they were eliminated since it did not seem constructive to model them again. The ZPPR-10 B and C cores contained a large quantity of drawers (leading to a large number of universes) to model which would likely take much longer to build the initial model. Thus they were eliminated.

This left the ZPPR-17A, 18A and C and 19B cores for consideration. The ZPPR 17A core had the advantage of having a Sodium Void Reactivity benchmark and did not contain any substituted enriched uranium. This core, however, contained an internal blanket, which is not present in TerraPower's design. Therefore, configurations which contained internal blankets were eliminated from consideration since configurations with only external blankets would pose a better benchmark calculation for TerraPower's needs.

The remaining cores under consideration at this point were the ZPPR-18A and C and 19B. The ZPPR-18C core contained a larger number of drawers and had less benchmark parameters so it was eliminated. Of the ZPPR 18A and 19B cores, it was suggested by TerraPower that the ZPPR-19B may have more completely defined data since it had been previously evaluated by the Japanese. Additionally, the ZPPR-19B contained a homogenous distribution of the enriched uranium within the outer core. Thus, the ZPPR-19 B was chosen as the facility to be modeled.

### 3.4 Facility Description

The ZPPR-19B experimental facility is arranged in two halves. One half is stationary and the other can translate to an open and closed position for the purpose of loading the core. The two halves are then moved closer together to achieve criticality. Each half core is composed of square matrix tubes which are 55.245 mm (2.175 inches) by 55.245 mm (2.175 inches) by 1524 mm (5 feet) [7] These tubes are stacked on top of each other to create a square lattice. Instead of the typical fuel elements seen in most reactor cores the ZPPR-19B is organized into drawers. A diagram of a matrix tube/drawer system is shown in Figure 3.

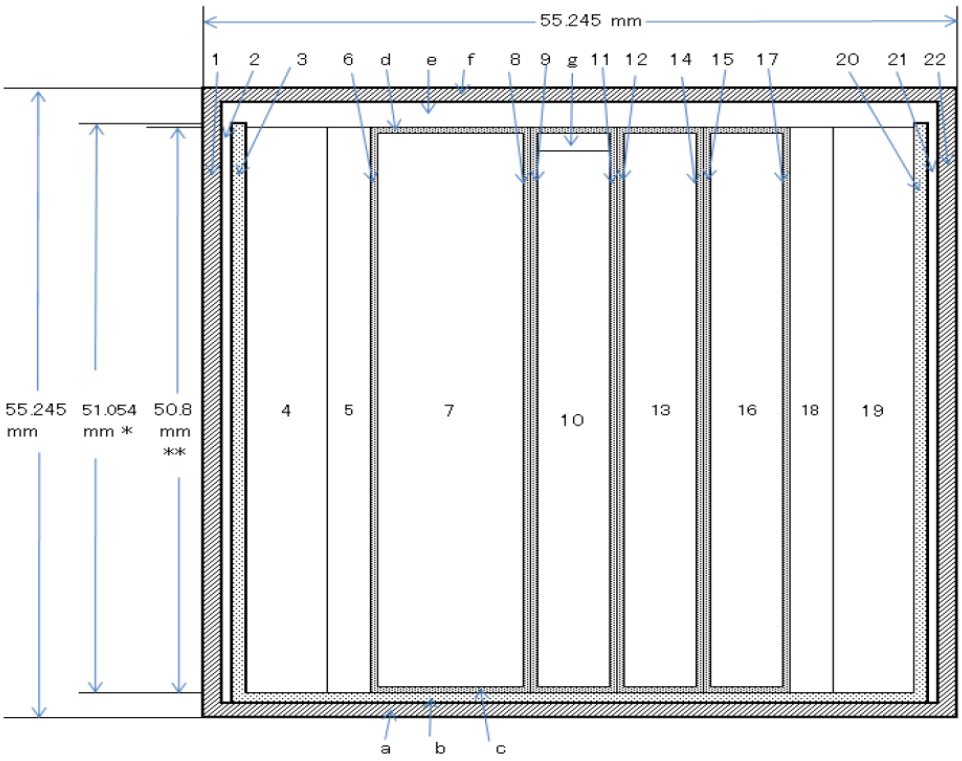


1 : Matrix tube (1.016 mm)
2 : Gap (0.4191 mm)
3 : Drawer (0.7874 mm)
4 : $U_3O_8$ plate (6.35 mm)
5 : Depletad uranium plate (3.175 mm)
6 : Can wall (0.381 mm)
7 : Sodium (11.938 mm)
8 : Can wall (0.381 mm)
9 : Can wall (0.381 mm)
10 : ZPPR-Pu fuel (5.588 mm)
11 : Can wall (0.381 mm)
12 : Can wall (0.381 mm)
13 : Sodium (5.588 mm)
14 : Can wall (0.381 mm)
15 : Can wall (0.381 mm)
16 : $Na_2CO_3$ (5.588 mm)
17 : Can wall (0.381 mm)
18 : $Fe_2O_3$ plate (3.175 mm)
19 : $U_3O_8$ plate (6.35 mm)
20 : Drawer (0.7874 mm)
21 : Gap (0.4191 mm)
22 : Matrix tube (1.016 mm)

a : Matrix tube (1.016 mm)
b : Drawer (0.7874 mm)
c : Can wall (0.381 mm)
d : Can wall (0.381 mm)
e : Gap (1.6256 mm)
f : Matrix wall (1.016 mm)
g : Gap (0.9144 mm)

* : Height of drawer side wall.
** : Height of plates.

Figure 3: Cross Section of a ZPPR Drawer [7]

The Matrix Tube is the material surrounding the outside of the drawer. The drawer itself has an air gap on both sides as well as the top. The function of the drawer is to tightly hold arrangements of different plate material and to allow this material to be easily removed from the core. In addition, some plates in the drawer have a can wall surrounding them as can be seen in cells 7, 10, 13 and 16 of Figure 3. These plates typically contain fissile material or sodium. In addition, there is a small gap between the top of the Pu-U-Mo fuel

plate and the can wall and this needs to be accounted for when modeling as seen in cell 10 of Figure 3.

The facility was very low power, thus little heat was produced during operation and testing. The only flow is results from natural convection of the air through gaps between the drawer and the matrix tube. The facility models a sodium fast reactor; therefore most of drawers contain sodium in plate form inside a can wall.

A typical drawer contains many types of materials and most have Pu-U-Mo fuel and sodium encased in a can wall, as well as slabs of uranium and stainless steel. Each drawer was inserted into one matrix tube and the core is assembled by separating the two halves of the core and inserting the drawers into the matrix tubes. The entire geometry in the core is rectilinear.

While the core was being assembled shim and safety rods were inserted to prevent any possible criticality. After the core was fully assembled the two halves of the core were slowly drawn together to a prescribed gap distance between the two halves. The interface gap distance is 54.5 mm for the critical core configuration #21 and 54.9 mm for the subcritical configuration #28. [7] After the correct gap has been achieved the shim and safety rods are withdrawn and the criticality of the system is measured. Excess reactivity for criticality was measured by using the positive period method, while delayed neutron fraction was measure by the rod drop method.

In addition to multiplication factor, reaction rates were also measured for fission in Pu-239 , U-238 and U-235 fission. The reaction rate for U-238 capture was also measured. Plutonium, depleted uranium and enriched uranium foils were inserted into different drawers with the reactor to measure these properties. The plutonium foils had a diameter of 10.80 mm or 8.00 mm and a thickness of 0.13 mm and were clad in aluminum with a thickness of 0.025 mm. The mass of the foil was 150 mg for the larger diameter and 90 mg for the smaller diameter foils. The enriched uranium and depleted uranium foils were essentially the same dimensions with a diameter of 12.70 mm and a thickness of 0.13 mm. The uranium foils were also coated in kef-f, a fluorocarbon based polymer [25], and covered on the top and bottom with .13mm thick aluminum disks. [7]

The foils were placed in holders with two possible orientations, orientation R and orientation A. Orientation R has the foils placed parallel to the front of the drawer while orientation A has the foils placed parallel to the side of the drawer. In addition, foils could

also be placed within the holder on top of the drawer to measure the reaction rates on top of the plates. [7] The primary orientation for foils in this experiment was orientation A. Figure 4 shows an example of the foil holder placed in orientation A, while Figure 5 shows a top down view of the foil holder placement within a drawer. It should be noted that most of the foils in the ZPPR-19B were placed in the GH position of Figure 5.

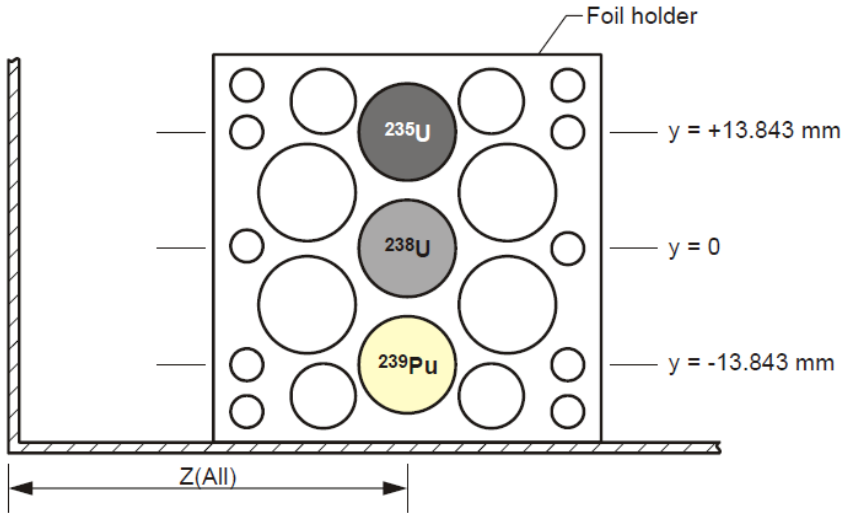


Figure 4: Foil Holder in Orientation A [7]

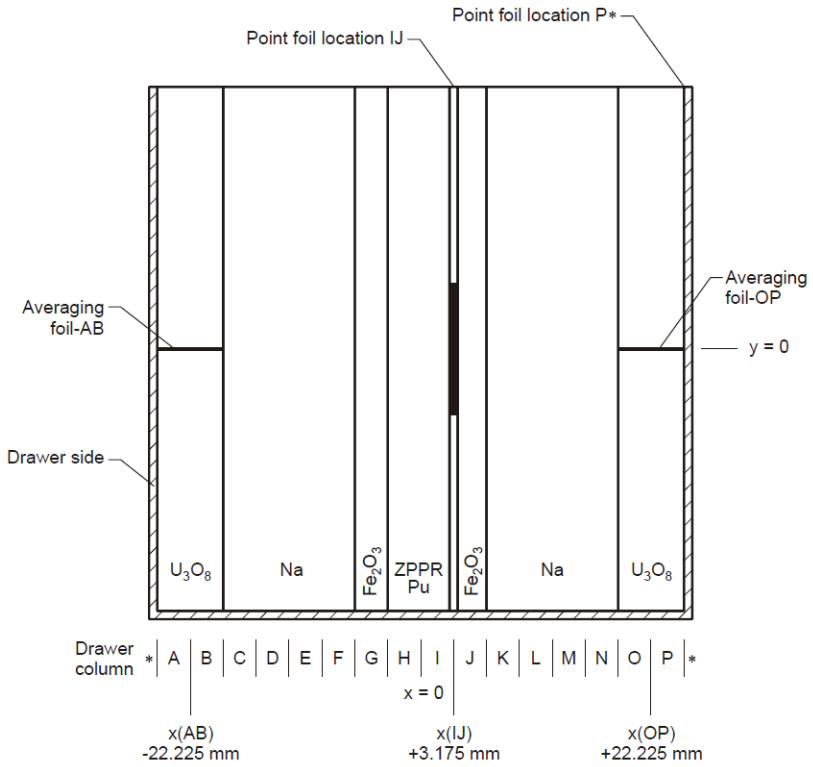


Figure 5: Top Down View of Foil Holder Placement [7]

Foils were placed in different locations throughout the core to measure the distribution of reaction rates for these fissile/fissionable materials within the core. The locations of these foils within the reactor core can be seen in Figure 6. As shown in this figure there were seven transverses of foil placements across the core. These included three axial transverses, a vertical transverse, a horizontal transverse and a 15° and 30° above the horizontal transverse. Of primary interest for this study were the three transverses containing plutonium foils, the horizontal transverse, the 15° transverse and the axial transverse at the center of the core located at the bottom left of the figure. Reaction rates of the foils were determined by using a Ge(Li) detector. Typically the foils were introduced to the detector about 18 hours after the end of radiation and were measured for 70 to 84 hours. Fission rates were determined by measuring counts of I-133 (529.9 keV), I-132 (667.7 keV), Nb-97 (658.1 keV) and Nb-97m (277.6 keV). U-238 capture was determined from the counts of Np-239 (277.6 keV).[7]

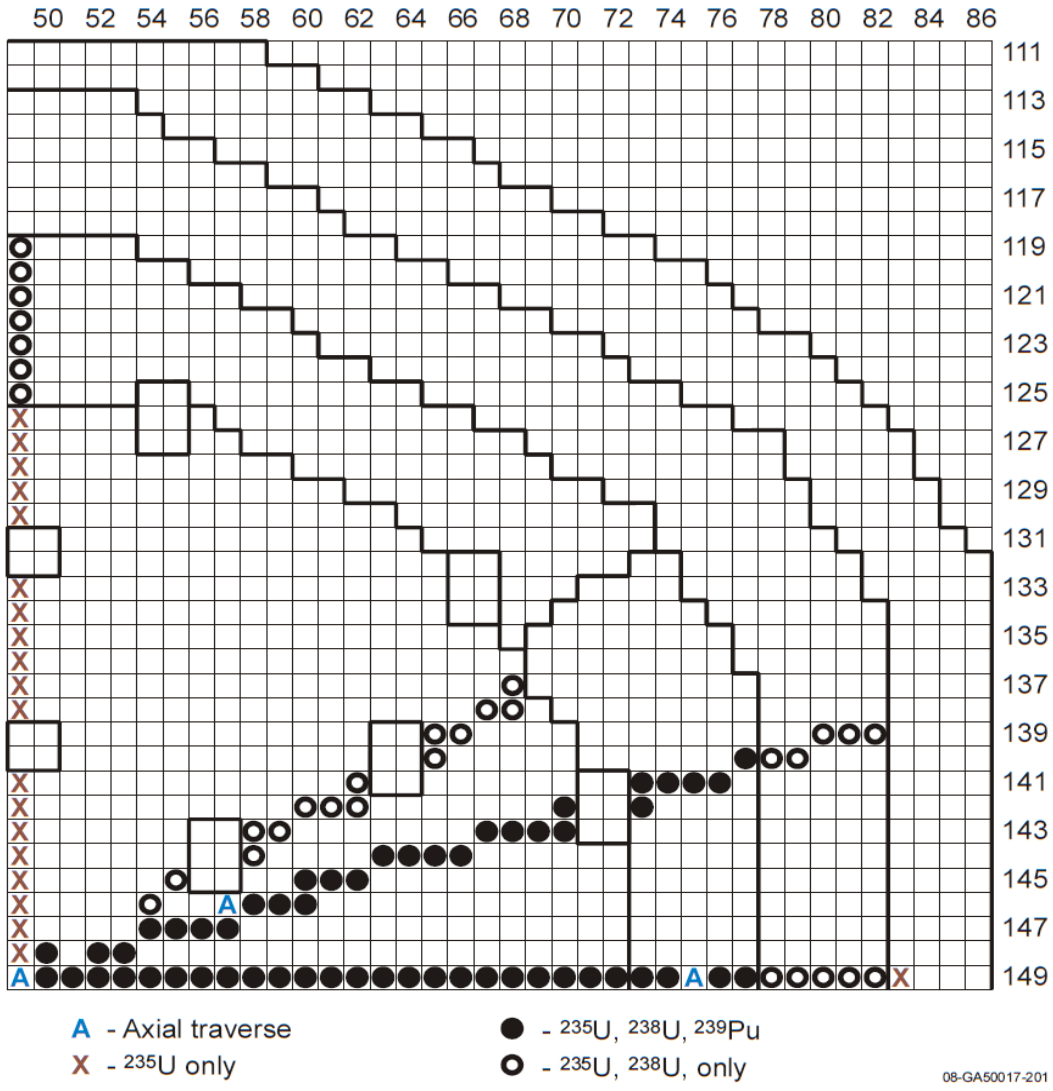


Figure 6: Foil Measurement Locations [7]

### 3.4 Core Geometry

The core for the ZPPR-19B is organized into a 77x75 matrix of drawers. Figure 7 shows the arrangement for the critical configuration for half of the core. The other half was organized similarly and thus not presented here. Because the core has so many elements this figure is hard to interpret but is presented for completeness. Figure 8 shows the 1/8th core with horizontal and vertical lines showing symmetry. It should be noted that while there is significant symmetry the locations of the pink counter drawers are not symmetric. The numbering system of the axis of Figure 7 is the number system used by the ZPPR program for describing the location of a particular matrix tube or drawer.

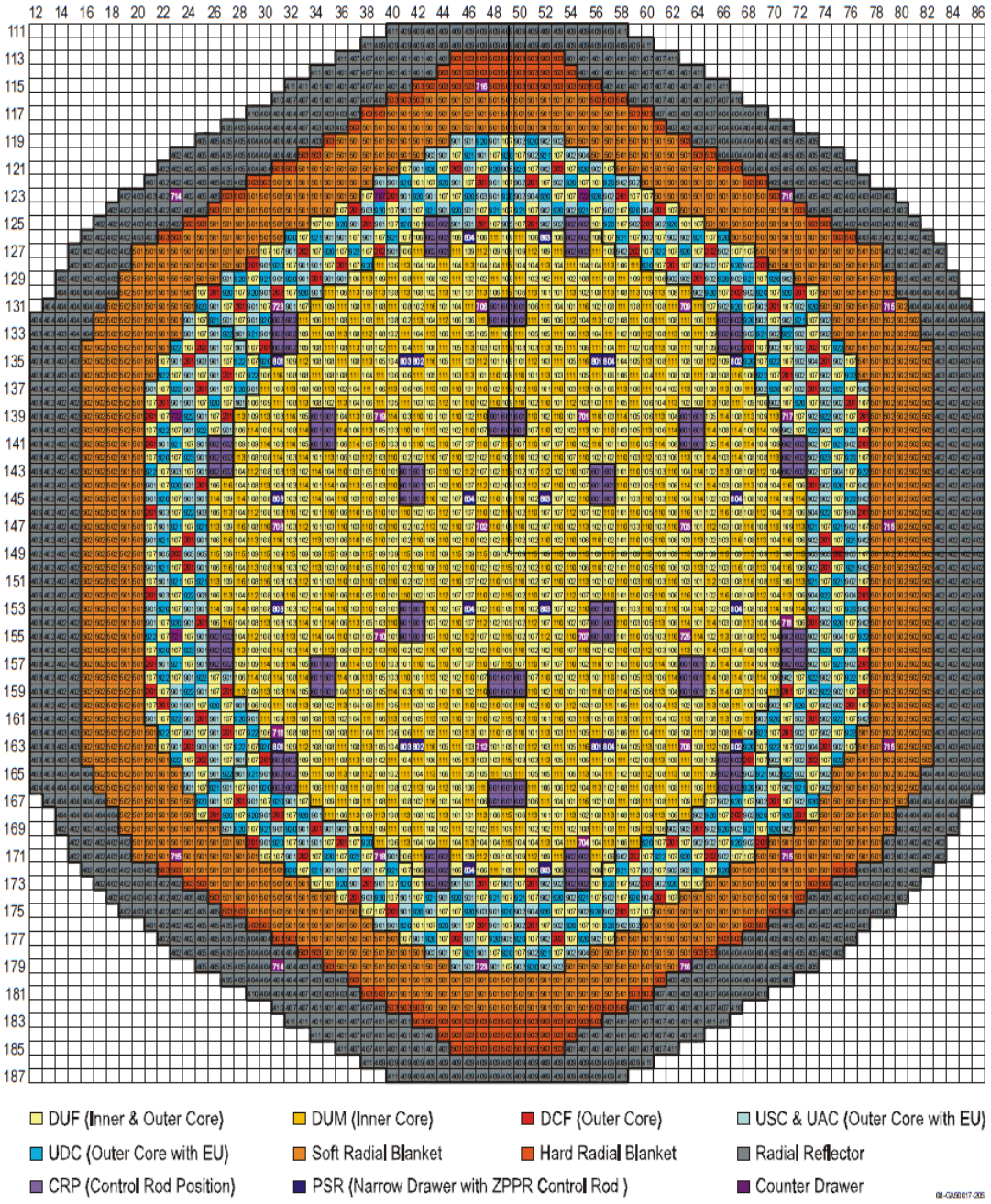


Figure 7: Critical Half Core Layout [7]

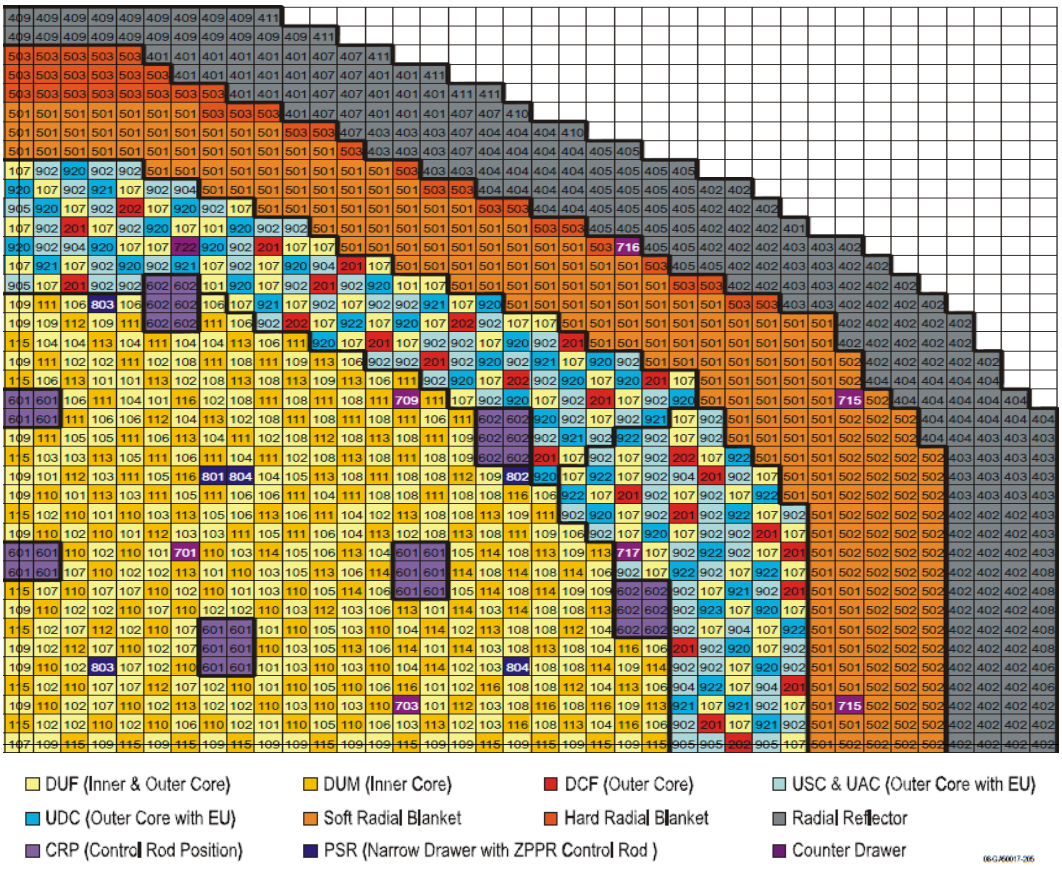


Figure 8: 1/8$^{th}$ core Layout [7]

As can be seen in Figure 8, the inner core was composed mostly of single fuel drawers which are denoted by the first digit being “1” (100 series) but also contained the 600 series of Control Rod Position (CRP) drawers, the 700 series of counter drawers and the 800 series of Poison Safety Rod (PSR) drawers. The “DUF” drawers were drawers 101-109 and they contain ZPPR fuel with $Fe_2O_3$ surrounding the fuel. The “DUM” drawers, 110-116, contained depleted uranium metal surrounding the ZPPR fuel in the same location where the $Fe_2O_3$ plates were located in the DUF drawers. While both drawers contained some oxidized depleted uranium, the DUM drawers contained significantly more depleted uranium in metallic form. These drawers were mostly distributed in a checkerboard pattern within the inner core.

The inner core also contained the 600 series of CRP drawers. For most core configurations, the 600 series of CRP drawers contained exclusively sodium but there are certain configurations where boron plates were inserted along with sodium to model the behavior of control rods within the core. The pure sodium CRP drawers are numbered 601

and 602 while any CRP of 603 or higher contains some amount of boron. It is important to clarify that these CRP drawers were not used for reactivity control and separate boron rods were used for the shim rods and safety rods.

The 800 series of PSR drawers were three quarters the thickness of normal drawers. The spaces between these narrow drawers and the matrix tubes were the locations where the shim and safety rods were inserted for reactivity control during assembly. These drawers contained similar material to the 100 series but one row of sodium plates is removed from the drawer.

The 700 series of counter drawers were located sporadically throughout the core and contained radiation detectors. These counter drawers were arranged to be approximately like the other drawers in the core region they were placed. Thus, there were many different types of counter drawers that could be built to be similar to DUM drawers, DUF drawers or any other drawer type within the reactor.

The outer core was composed of DCF, USC, UAC, UDC and the same DUF and DUM drawers contained within the inner core. DCF (Double Column plutonium Fuel) drawers contained twice as much plutonium fuel as the 100 series previously mentioned. The 900 series of drawers contained enriched uranium rather than the ZPPR fuel in the 100 and 200 series. The reason enriched uranium had to be employed in these drawers was that the ZPPR 19B was the largest core modeled within the ZPPR experimental facility and there was not enough fuel material to build the entire core  out of plutonium plates. It should be noted, that all of the enriched uranium drawers were well mixed and homogenized within the outer core.

The next layer of the core was the soft/hard radial blanket. These 600 series of drawers contained large amounts of depleted uranium but no enriched uranium or ZPPR plutonium fuel. The difference between the soft blanket and hard blanket was the presence or absence of sodium within the drawer.

Finally, the last layer was the radial reflector. This 400 series of drawers contained exclusively stainless steel and was included to reflect neutrons back into the system.

Overall both of the core halves are similar with respect to the distribution of drawers and location of different layers of the reactor core. The main differences between the two halves have to do with the locations of the 700 series of counter drawers within the core.

### 3.6 Plate Distribution within Drawers

The layouts of the different types of drawers had some major similarities and it is important that these be discussed before considering the specific details of each drawer. Figure 9 shows a photograph of a typical ZPPR drawer. The plates making up the drawer are elevated from the bottom of the drawer in this figure in order that they can be better seen but in the actual drawers the plates were flush with the top of the stainless steel drawer container.

Figure 9: Photograph of a Representative ZPPR Drawer [7]

Figure 9 is presented to give the reader a physical sense of what a drawer loaded with plates physically looks like, but this specific arrangement is not present in the ZPPR-19B. The drawers in the ZPPR-19B were divided into three regions, the core (the section which is closest to the interface gap), the axial blanket and the axial reflector. Figure 10 shows the dimensions and the distribution of these regions within a drawer.

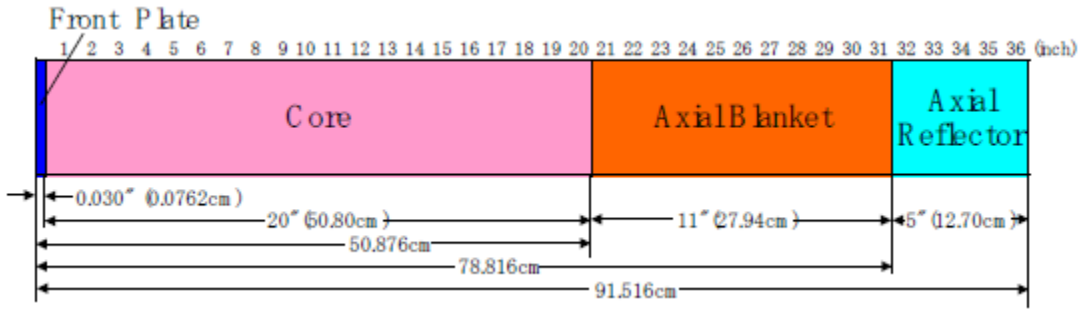


Figure 10: Dimensions of Regions within a Drawer [7]

There are two types of drawers in the 100 series. The first type of drawers contained stainless steel next to the fuel while the second type of drawers contained depleted uranium metal in this location. Figures 11 and 12 demonstrate the general distribution of plates within these two types of drawers from a top down view.

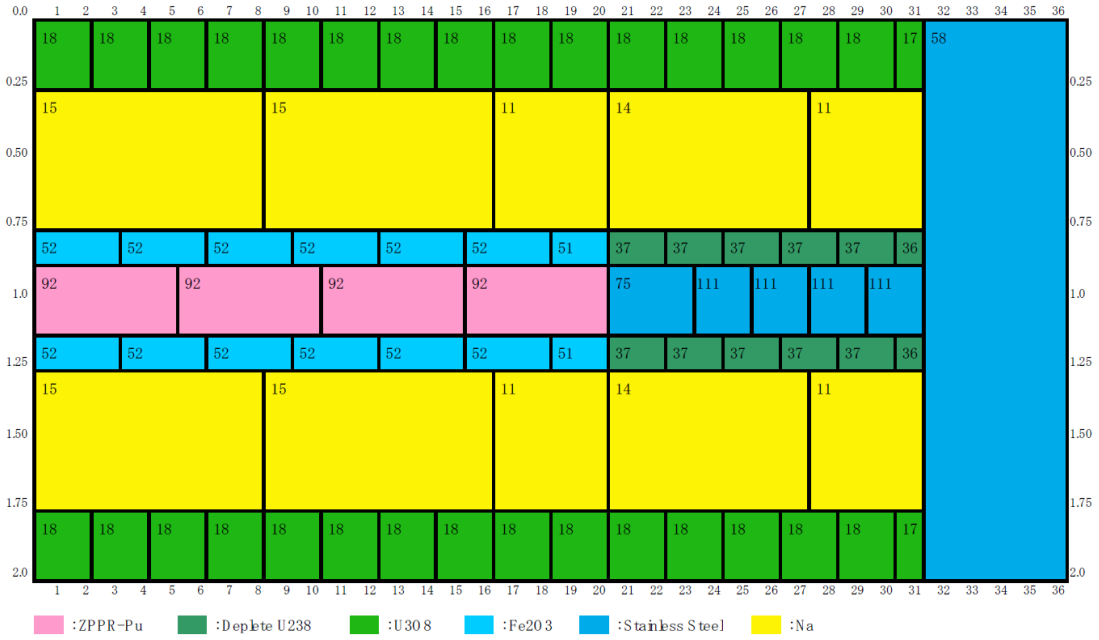


Figure 11: Drawer 101 Schematic Arrangement [7]

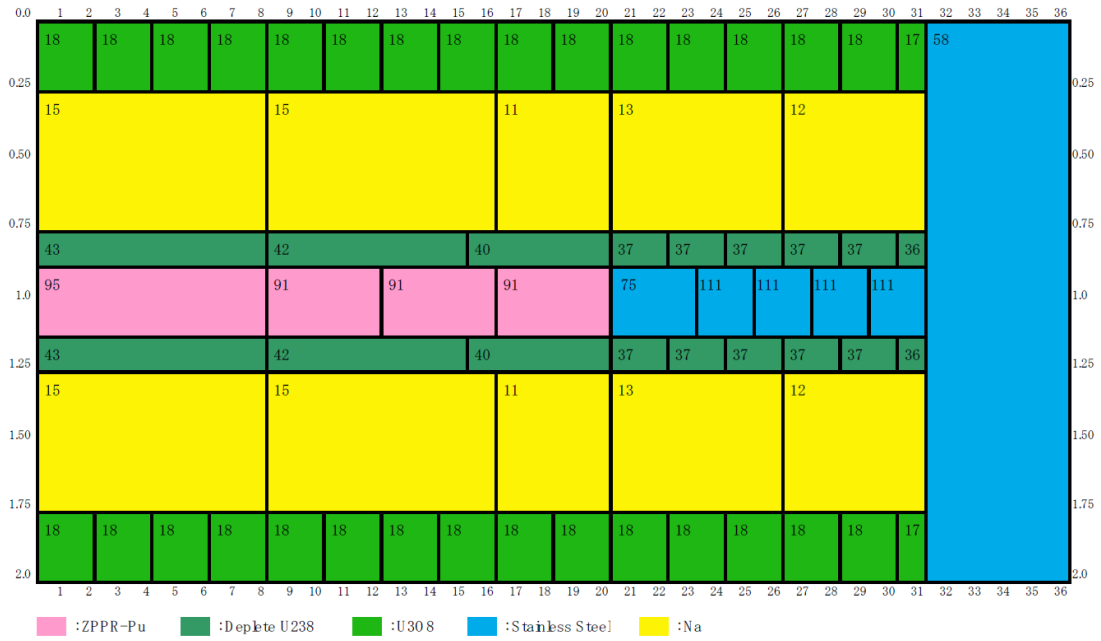


Figure 12: Drawer 110 Schematic Arrangement [7]

All dimensions shown here are in inches. The color of the plates indicates the general type of material present within the plates while the number on the plates explicitly categorizes the exact material composition of the plates. Thus, while material number 91 and 96 are both pink indicating both are ZPPR-Pu, the exact isotopic composition and dimensions of these plates are different.

In these two figures one can clearly see that the fuel ends at the boundary of the core, twenty inches from the front, while the axial blanket contains only sodium depleted uranium and stainless steel. The axial reflector contains only stainless steel. Within the DUF 101-109 series of drawers, the locations of plate boundaries and exact material compositions may vary, but the locations of the six types of material present remains constant. Thus, the plutonium fuel is always located in the center of the drawer with the same width and always extends to 20 inches. The same is true for all other materials within the drawer. This core contains approximately 80 different numbered drawers and it would be overwhelming to present all of this information here. However, it is not necessary to present the details for all drawers explicitly since the types of materials present and their locations are fairly similar for specific groups of drawers.

The next group of drawers is the DUM series, drawers 110 -116. The significant difference between the DUF and DUM series of drawers is that the DUF series contained oxidized iron plates on both side of the ZPPR fuel while the DUM series has depleted

uranium metal in these locations. This significantly affects the neutronic behavior of these two types of drawers.

The DCF 200 series of drawers contained two similar drawers, 201 and 202. The layout of drawer type 201 is shown in Figure 13.

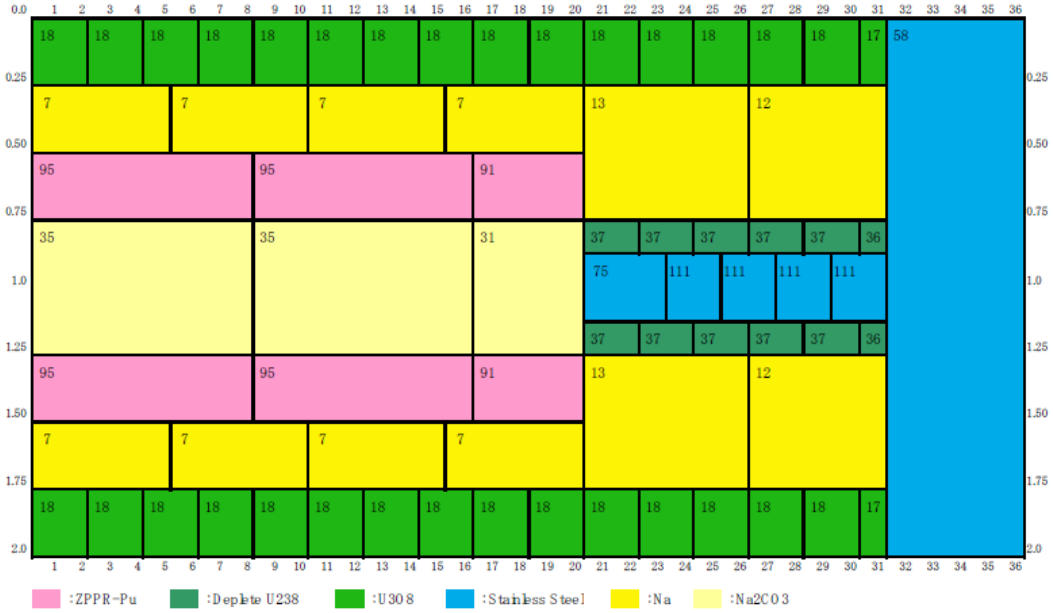


Figure 13: Drawer 201 Schematic Arrangement [7]

The layout of this drawer is fairly similar to the layout of the 100 series but instead of one column of ZPPR fuel there are two columns. In addition, they are separated by $Na_2CO_3$. The materials present within the axial blanket and axial reflector are exactly the same as the 100 series while the core was different. Another significant difference was the absence of iron oxide or uranium metal surrounding the fuel. The other 200 series drawer, 202, was similar in material locations but as with drawers 100-109 plate boundaries and exact material numbers differ.

The 400 series of drawers were the radial reflector drawers. They were composed completely of stainless steel in many different arrangements. An example of one of these arrangements is shown in Figure 14.

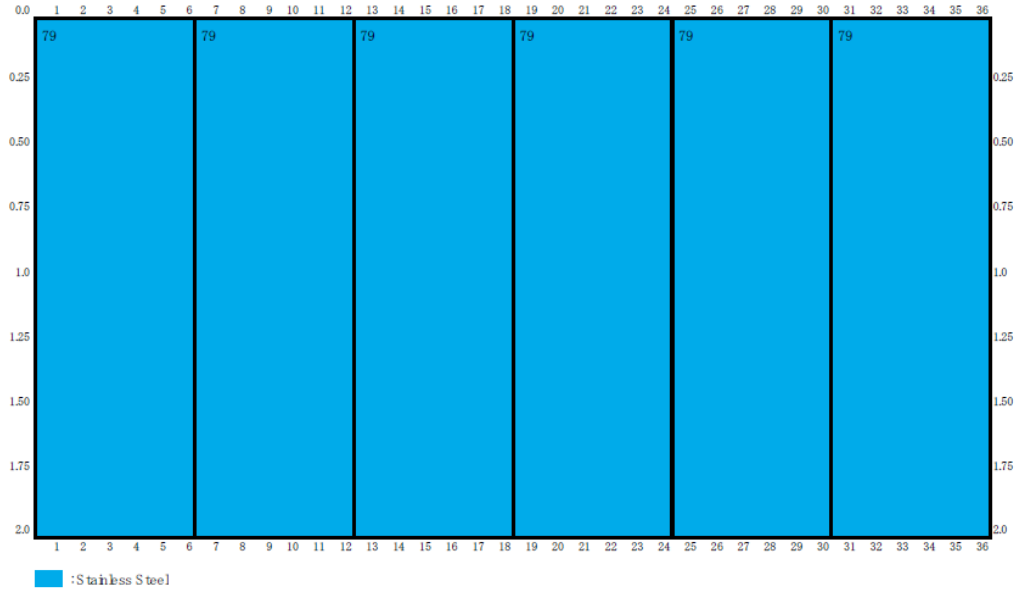


Figure 14: Drawer 401 Schematic Arrangement [7]

The 500 series of drawers is split into soft radial blanket (501 and 502) and hard radial blanket (503). Renditions of these drawers are in Figures 15 and 16. The soft radial blanket drawers contained uranium metal, $U_3O_8$, sodium and stainless steel while the hard radial blanket contained only uranium metal and stainless steel. Because the hard blanket had an absence of sodium and oxidized uranium with a larger amount of uranium metal it had a much higher local density of uranium atoms. This is partially because the density of metallic uranium is much larger than the density of oxidized uranium, but also because the hard radial blanket contained a larger volume of uranium. Because the hard radial blanket contained a much higher atom density of uranium it is likely to have a harder neutron spectrum.

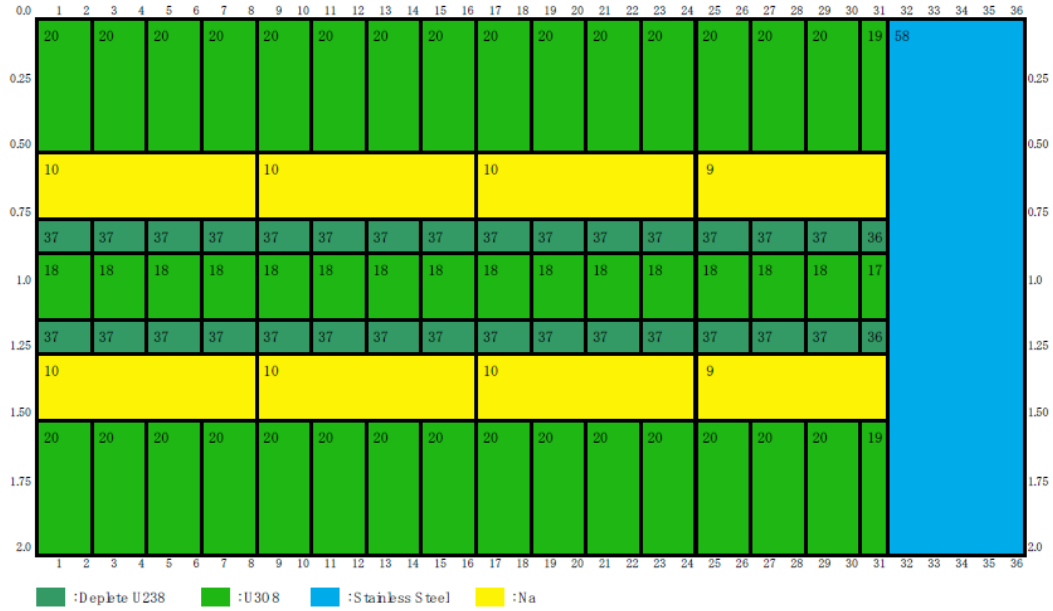


Figure 15: Drawer 501 Schematic Arrangement [7]

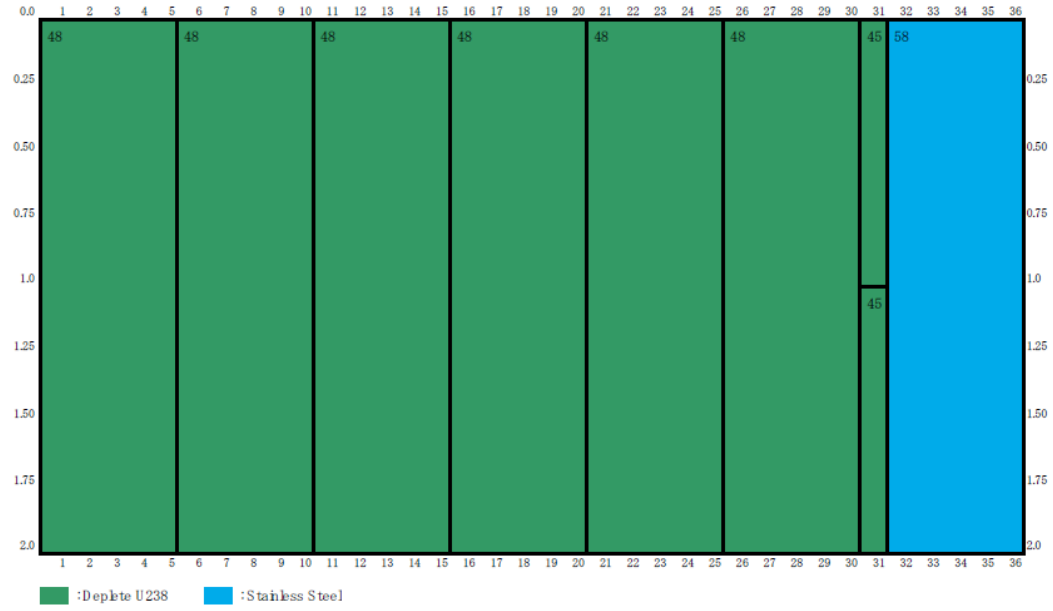


Figure 16: Drawer 503 Schematic Arrangement [7]

The 600 series of control rod positioner drawers typically contained exclusively sodium. There were some core configurations where boron plates are also included to simulate control rod insertion and investigate the effects on reactivity of the system but for most of the work done in this thesis only the 601 and 602 drawers containing only sodium were used. These drawers are important to the physics of the core since an actual core will also have control rods and when they are withdrawn there will be large areas of sodium

instead of fuel in these locations. Interestingly these drawers do not contain any sort of axial blanket or reflector. Figure 17 shows the physical layout of one of these drawers.

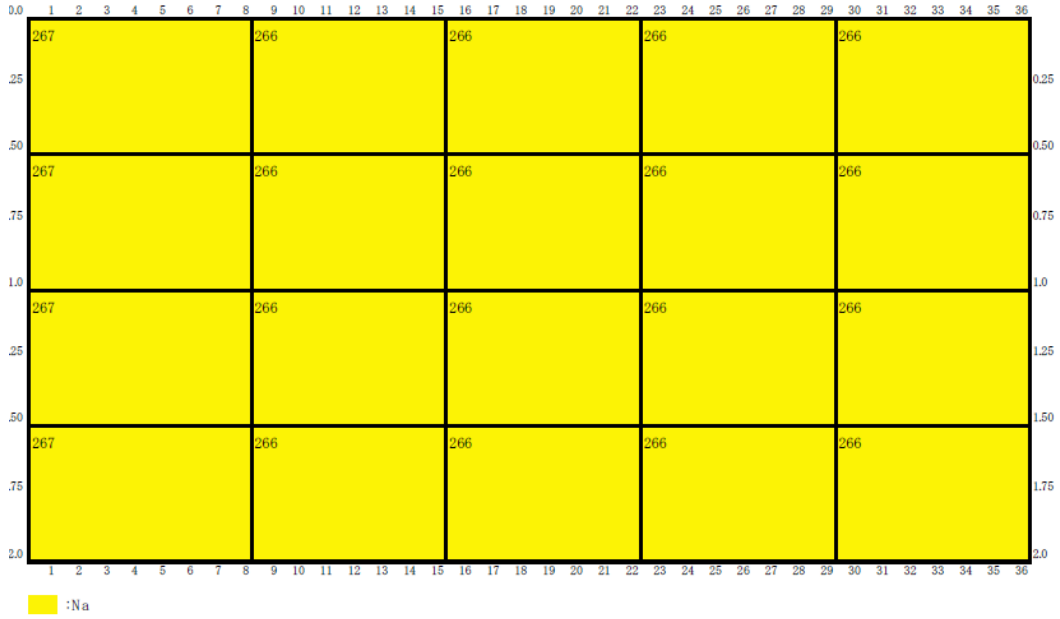


Figure 17: Drawer 601 Schematic Arrangement [7]

The 900 series of drawers contained drawers that included enriched uranium as fuel rather than the ZPPR fuel used in the 100 and 200 series of drawers. Most plates within the core had a height of two inches, lengths that were a multiple of one inch and widths that were a multiple of one quarter of an inch. The uranium plates, however, did not follow this pattern. The reason for this was that the decision was made, after the plates were designed and fabricated, that they should be clad. This resulted in the enriched uranium tending to have odd dimensions which lead to air gaps in certain spots within the drawer. The UAC and USC drawers are shown in Figures 18 and 19.

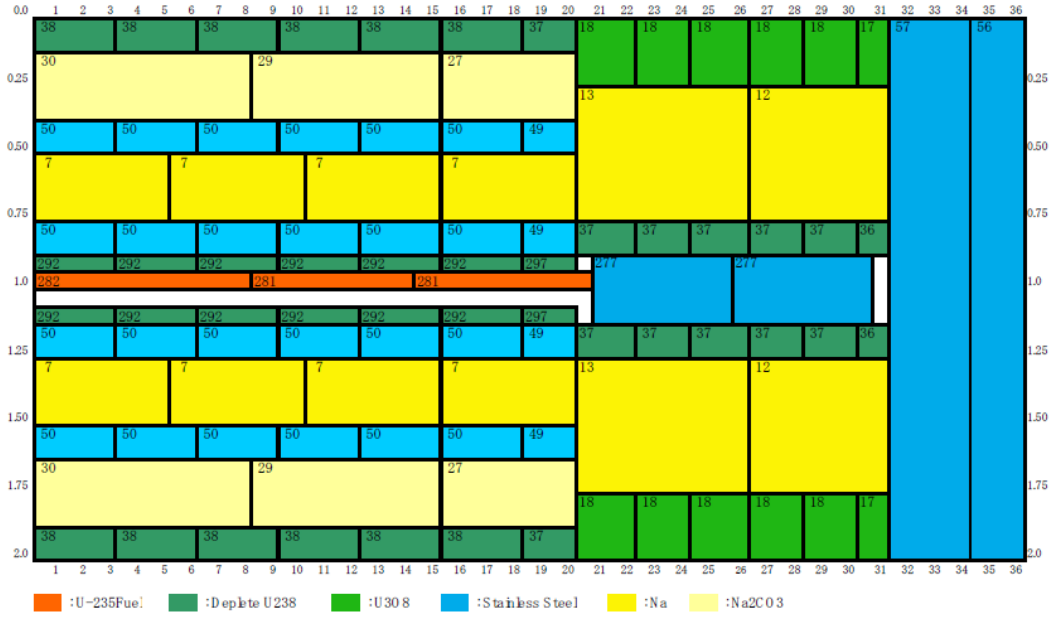


Figure 18: Drawer 905 Schematic Arrangement [7]

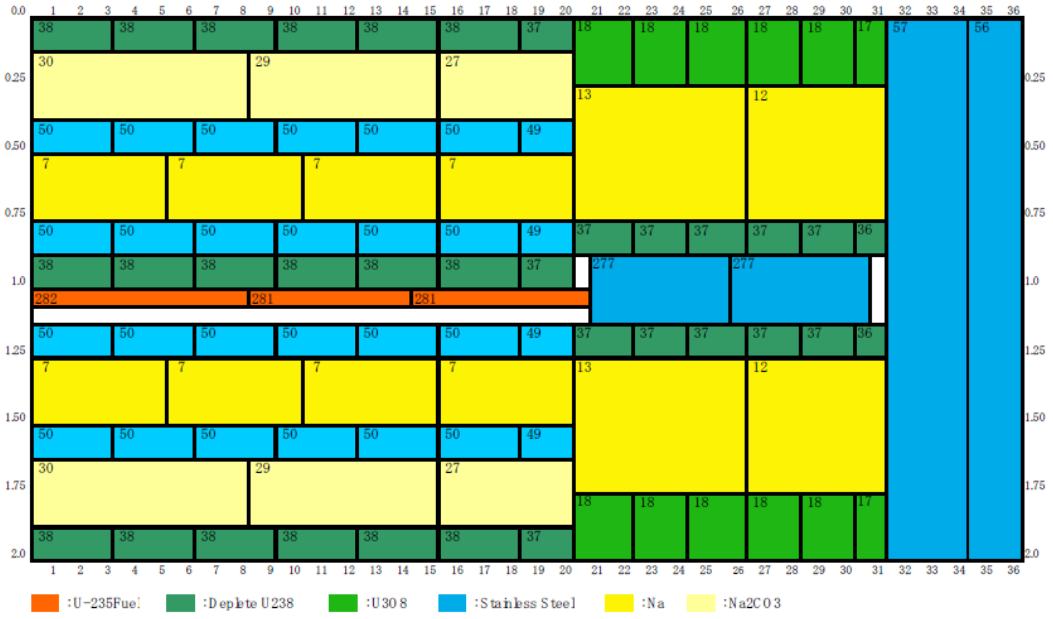


Figure 19: Drawer 901 Schematic Arrangement [7]

Drawer 905 is the only symmetric single column enriched uranium drawer. Drawers 901 through 904 are all asymmetric drawers. The main difference between the asymmetric and symmetric drawers was the location of the enriched uranium fuel. In the symmetric drawers the fuel located close to the center of the drawer, while the asymmetric drawers have the fuel significantly offset from the center. Of the asymmetric drawers, drawers 901

and 903 have the fuel offset to the right side if looking in from the front of the drawer. Drawers 902 and 904 had the fuel offset to the other side.

Drawers 920 to 923 were UDC (Uranium Double-Column fuel) drawers and used the same types of fuel as used in drawers 901-905. A representation of this drawer is shown in Figure 20.

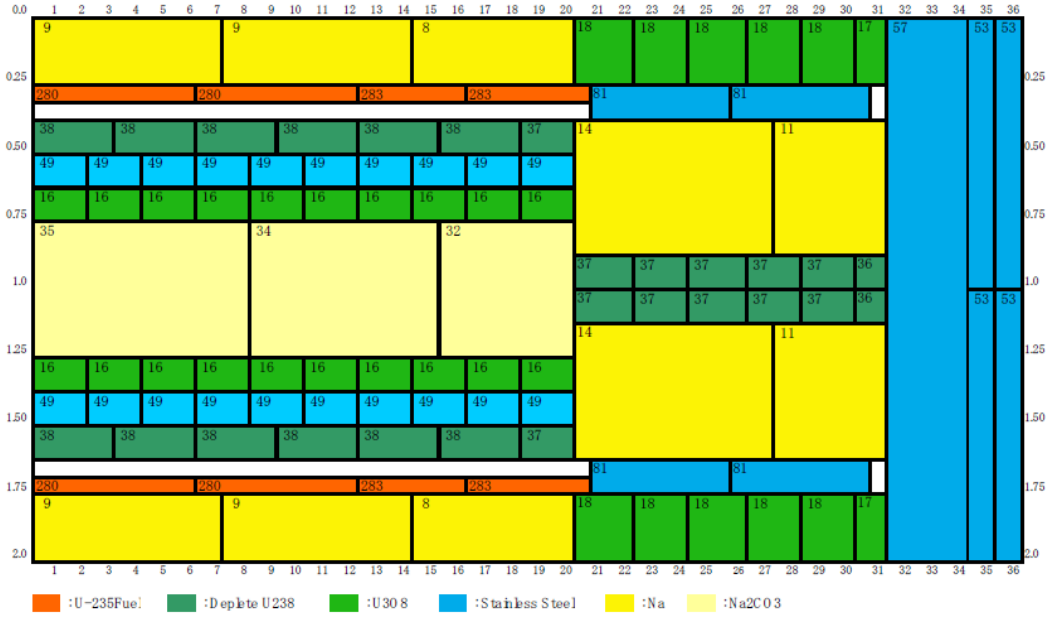


Figure 20: Drawer 920 Schematic Arrangement [7]

As a group, the significant aspects of the 900 series of drawers were that there were gaps within the plates in the drawers. In addition, they all contained enriched uranium as well as $Na_2CO_3$. $Na_2CO_3$ is not present in the any of the inner single column 100 series of drawers. It should be recognized that the 900 series of drawers were only located in the outer core along with the 200 series, which also contained $Na_2CO_3$. Thus, the sodium in the inner core was exclusively pure plated sodium while the sodium in the outer core was a mix of $Na_2CO_3$ and pure sodium.

### 3.3 Facility material properties

Before extensively discussing the material properties of the plates in the core it is important to address the issue of cladding or can walls surrounding certain material plates. The can walls of all plates were 0.381mm thick. The clad on the enriched uranium had variable thickness of .00575 inches horizontally, .005 inches vertically and .055 inches along the plate's axial length. Any plates continuing plutonium, sodium or enriched uranium was

encased in a can wall to avoid chemical reactivity from sodium and possible radiation exposure from the fissile material. In addition, a few of the boron plates within the 600 series were also manufactured with a can wall.

Table 4 contains a sample of the material properties of the core. One type of each common plate type is shown in this table.

Table 4: Examples of Plate Material Composition (adapted from [7])

| NO | 1 | 6 | 16 | 29 | 36 | 50 | 53 | 280 |
|---|---|---|---|---|---|---|---|---|
| NAME | PUMD | NA | UOD8 | NACO | UD | FEO | FE | U93A* |
| PLATE DENSITY (g/cc) | 15.81276 | 0.873223 | 7.074849 | 1.997515 | 18.23878 | 4.658146 | 7.696071 | 17.91413 |
| CLAD DENSITY (g/cc) | 9.660204 | 7.942203 | NO CLAD | 7.778203 | NO CLAD | NO CLAD | NO CLAD | 6.900464 |
| WIDTH (IN) | 0.250 | 0.250 | 0.125 | 0.250 | 0.125 | 0.125 | 1.000 | 0.074 |
| HEIGHT(IN) | 2.000 | 2.000 | 2.000 | 2.000 | 2.000 | 2.000 | 1.000 | 2.010 |
| LENGTH(IN) | 4.000 | 4.000 | 2.000 | 7.000 | 1.000 | 3.000 | 2.000 | 6.110 |
| WIDTH (cm) | 0.635 | 0.635 | 0.318 | 0.635 | 0.318 | 0.318 | 2.540 | 0.188 |
| HEIGHT (cm) | 5.080 | 5.080 | 5.080 | 5.080 | 5.080 | 5.080 | 2.540 | 5.105 |
| LENGTH (cm) | 10.160 | 10.160 | 5.080 | 17.780 | 2.540 | 7.620 | 5.080 | 15.519 |
| CLAD THICKNESS (cm) | 0.0381 | 0.0381 | 0.0000 | 0.0381 | 0.0000 | 0.0000 | 0.0000 | DIFFERS |
| GAP (cm) | 0.09144 | 0.00000 | 0.00000 | 0.00000 | 0.00000 | 0.00000 | 0.00000 | 0.00000 |
| MASS PLATE (g) | 437.702 | 24.621 | 57.968 | 98.881 | 74.720 | 57.250 | 252.232 | 220.170 |
| MASS CLAD (g) | 44.230 | 36.364 | 0.000 | 61.080 | 0.000 | 0.000 | 0.000 | 17.957 |
| VOLUME PLATE (cc) | 27.680 | 28.196 | 8.194 | 49.502 | 4.097 | 12.290 | 32.774 | 12.290 |
| VOLUME CLAD (cc) | 4.579 | 4.579 | 0.000 | 7.853 | 0.000 | 0.000 | 0.000 | 2.602 |
| PU38 | 0.046 | ---- | ---- | ---- | | ---- | ---- | ---- |
| PU39 | 107.856 | ---- | ---- | ---- | ---- | ---- | ---- | ---- |
| PU40 | 14.380 | ---- | ---- | ---- | ---- | ---- | ---- | ---- |
| PU41 | 1.329 | ---- | ---- | ---- | ---- | ---- | ---- | ---- |
| PU42 | 0.212 | ---- | ---- | ---- | ---- | ---- | ---- | ---- |
| AM41 | 0.817 | ---- | ---- | ---- | ---- | ---- | ---- | ---- |
| U235 | 0.664 | ---- | 0.106 | ---- | 0.160 | ---- | ---- | 205.154 |
| U238 | 301.320 | ---- | 49.109 | ---- | 74.560 | ---- | ---- | 12.043 |
| U234 | ---- | ---- | ---- | ---- | ---- | ---- | ---- | 2.004 |
| U236 | ---- | ---- | ---- | ---- | ---- | ---- | ---- | 0.969 |
| MO | 11.078 | ---- | ---- | ---- | ---- | ---- | ---- | ---- |
| O | ---- | 0.001 | 8.753 | 44.750 | ---- | 16.760 | ---- | ---- |
| C | ---- | 0.001 | ---- | 11.180 | ---- | ---- | 0.432 | ---- |
| NA | ---- | 24.608 | ---- | 42.850 | ---- | ---- | ---- | ---- |
| CA | ---- | 0.010 | ---- | ---- | ---- | ---- | ---- | ---- |
| CL | ---- | 0.001 | ---- | 0.087 | ---- | ---- | ---- | ---- |
| S | ---- | ---- | ---- | 0.005 | ---- | ---- | ---- | ---- |
| H | ---- | ---- | ---- | 0.009 | ---- | ---- | ---- | ---- |
| FE | ---- | ---- | ---- | ---- | ---- | 40.490 | 251.800 | ---- |
| CR | ---- | ---- | ---- | ---- | ---- | ---- | 0.076 | ---- |
| MN | ---- | ---- | ---- | ---- | ---- | ---- | 1.805 | ---- |
| P | ---- | ---- | ---- | ---- | ---- | ---- | 0.038 | ---- |
| S | ---- | ---- | ---- | ---- | ---- | ---- | 0.064 | ---- |
| FE | 30.350 | 24.941 | ---- | 41.980 | ---- | --- | --- | 12.615 |
| CR | 8.210 | 6.686 | ---- | 11.380 | ---- | ---- | ---- | 3.312 |
| NI | 4.640 | 3.868 | ---- | 6.400 | ---- | ---- | ---- | 1.537 |
| MN | 0.740 | 0.527 | ---- | 0.870 | ---- | ---- | ---- | 0.275 |
| SI | 0.210 | 0.225 | ---- | 0.290 | ---- | ---- | ---- | 0.110 |
| CU | 0.060 | 0.044 | ---- | 0.080 | ---- | ---- | ---- | 0.015 |
| MO | ---- | 0.007 | ---- | 0.060 | ---- | ---- | ---- | 0.063 |
| AL | 0.020 | 0.018 | ---- | 0.020 | ---- | ---- | ---- | ---- |
| CO | ---- | 0.011 | ---- | ---- | ---- | ---- | ---- | 0.012 |
| C | ---- | 0.009 | ---- | ---- | ---- | ---- | ---- | 0.010 |
| P | ---- | 0.005 | ---- | ---- | ---- | ---- | ---- | 0.005 |
| S | ---- | ---- | ---- | ---- | ---- | ---- | ---- | 0.003 |
| LIP | ---- | 0.008 | ---- | ---- | ---- | ---- | ---- | ---- |
| HIP | ---- | 0.015 | ---- | ---- | ---- | ---- | ---- | ---- |

The masses in the table are grouped into two parts, one part for plate material and the other for can wall material. The material above the double bar (Pu38 through S) shows

masses for the plate material while the material below the double bar (Fe through HIP) in the bottom half of Table 4 indicates the masses of the can wall material. In the core there are roughly 120 different plates that are used in different core configurations. Many of the plates have similar material properties, but since individual plate composition was provided it was decided to model the core as closely to the specifications as possible. The numbers on these plates correspond to the numbers on the plate layout diagrams for the drawers. Each plate number can possibly be contained in many different drawers. For example, plate 92 is contained in drawer 101 but it is also contained in many other drawers such as drawers 111 and 114. It is likely that each plate was produced in a batch with an identification number corresponding to its batch. Because of this, the density and exact material composition of plates of the same type but different material identification number can vary significantly. The plate properties shown in gray were added to the material information provided in the benchmark document. [1] The can wall density and plate density shown in these tables were used directly in the MCNP cell card as the density of the cells. Sample calculations for these variables for plate 1 are shown below:

$$Plate\ Density = \frac{plate\ mass}{plate\ volume} = \frac{plate\ mass}{(length)(width)(heigth)}$$

$$= \frac{437.702\ g}{(10.160 - 2 \times 0.0381)(0.635 - 2 \times 0.0381)(5.080 - 2 \times 0.0381 - 0.09144)cm^3}$$

$$= \frac{437.702\ g}{27.68\ cm^3} = 15.81\ g/cm^3$$

$$Clad\ Density = \frac{clad\ mass}{clad\ volume} = \frac{clad\ mass}{total\ volume - non\ clad\ volume}$$

$$= \frac{44.230\ g}{((0.635 \times 5.080 \times 10.160) - (0.635 - 0.076)(5.080 - 0.076)(10.16 - 0.076))cm^3}$$

$$= \frac{44.230\ g}{4.579\ cm^3} = 9.660\ g/cm^3$$

For the sake of brevity, there are a few types of plates and materials not shown in this table, such as void cans which contained measuring equipment or detectors and matrix tubes and drawer materials which were similar to the can material. These materials do not contain any new elements or isotopes.

### 3.8 MCNP Model and Assumptions

The ZPPR-19B facility was modeled as closely as possible to the "as built data" presented within the Benchmark Document. [1] In totality, the resulting MCNP input file is approximately 30,000 lines long. All cells in the facility were modeled with planes since the geometry was exclusively rectilinear. Each drawer was built individually, in its own universe, with MCNP. The lattice card was used to construct the full facility out of these universes.

Significant effort was utilized to preserve any of the nomenclature presented in the benchmark document. The universes for each drawer were named according to their drawer number, thus drawer 101 was built in universe 101. The same standard was applied to all drawers. The materials were also modeled according to their material number within the benchmark. The exception was the can wall. Since the can wall material composition was presented under the same material number as the plate within the can, this was not possible. The simple solution was to add 500 to the material number to describe the can's material composition. For example, material 1 had a plate number of 001 while the can material would be 501. Since there were no material numbers above 500 within the benchmark document, there would be no overlap. These nomenclatures lead to much improved readability and verification that the model was constructed correctly.

It was also helpful to use intelligently "named" surfaces to build the model. Each surface in MCNP has a number used to identify it. However, there is no requirement that the first surface start at 00001 and the next one be labeled 00002. Thus, the numbers were divided into three parts to identify the location and orientation of a surface without having to refer back to the surface card every time. For example surface "11601" contains the three parts, 1, 16 and 01. The first digit "1" means that it is a plane orthogonal to the x direction. (2 indicates y plane and 3 indicates z) The second 2 digits, "16" indicate that the plane resides close to 16/16ths of an inch (or one inch) form the origin. The outer dimensions of most plates in the drawer were multiples of 1/16 inch so this nomenclature can be used to describe any outer width of the plate. The y direction was also divided into 1/16 inch segments while the z direction was divided into segments of one-half of an inch. The last two identifying digits are reserved for can wall or other gaps. The digits 01 indicate it is the surface for a can wall just after 16/16ths of an inch. If these last two digits were 10

it would indicate the surface for the can wall right before one inch while 00 would be exactly one inch. By looking at the surface number one can tell exactly where and how a plane is oriented.

A description of the assumptions used to model the facility is presented here. Due to the vast complexity of the facility, not every nuance was described completely within the benchmark document. [7] Therefore any assumptions made, no matter how strong they were, are presented to show exactly how the facility was modeled based upon the availability of information.

1. The shim rods used to control the reactivity during the core assembly were assumed to be completely withdrawn during any experimentation. There was no information present in the benchmarking documentation concerning their composition or geometry. In addition the plate stretch and analytical model portion gave not mention of modeling these features. [7]

2. Any air within the system was modeled as oxygen, nitrogen, carbon dioxide and argon. In reality, air has other elements that but they are all much less than 1% so they will not have an observable effect on reactivity, especially considering that air has a density that is many orders of magnitude less than the density of the rest of the materials within the core.

3. The gap in the top of the plutonium elements was assumed to be void. Little information was given concerning this gap and the fill gas is completely unknown. Rather than assuming it to be air it was assumed to be void.

4. There was a significant amount of machining on the matrix tubes and drawers such as slits and holes. The data for the material properties of these components was given in mass per unit length. These reported values included this machining since the first inch of the matrix tubes that had significantly more machining had different material properties reported. Thus, it was reasonable to simply redistribute the mass evenly throughout that cell to account for the holes.

5. Each drawer had a retainer spring in the back which was used to push the plates forward to the front of the drawer. This spring was small and light so it was not modeled. The ZPPR-19B report confirmed that these springs have negligible effect on reactivity.

6. The guide tubes, which were similar in composition to the matrix tubes and drawers, were assumed to be blocks. They likely had a hollow center but the thickness of

the tubes was not provided. They were assumed to be solid blocks with the mass of the guide tubes equally distributed throughout. This led to significantly reduced density of the metal since in actuality most of the material likely resides in the outside. The important factor was that mass was conserved. Since the ZPPR-19B models a fast reactor where neutrons have a longer mean free path, this should not have a significant effect on the results.

7. Insufficient information was present regarding the exact position of the narrow drawers within the matrix tube. It was decided that the narrow drawer should have the same gap size between it and the wall of the matrix tube as a normal drawer. In addition, this resulted in an equal gap between the narrow drawer and the matrix tube and the gap between the guide tube and the matrix tube. The exact location of these gaps should not affect criticality strongly since all the correct amount of material is present and these gaps are small.

8. The front of the narrow drawers was reduced from 0.035'' to 0.03'' to make them the same thickness as the normal drawers. The density of the front of these drawers was increased to conserve mass.

9. Nominal dimensions are assumed. Edges and corners of plates tend to be round and not pointed but there was no way of knowing how rounded they were and boxes are much easier to model than rounded edges. Thus they were modeled as boxes with the nominal dimensions given. Individual plates may not have these exact dimensions but the model was built so that mass of all material was conserved. This method leads to an interesting variety in the density calculations that can vary as much as 5-10%. In reality it is unlikely that all the can wall is exactly the same thickness so this uncertainty likely had a lot to do with the variety of densities present.

10. Since all width dimensions of plates tended to be in inches it was assumed that by 0.063, 0.0625 (1/16 of an inch) was implied. Only three decimal places were given so this is likely the result of rounding. If these plates were 0.063 they would not be able to fit in the space within the drawers. In addition densities were calculated so that material mass was conserved so this should not have a significant impact on reactivity. In addition, plates 51 and 52 were stretched from a width of .109 inches to .125 inches because the thickness of these plates would cause a small gap in the drawer. There was no information on which

side this of the plates this gap would occur so the plates were stretched and mass was conserved.

11. As with the modeling present in the benchmark document light impurities and heavy impurities were modeled as carbon and copper respectably. There was no other information given regarding these materials so it seemed to be a reasonable assumption.

12. The enriched uranium fuel, located in the outer core, was not described within the ZPPR-19B document but was described in the ZPPR-20C document [27] which used this fuel more extensively. In this document, the enriched uranium clad thickness in the axial direction was taken to be 0.0115'', not 0.015''. Both these values were reported in the literature but the 0.0115'' matches the rest of the description well. 0.015'' makes the total length of the plate too long. This other reported value is believed to be a simple typographic error in the document.

13. Not all the materials located within the 19B were presented within the material tables in the 19B document. They were however located in the ZPPR-18C document which had most of the same materials with exactly the same mass values. These masses were used when the ZPPR-19B document did not provide the values needed to model the core. The material information used from the ZPPR-18C [26] document were material numbers 19, 45, 265, 350, 352, and 387.

14. Nothing outside of the matrix tubes and the air gap between the two cores was modeled. Thus neither the building nor concrete floor were modeled. This will likely lead to a slight underestimate in $k_{eff}$ since it is possible but certainly not likely for a neutron to escape the matrix tubes, and reenter after scattering interactions outside of the matrix tubes. It is highly unlikely that the neutron would make it all the way back to the fissile material since there is a large amount of stainless steel in the reflector and depleted uranium in the uranium blanket, both strong thermal neutron absorbers.

15. It is assumed that the matrix tubes surrounding the radial reflector are completely empty. Therefore, they are modeled simply with air. No information was provided describing these tubes, thus a reasonable assumption for how this should be modeled.

16. The upper axial reflector, which is a plate of steel shielding located behind the drawers, was not well described in the facility description section of the benchmark. The

composition of this portion of the facility was described in the plate stretch portion of the benchmark and this composition was used to model this part of the facility. [7]

17. Some of the isotopes present within the facility did not have explicit cross sectional data available in MCNP. Notably, oxygen-18 which is naturally occurring was not present in any of the nuclear data libraries. Thus, it was assumed that oxygen 18 acted similar to oxygen 16, the most common isotope of oxygen and was modeled as such.

18. Plutonium-241, was assumed to be the only isotope short-lived enough to model its decay between the time when the material composition of the fuel was measured and its use in the facility. It has a half-life of 14.29 years and beta decays to Americum-241. Americium-241 was considered to be stable since its half-life is 432 years. The only other isotope within the facility with a “short” half-life was Pu-238. It has a half-life of 87.7 years and decays to U-234. Since U-234 was not tracked in the Pu-U-Mo material data,[7] while americium was, it appears reasonable to assume that its decay is not significant or important.

19. Because the total width of all plates along the width of the drawer were recorded as 2 inches and the inner width of the drawer was also recorded as 2 inches, there were no room for the modeling of the foil holders and foils. [7] Thus the foil holder was not model at all while the foils simply displaced the material on the left and right of the foils, typically clad, iron oxide or depleted uranium. The total volume of all displaced material over the full core for three transverses was approximately 3 cubic cm. Reaction rates of the four different reaction types were calculated using FM tallies at the location of these foils. Figure 21 shows how these foils were modeled in MCNP. Foil compositions were taken from Table 3.7.2. [7]

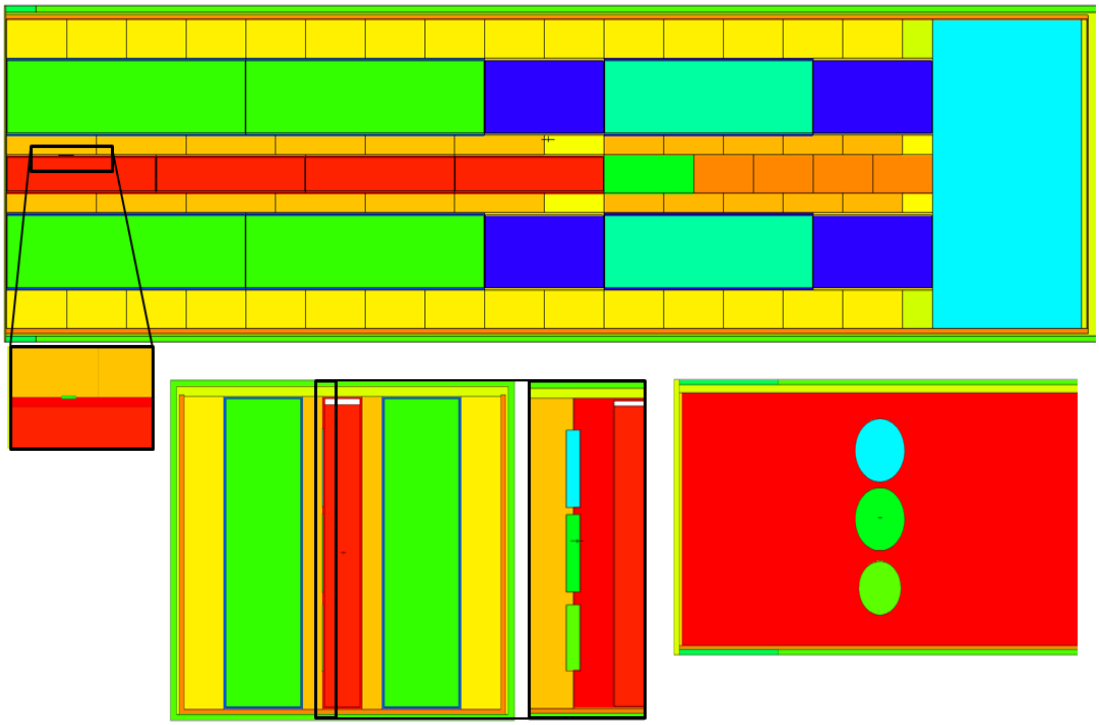

Figure 21: Foil Modeling Material Displacement in MCNP

# 4 RESULTS AND DISCUSSION

## 4.1 Drawer Criticality Calculations

This section focuses on the efforts to confirm that the model of the ZPPR-19B facility was built correctly. After the model was constructed in MCNP, each of the drawers was isolated individually and analyzed. The purpose of this analysis was to compare drawers that were similar to inspect whether their $k_{eff}$ values were similar. For example, the DUF series of drawers, drawers 101-109, were all run through a drawer multiplication factor calculation individually and then compared against each other. Two of the same drawers were put together facing each other with a small gap between to simulate the gap between the two core halves. Figures 22 and 23 show the configuration of the drawers used in the drawer multiplication factor calculation. The color of the cells in these figures corresponds to the material contained in the cells.

Two cases were run for each individual drawer. One case was simply the two bare drawers facing each other surrounded by void. This case had a large amount of leakage.

The second case had four reflector planes placed around the four sides of the drawer shown in Figure 22. This was done to simulate an infinitely tall and wide core composed entirely of one type of drawers. No reflectors were placed on the left and right side of Figure 23 since this is the axial direction.

The reason for modeling the bare case was that this case may show if the model of any particular drawer had significantly more leakage then other drawers which would be indicated by a decreased multiplication factor. The four reflectors were used to significantly decrease leakage and give insight into any excess absorption that may be occurring within a specific drawer.

It should be noted that after these drawer criticality calculations were completed, it was discovered that the wrong gap thickness was used. The gap thickness between two halves of the core in these models is larger than the actual gap thickness. This error will be present in all results but will affect each set of results similarly. Because the purpose of this analysis was to compare the drawers of similar type rather than to compare results to the experimental facility, these results are still useful. The gap error will affect the bare arrangement much more than the reflected arrangement since the excess neutron stream escaping through the gap will be reflected in the reflected arrangement.

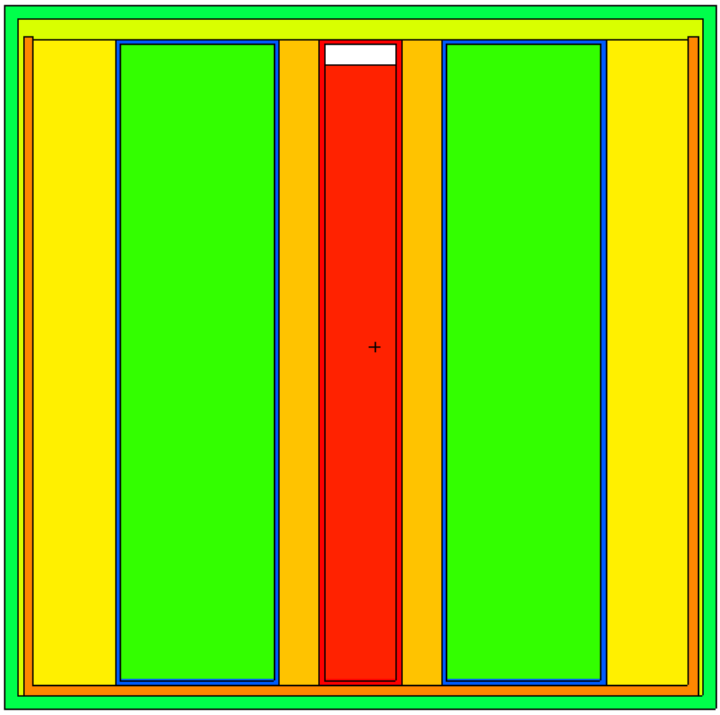

Figure 22: Cross Sectional View of Drawer 101 in K-Code

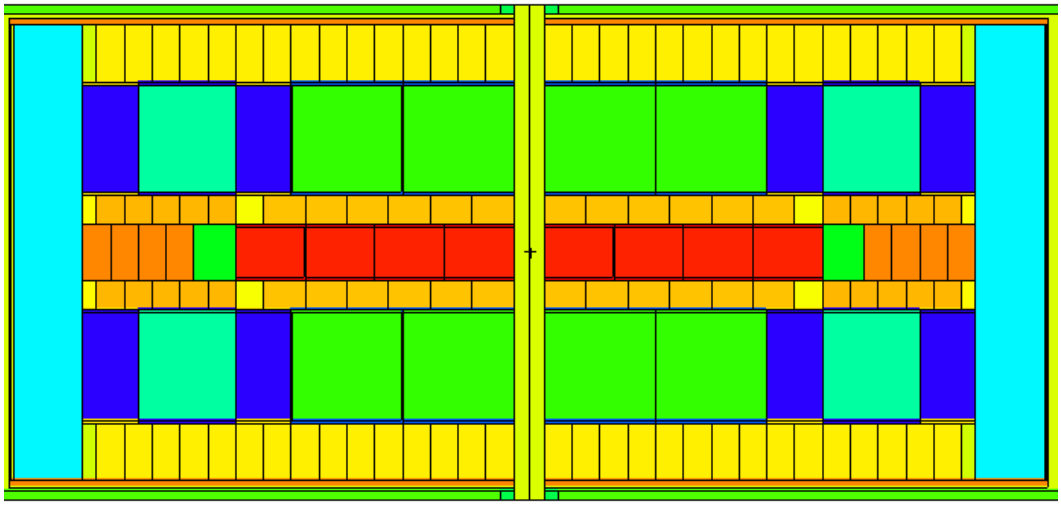

Figure 23: Top down View of Drawer 101 in K-code

Table 5 and 6 show $k_{eff}$ for both a bare and reflected configuration of the DUF drawers, drawers 101 through 109, highlighting that the $k_{eff}$ for all drawers is within 1% of the average. In addition, the standard deviation of this value is small compared to the maximum and minimum values for this percent deviation. This gives reasonable evidence that the drawers are constructed correctly, at least with respect to each other. However, it

is conceivable that there still could possibly be errors present in all drawers of this type that affect them all similarly. Later, a simplified full core model was built to investigate this possibility. In addition, the deviation from the average can be fairly well accounted for by looking at the fuel within the drawer. The Pu Mass column is the sum of all plutonium mass within each drawer. Table 5 also shows that Drawer 101 contains the smallest mass of plutonium and, as expected, it has the lowest values for $k_{eff}$.

Table 5: DUF Bare Drawer Results

| Drawer | $k_{eff}$ | stdv | % deviation from average | stdv of % dev | Pu Mass (g) |
|---|---|---|---|---|---|
| 101 | 0.08387 | 0.00003 | -0.841 | 0.03724 | 622.140 |
| 102 | 0.08480 | 0.00003 | 0.259 | 0.03728 | 631.408 |
| 103 | 0.08489 | 0.00003 | 0.365 | 0.03728 | 632.337 |
| 104 | 0.08527 | 0.00003 | 0.814 | 0.03730 | 633.081 |
| 105 | 0.08458 | 0.00002 | -0.001 | 0.02627 | 626.098 |
| 106 | 0.08415 | 0.00003 | -0.510 | 0.03725 | 626.040 |
| 107 | 0.08451 | 0.00003 | -0.084 | 0.03727 | 627.658 |
| 108 | 0.08449 | 0.00003 | -0.108 | 0.03727 | 627.658 |
| 109 | 0.08467 | 0.00003 | 0.105 | 0.03728 | 628.708 |
| average | 0.08458 | 0.00001 | | | |

Table 6: DUF Reflected Drawer Results

| Drawer | $k_{eff}$ | stdv | % deviation from average | stdv of % dev | Pu Mass (g) |
|---|---|---|---|---|---|
| 101 | 1.07470 | 0.00044 | -0.529 | 0.0431 | 622.140 |
| 102 | 1.08343 | 0.00048 | 0.279 | 0.0467 | 631.408 |
| 103 | 1.08327 | 0.00047 | 0.265 | 0.0458 | 632.337 |
| 104 | 1.08550 | 0.00048 | 0.471 | 0.0467 | 633.081 |
| 105 | 1.08032 | 0.00032 | -0.009 | 0.0329 | 626.098 |
| 106 | 1.07928 | 0.00051 | -0.105 | 0.0493 | 626.040 |
| 107 | 1.07819 | 0.00048 | -0.206 | 0.0467 | 627.658 |
| 108 | 1.07944 | 0.00049 | -0.090 | 0.0476 | 627.658 |
| 109 | 1.07958 | 0.00048 | -0.077 | 0.0467 | 628.708 |
| average | 1.08041 | 0.00015 | | | |

Figures 24 and 25 show the relationship between the mass of plutonium and $k_{eff}$. The error bars present in these figures represent one standard deviation. There are no error bars on plutonium mass because no uncertainties were given for any mass values. The trend shows that, as expected, a larger plutonium as results in a larger $k_{eff}$. The high degree of linearity indicates that the plutonium mass within the drawer can be used to account for most of the differences in $k_{eff}$ between the drawers. The deviations from this trend can be attributed to different composition of plates within the drawer. Even if the total mass of plutonium is similar in two drawers, this does not guarantee that the drawers contained the exact same plutonium plates. Therefore the isotopic ratio of the four types of plutonium included in plutonium plates may be different which will also affect $k_{eff}$.

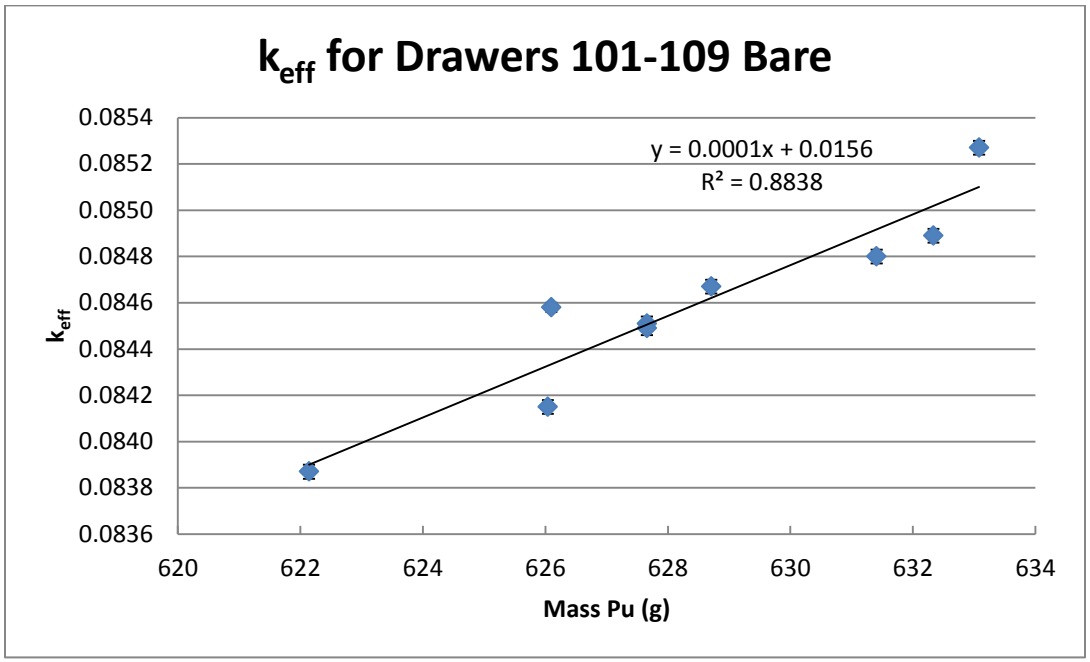


Figure 24: $k_{eff}$ vs. Plutonium Mass for Bare DUF

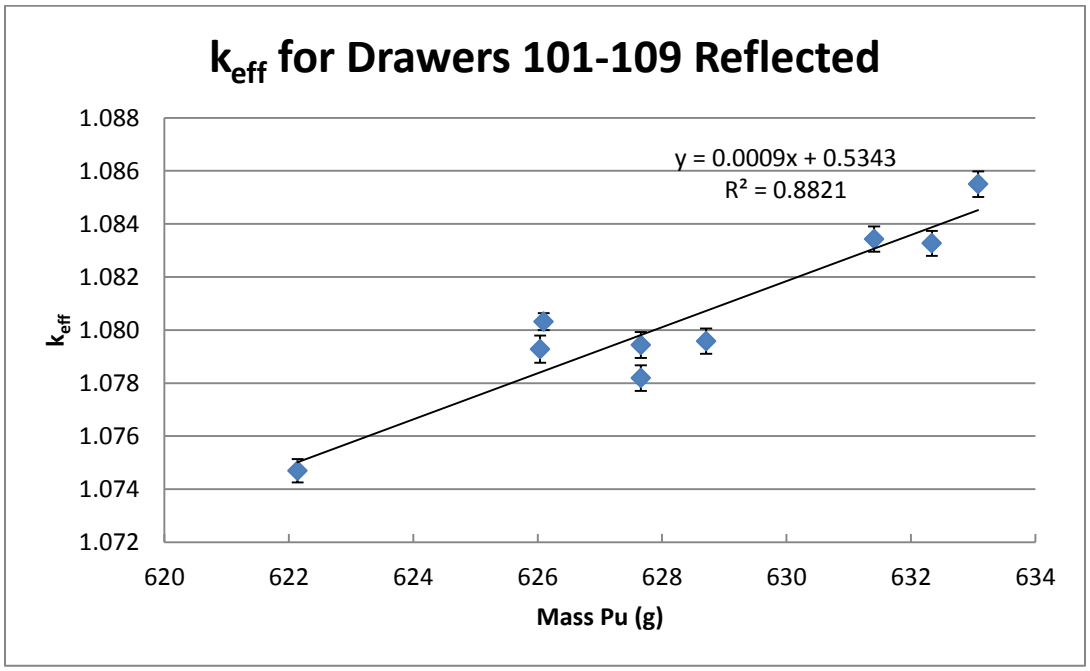


Figure 25: $k_{eff}$ vs. Plutonium Mass for Reflected DUF

Tables 7 and 8 show similar data tables for DUM drawers 110-116. These tables show similar results to those of the DUF drawers with all drawers remaining within 1 % deviation of the average. In addition, the average multiplication factor for the DUM drawers

is larger than the DUF Drawers multiplication factor for the bare case but smaller for the reflected case.

Table 7: DUM Bare Drawer Results

| Drawer | $k_{eff}$ | stdv | % deviation from average | stdv of % dev | Pu Mass (g) |
|---|---|---|---|---|---|
| 110 | 0.10065 | 0.00004 | 0.265 | 0.0427 | 621.733 |
| 111 | 0.10044 | 0.00004 | 0.056 | 0.0426 | 622.140 |
| 112 | 0.09951 | 0.00004 | -0.871 | 0.0426 | 614.535 |
| 113 | 0.10110 | 0.00003 | 0.713 | 0.0336 | 628.708 |
| 114 | 0.10029 | 0.00005 | -0.094 | 0.0521 | 622.140 |
| 115 | 0.10030 | 0.00004 | -0.084 | 0.0426 | 622.140 |
| 116 | 0.10040 | 0.00004 | 0.016 | 0.0426 | 622.140 |
| average | 0.10038 | 0.00002 | | | |

Table 8: DUM Reflected Drawer Results

| drawer | $k_{eff}$ | stdv | % deviation from average | stdv of % dev | Pu Mass(g) |
|---|---|---|---|---|---|
| 110 | 0.97142 | 0.00045 | 0.124 | 0.0493 | 621.733 |
| 111 | 0.97044 | 0.00042 | 0.023 | 0.0464 | 622.140 |
| 112 | 0.96455 | 0.00043 | -0.584 | 0.0474 | 614.535 |
| 113 | 0.97530 | 0.00041 | 0.524 | 0.0455 | 628.708 |
| 114 | 0.97000 | 0.00047 | -0.022 | 0.0513 | 622.140 |
| 115 | 0.97035 | 0.00043 | 0.014 | 0.0474 | 622.140 |
| 116 | 0.96943 | 0.00041 | -0.081 | 0.0455 | 622.140 |
| | 0.97020 | 0.00016 | | | |

Figures 26 and 27 show the relationship between plutonium mass and $k_{eff}$ for the DUM series. The deviations from linear behavior are likely caused again by the composition of the specific plates which make up the drawer. This is especially evident for the drawers with about 622 g of plutonium since they are all similar in mass of plutonium but can deviate significantly from each other in non-fuel plate composition, such as sodium plates.

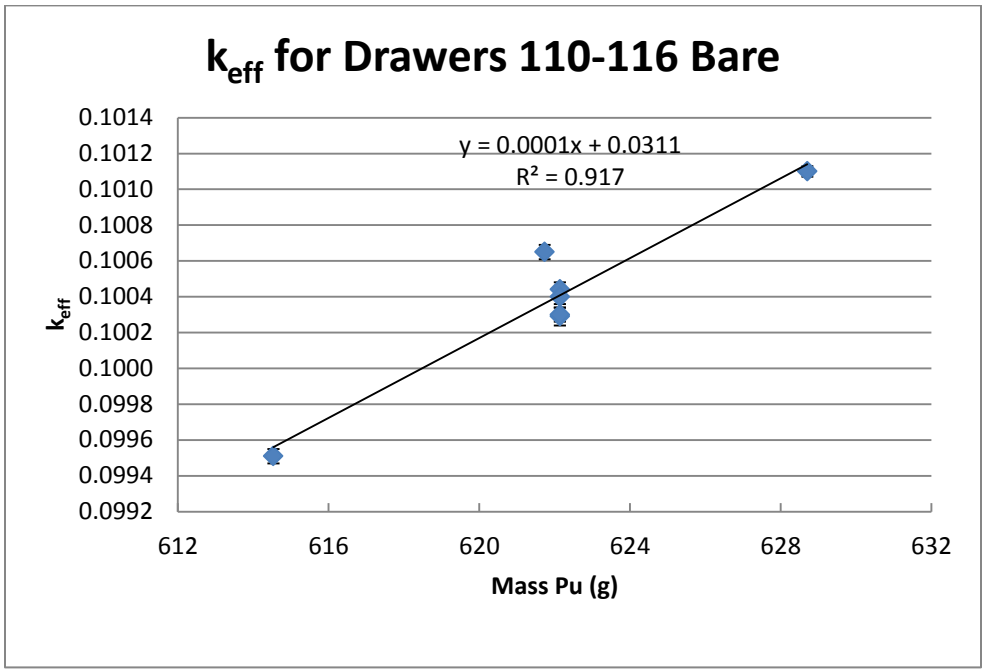


Figure 26: $k_{eff}$ vs. Plutonium Mass for Bare DUM

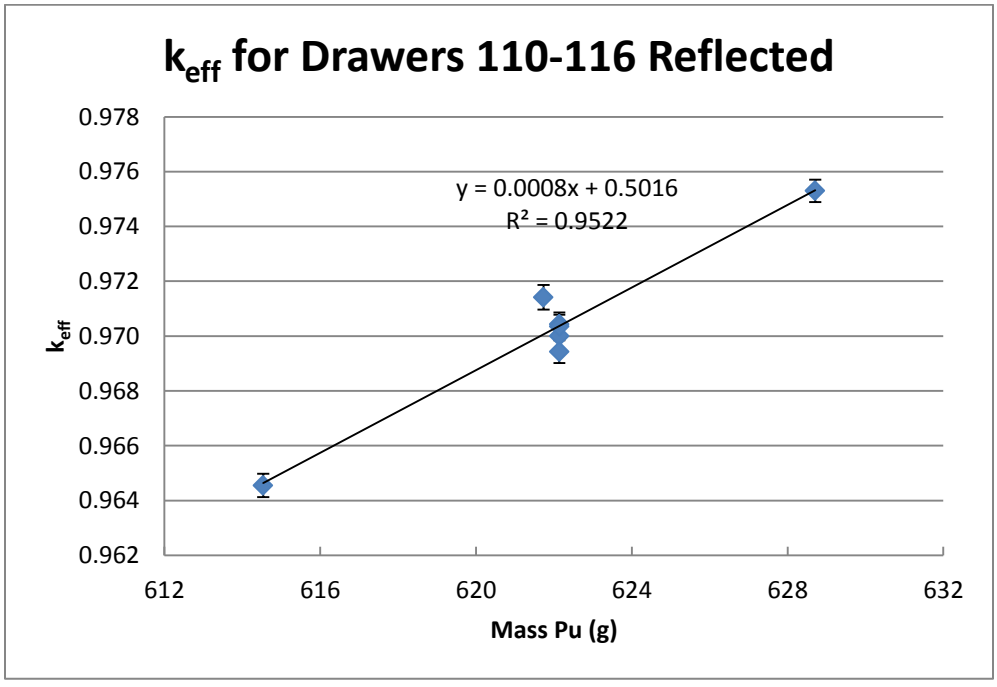


Figure 27: $k_{eff}$ vs. Plutonium Mass for Reflected DUM

As previously noted, the difference between the DUM and DUF drawers is that the fuel in DUF drawers is surrounded by $Fe_2O_3$ while it is surrounded by depleted uranium metal in DUM drawers. The likely explanation for the significant difference in multiplication

factor between the DUF and DUM drawers is this material surrounding the fuel. In the bare case, the additional depleted uranium in the DUM drawer causes some fission to occur from neutrons that would have otherwise escaped the system. This increases $k_{eff}$ for the DUM drawer bare case since there are more fissions occurring due to neutrons that would likely have been lost anyway. In the reflected case, the depleted uranium acts more like a shield to the plutonium fuel and absorbs neutrons that could have caused fission in the plutonium. This decreases $k_{eff}$ in the in the reflected DUM case since η is much smaller in depleted uranium than in plutonium.

When determining the effects of depleted uranium on the system, it is important to consider where a neutron is likely to end its life. If depleted uranium is added in a location where neutrons are likely to leak out of the system, depleted uranium will increase $k_{eff}$ as demonstrated by the bare case. However, if depleted uranium is added in a location where neutrons are likely to cause fission in plutonium or some other material with a higher η value than depleted uranium, this will decrease the multiplication factor as shown by the reflected case. This is analogous to surrounding the outside of a core with depleted uranium. Even though depleted uranium has an η value of less than one, this will increase the multiplication factor since the depleted uranium will affect only neutrons that would have escaped the system anyway. One final conclusion that can be made from these data is that the macroscopic absorption cross section for the depleted uranium plates must be higher than the macroscopic absorption cross section for $Fe_2O_3$ since if $Fe_2O_3$ absorbed more neutrons the $k_{eff}$ for the DUF series of drawers would be smaller.

Tables 9 and 10 show results for the 200 series of DCF drawers. The multiplication factor tends to be significantly higher than the 100 series of drawers since there is double the mass of fuel in these DCF drawers. Masses of plutonium are not shown since both the DCF drawers contain the exact same plutonium plates, and thus have the exact same mass.

Table 9: DCF Bare Drawer Results

| Drawer | $k_{eff}$ | stdv | % deviation from average | stdv of % dev |
|---|---|---|---|---|
| 201 | 0.10793 | 0.00002 | 0.023 | 0.0250 |
| 202 | 0.10788 | 0.00003 | -0.023 | 0.0324 |
| average | 0.10791 | 0.00002 | | |

Table 10: DCF Reflected Drawer Results

| Drawer | $k_{eff}$ | stdv | % deviation from average | stdv of % dev |
|---|---|---|---|---|
| 201 | 1.38921 | 0.00055 | 0.015 | 0.0478 |
| 202 | 1.38880 | 0.00050 | -0.015 | 0.0448 |
| average | 1.38901 | 0.00037 | | |

The uncertainty in the deviation from the average is greater than the deviation itself, showing that these drawers perform nearly identically. While the fuel plate distribution in the drawers was exactly the same, the sodium plates were slightly different. This shows that the fuel plates have a much larger impact on $k_{eff}$ than sodium plates. Looking at the magnitude of the $k_{eff}$ results, for the bare case the $k_{eff}$ is similar to that of the DUM drawers which was on average 0.10038. One would initially expect it to be significantly larger since there is much more fuel in these drawers. One explanation for these values being similar is that in the DCF drawers the fuel is no longer located in the center of the drawer but rather on the outside. Leakage is likely larger since there is less material between the fuel and the void on the outside of the drawer. For the reflected case, the system goes highly supercritical. $k_{eff}$ is much larger in this system that for any of the single fuel drawers. This is to be expected since there is twice as much fuel and leakage is not a factor since there are reflective planes on the outside of the drawer. Furthermore, even though this drawer has twice the mass of fuel as the 100 series, this does not correlate to doubling $k_{eff}$. This is largely because for any system $k_{eff}$ cannot be larger than the η of the fuel and will asymptotically approach this value no matter how much fuel is added.

The 400 and 500 and 600 series of drawers contained no fuel. Because of this, they could not be analyzed in exactly in the same way as the other drawers. Instead of two drawers facing each other it was decided to have two three-by-three arrays of drawers facing each other with a fuel drawer in the center. Figures 28 and 29 show this arrangement.

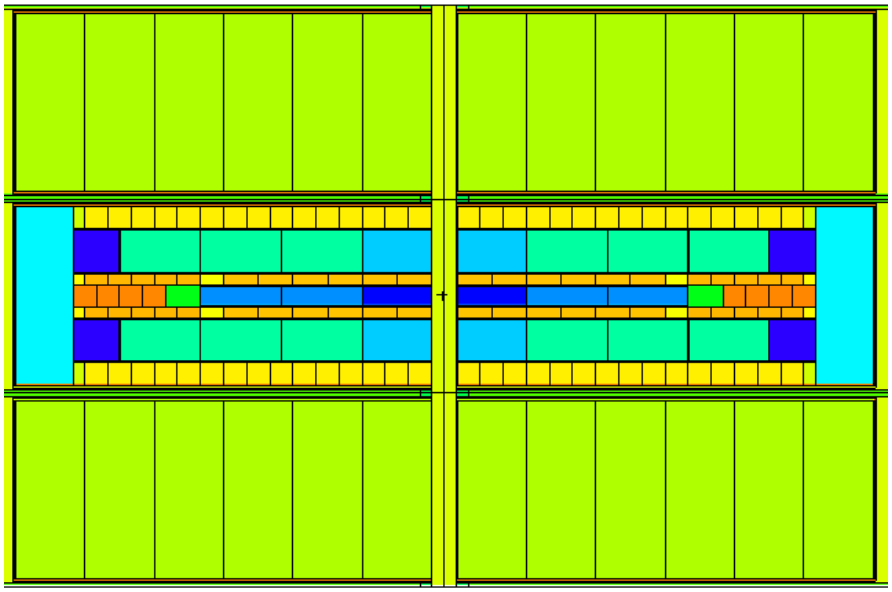

Figure 28: Top down View of Drawer 401 in K-code

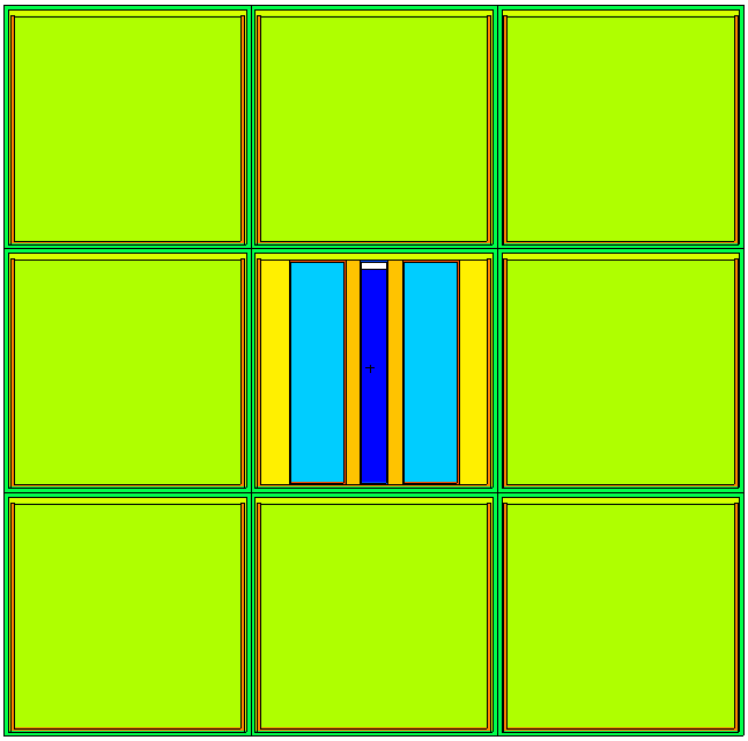

Figure 29: Cross Sectional View of Drawer 401 in K-Code

Similarly to the single drawer case, reflective planes were placed around the four sides of Figure 29 in an attempt to investigate leakage and absorption. The same drawer

was used as the center drawer in all cases so that this parameter was constant. Drawer 107 was arbitrarily chosen for this purpose.

Table 11 and Table 12 show drawer criticality calculation results for the 400 series of stainless steel reflector drawers. For the bare case all results were within 1% of the average while for the reflected plane case all results were within 3.5% of the average. The difference in the deviation of these results can be attributed to the fact that the bare case shows how effective a reflector these drawers are since neutrons are free to leak, while the reflected plane case shows the absorptive properties of the stainless steel drawers. Therefore, these results show that there is a higher deviation in the absorptive properties of these drawers than the reflective properties. In addition, there is a relationship between a drawer being a good reflector and a good absorber. All drawers which had $k_{eff}$ below average in the bare case had an above average $k_{eff}$ in the reflected case showing that drawers that are better reflectors are also have higher absorption. This can likely be attributed to higher atom density drawers being more effective reflectors and absorbers simply because there are more atoms to reflect or absorb within the drawer.

Table 11: Stainless Steel Reflector Bare Drawer Results

| Drawer | $k_{eff}$ | stdv | % deviation from average | stdv of % dev |
|---|---|---|---|---|
| 401 | 0.09421 | 0.00002 | -0.738 | 0.0221 |
| 402 | 0.09426 | 0.00003 | -0.686 | 0.0323 |
| 403 | 0.09533 | 0.00002 | 0.442 | 0.0221 |
| 404 | 0.09531 | 0.00002 | 0.420 | 0.0221 |
| 405 | 0.09555 | 0.00002 | 0.673 | 0.0221 |
| 406 | 0.09558 | 0.00002 | 0.705 | 0.0221 |
| 407 | 0.09544 | 0.00002 | 0.557 | 0.0221 |
| 408 | 0.09423 | 0.00002 | -0.717 | 0.0221 |
| 409 | 0.09543 | 0.00002 | 0.547 | 0.0221 |
| 410 | 0.09433 | 0.00002 | -0.612 | 0.0221 |
| 411 | 0.09435 | 0.00002 | -0.591 | 0.0221 |
| average | 0.09491 | 0.00001 | | |

Table 12: Stainless Steel Reflector Reflected Drawer Results

| Drawer | $k_{eff}$ | stdv | % deviation from average | stdv of % dev |
|---|---|---|---|---|
| 401 | 0.37908 | 0.00033 | 2.929 | 0.0936 |
| 402 | 0.38014 | 0.00031 | 3.217 | 0.0885 |
| 403 | 0.36446 | 0.00032 | -1.041 | 0.0907 |
| 404 | 0.36164 | 0.00033 | -1.807 | 0.0933 |
| 405 | 0.35995 | 0.00033 | -2.265 | 0.0933 |
| 406 | 0.36078 | 0.00030 | -2.040 | 0.0855 |
| 407 | 0.36268 | 0.00032 | -1.524 | 0.0907 |
| 408 | 0.38046 | 0.00034 | 3.303 | 0.0963 |
| 409 | 0.36269 | 0.00030 | -1.522 | 0.0855 |
| 410 | 0.37044 | 0.00035 | 0.583 | 0.0987 |
| 411 | 0.36891 | 0.00032 | 0.167 | 0.0908 |
| average | 0.36829 | 0.00001 | | |

Tables 13 and 14 show results for the 500 series of drawer criticality calculations for the radial blanket drawers. Drawers 501 and 502, the soft radial blanket, contain large amounts of depleted uranium with some sodium. Drawer 503, the hard radial blanket contains almost exclusively depleted uranium and thus is not included in the soft radial blanket average.

Table 13: Radial Blanket Bare Drawer Results

| Drawer | $k_{eff}$ | stdv | % deviation from average | stdv of % dev |
|---|---|---|---|---|
| 501 | 0.11896 | 0.00004 | 0.308 | 0.0398 |
| 502 | 0.11823 | 0.00003 | -0.308 | 0.0329 |
| average | 0.11860 | 0.00003 | | |
| 503 | 0.19662 | 0.00005 | n/a | n/a |

Table 14: Radial Blanket Reflected Drawer Results

| Drawer | $k_{eff}$ | stdv | % deviation from average | stdv of % dev |
|---|---|---|---|---|
| 501 | 0.35032 | 0.00032 | -0.117 | 0.111 |
| 502 | 0.35114 | 0.00031 | 0.117 | 0.109 |
| average | 0.35073 | 0.00022 | | |
| 503 | 0.37362 | 0.00037 | n/a | n/a |

The two soft radial blanket drawers produced similar results while the hard radial blanket had a higher $k_{eff}$ for both the bare and reflected cases. The reason it is larger for the bare case is that there is more depleted uranium so more neutrons that would have leaked instead cause fission, increasing $k_{eff}$. The likely reason for the hard radial blanket producing a higher $k_{eff}$ in the reflected system is that the probability of axial leakage versus fuel absorption is much more significant in this system since only one of every nine drawers contains fuel. Neutron interaction in depleted uranium is more favorable for $k_{eff}$ than neutron leakage.

Tables 15 and 16 show CRP drawer results. These drawers contain exclusively sodium and are composed of exactly the same plates. The only difference is that one has a button and one does not. There was no explanation in any of the literature as to what a button was. By how it was mentioned, it would seem that it was some sort of machining on the front of the drawer. Ultimately there was no way of knowing, so the drawers were modeled the same and produced similar results.

Table 15: CRP Bare Drawer Results

| Drawer | $k_{eff}$ | stdv | % deviation from average | stdv of % dev |
|---|---|---|---|---|
| 601 | 0.08888 | 0.00002 | -0.028 | 0.0275 |
| 602 | 0.08893 | 0.00002 | 0.028 | 0.0276 |
| average | 0.08891 | 0.000014 | | |

Table 16: CRP Reflected Drawer Results

| Drawer | $k_{eff}$ | stdv | % deviation from average | stdv of % dev |
|---|---|---|---|---|
| 601 | 0.51852 | 0.00045 | -0.011 | 0.107 |
| 602 | 0.51863 | 0.00046 | 0.011 | 0.108 |
| average | 0.51858 | 0.00032 | | |

Tables 17 and 18 show results for the 800 series of drawers. These drawers were the narrow drawers which were half an inch thinner than other drawers in the system. Reactivity control such as safety and shim rods were inserted next to these drawers when needed. Drawer 801 and 802 are similar to the DUF series with one less row of sodium plates while 803 and 804 were similar to the DUM series with one less row of sodium plates. Drawers 801 and 802 contained exactly the same plates but the gap for the shim and safety rods were on the opposite side. The same is true of drawers 803 and 804.

Table 17: Narrow Drawer Bare Results

| Drawer | $k_{eff}$ | stdv | % deviation from average | stdv of % dev |
|---|---|---|---|---|
| 801 | 0.08891 | 0.00002 | 0.022 | 0.0276 |
| 802 | 0.08887 | 0.00002 | -0.022 | 0.0276 |
| average | 0.08889 | 0.00001 | | |
| 803 | 0.10624 | 0.00003 | 0.000 | 0.0346 |
| 804 | 0.10624 | 0.00003 | 0.000 | 0.0346 |
| average | 0.10624 | 0.00002 | | |

Table 18: Narrow Drawer Reflected Results

| Drawer | $k_{eff}$ | stdv | % deviation from average | stdv of % dev |
|---|---|---|---|---|
| 801 | 1.08583 | 0.00047 | 0.018 | 0.0536 |
| 802 | 1.08545 | 0.00050 | -0.018 | 0.0559 |
| average | 1.08564 | 0.00034 | | |
| 803 | 0.99269 | 0.00044 | -0.026 | 0.0543 |
| 804 | 0.99320 | 0.00044 | 0.026 | 0.0543 |
| average | 0.99295 | 0.00031 | | |

For these drawers, the uncertainty of the deviation was larger than the deviation themselves showing that the drawer runs gave almost identical results. The results were also similar to the DUF and DUM results from the 100 series which is to be expected since they contain similar plates.

The 900 series of drawers contained USC, UAC and UDC, the three types of enriched uranium drawers in the facility. Since USC and UAC had similar plate composition and the only significant difference was a slight offset in the position of the enriched uranium fuel, they were grouped together. Tables 19 and 20 show the drawer criticality calculation results for these drawers.

Table 19: USC and UAC Bare Drawer Results

| Drawer | $k_{eff}$ | stdv | % deviation from average | stdv of % dev |
|---|---|---|---|---|
| 901 | 0.06815 | 0.00002 | -0.170 | 0.0321 |
| 902 | 0.06818 | 0.00002 | -0.126 | 0.0321 |
| 903 | 0.06811 | 0.00002 | -0.229 | 0.0321 |
| 904 | 0.06816 | 0.00002 | -0.155 | 0.0321 |
| 905 | 0.06873 | 0.00002 | 0.680 | 0.0321 |
| average | 0.06827 | 0.000009 | | |

Table 20: USC and UAC Reflected Drawer Results

| Drawer | $k_{eff}$ | stdv | % deviation from average | stdv of % dev |
|---|---|---|---|---|
| 901 | 1.01858 | 0.00045 | -0.044 | 0.0484 |
| 902 | 1.01968 | 0.00047 | 0.064 | 0.0503 |
| 903 | 1.01965 | 0.00046 | 0.061 | 0.0494 |
| 904 | 1.01951 | 0.00043 | 0.048 | 0.0467 |
| 905 | 1.01770 | 0.00046 | -0.130 | 0.0493 |
| average | 1.01902 | 0.00020 | | |

901 through 904 were the UAC drawers while 905 was the USC, containing its fuel closer to the center. These results show that for the bare drawer, having the fuel closer to the center produced larger $k_{eff}$ results. This is likely due to slightly reduced leakage because the fuel is in the center. For the reflected results this effect was not observable due to significantly reduced leakage from the reflected surfaces. The results were all less than 1% of each other and it seems as though these drawers act similar to DUF drawers' with lower $k_{eff}$ for both the reflected and the bare case. Tables 21 and 21 show UDC results:

Table 21: UDC Bare Drawer Results

| Drawer | $k_{eff}$ | stdv | % deviation from average | stdv of % dev |
|---|---|---|---|---|
| 920 | 0.07142 | 0.00002 | -0.352 | 0.0312 |
| 921 | 0.07168 | 0.00002 | 0.010 | 0.0312 |
| 922 | 0.07183 | 0.00002 | 0.220 | 0.0312 |
| 923 | 0.07176 | 0.00002 | 0.122 | 0.0312 |
| average | 0.07167 | 0.00001 | | |

Table 22: UDC Reflected Drawer Results

| Drawer | $k_{eff}$ | stdv | % deviation from average | stdv of % dev |
|---|---|---|---|---|
| 920 | 1.34916 | 0.00053 | -0.125 | 0.0439 |
| 921 | 1.35093 | 0.00054 | 0.006 | 0.0446 |
| 922 | 1.35055 | 0.00051 | -0.022 | 0.0426 |
| 923 | 1.35277 | 0.00055 | 0.142 | 0.0453 |
| average | 1.35085 | 0.00027 | | |

For the reflected case these drawers gave similar results to the DCF. This is to be expected since both these sets of drawers contained two columns of fuel. For the bare case $k_{eff}$ was only slightly larger than for the USC and UAC drawers. This is likely a result of the

fuel being located close to the edges of the drawer which maximizes leakage. These results were all within 0.4% of the average helping to confirm that they were modeled correctly.

Drawer criticality calculations were also completed for the 700 series of counter drawers. Because there were twenty five different counter drawers and they emulated many different standard drawers, there are few observation that can be made about this set as a whole. These calculations were completed only to verify the drawers were modeled correctly. The results of these calculations show that for these drawers, the criticality calculation values are all within 1% for the bare case and 4% for the reflective case. The higher deviation in the reflective case is likely the result of absorptive material being replaced with detectors which were essentially modeled as void cans which results in less absorptive material within the drawer. If the reader is interested these results are in Appendix A.

**4.2 Criticality Results**

Multiplication factor results were obtained for 2,000 cycles of 500,000 neutrons per cycle. Only 10 cycles were skipped since a neutron source file had already been developed for the core. On TerraPower's cluster this run took approximately four days. The following are the results for $k_{eff}$:

$$k_{eff,MCNP} = 0.99892 \ \pm \ 0.00001$$

The measured multiplication factor for this core arrangement was:

$$k_{eff,Facility} = 1.000804 \ \pm \ 0.000027$$

The delayed neutron fraction from the benchmark was used because another time intensive MCNP run would have to be done to calculate the delayed neutron fraction in MCNP. With delayed neutron fraction from the benchmark document being used:

$$\beta = .003866$$

Calculating the Bias:

$$Bias = \frac{k_{eff,MCNP} - k_{eff,Facility}}{\beta} = \frac{0.99892 \ - 1.000804}{.003866} = -\$.487$$

Thus the MCNP model underpredicted the multiplication factor of the ZPPR facility. It should be noted that all uncertainties present in this thesis only account for statistical

uncertainties. Other uncertainties in factors such as material composition and nuclear data are unaccounted for. Thus in reality the uncertainty is for all results is larger then what is presented.

### 4.3 Gap Worth Results

Results were also obtained for the multiplication factor as a function of the gap thickness between the two halves of the core. The spreadsheet software used to build the model read a gap thickness value and generated surfaces that the core was built from dependent on this value. Thus, it was a simple matter of changing this one cell within the spreadsheet and running the input decks for different gap values. The results obtained for this investigation have larger uncertainty since they ran significantly less neutrons to save time. Input decks for five different gap thicknesses were built. The center value was 54.5 mil and two values on either side of this were also run. It should be noted that the gap of 54.5 mil was "on scale with arbitrary zero" implying that because all the matrix tubes were not necessarily completely flush an arbitrary zero gap thickness was chosen. They are shown in Figure 30.

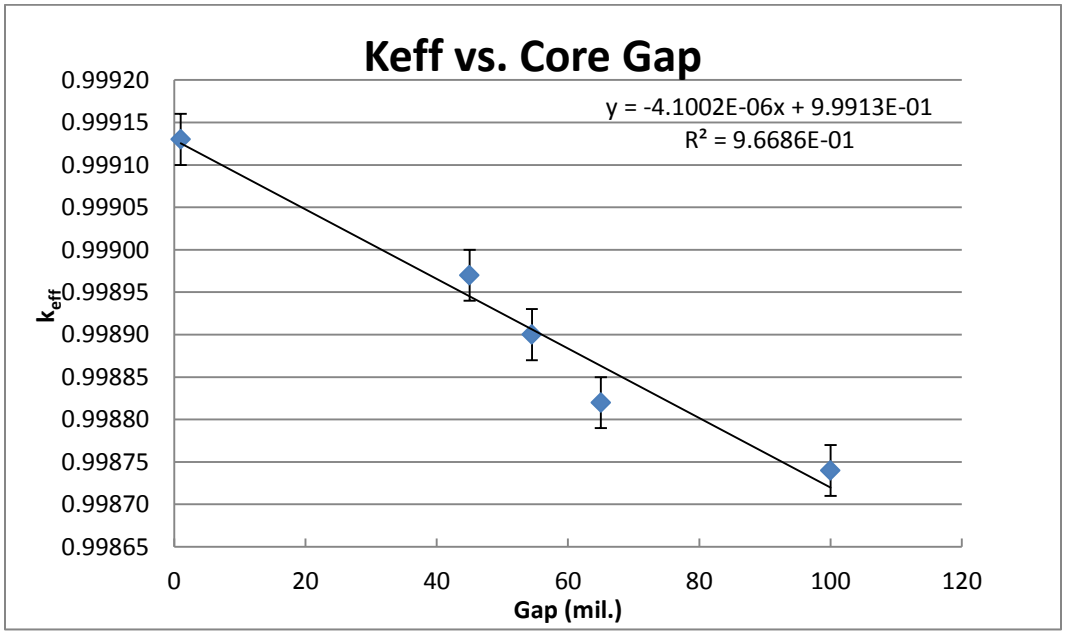


Figure 30: Multiplication Factor at Different Gap Thicknesses

As the gap between the two core halves increases the multiplication factor decreases. This is a direct result of more neutrons streaming out of the reactor as the gap increase. The ZPPR facility measured the gap worth to be:

$$Gap\ Worth = -0.090 \pm .010\ ¢/mil$$

Converting the MCNP obtained gap worth:

$$\frac{(-4.1002)(10^{-6}/mil)}{0.003866} = .106\ ¢/mil$$

This result does not agree exactly but is within two standard deviations of the results obtained at the ZPPR facility. One possible reason for disagreement is that the exact gap present at the facility was not well described. The measurements for gap thickness are referred to as "on scale with an arbitrary zero." [7] This likely is the result of the matrix tubes not being completely flush with each other at all locations, therefore it is hard to select a specific reference thickness since this value will change dependent on which matrix tubes it is measured between and no one reference thickness has any advantage over another. It is also unclear exactly what range of gap thicknesses the facilities' worth measurement was obtained for. Their range of thicknesses could be smaller or larger than is shown in Figure 30. It should also be stressed that this experimental measurement is not listed as an acceptable benchmark, implying that the uncertainty may be high and the results may be problematic to match with a computational model. However, the fact that the MCNP model provides similar results increases confidence in the model.

### 4.4 Comparison to ZPPR-9 Neutron Absorption

The underprediction of the multiplication factor could be the result of the possibility that there was some sort of excess absorption within the core. The most absorptive isotopes within the core were investigated and compared to a similar core, the ZPPR-9 for which an MCNP input was already available. This core was smaller but contained many of the same plates that were in the ZPPR-19B. One of the most significant differences between the ZPPR-9 and the ZPPR-19B was that the ZPPR-9 did not contain any enriched uranium which was present in the outer core of the ZPPR-19B. Table 23 shows the ten most absorptive isotopes for the ZPPR-9. Table 24 shows the ten most absorptive isotopes for the ZPPR-19B along with the deviation of rank from the ZPPR-9. The weight values shown for capture indicate the probability of the neutron ending its life by being captured by the material indicated while the values shown for fission indicate the probability that the neutron will end its life by causing fission in that material. Thus these weight values are dependent on the amount of material in the reactor since more material will give a higher probability of interaction. In

addition the location of the material within the reactor is also important since the flux and flux spectrum are location dependent and these variables can influence neutron interactions.

The ten most absorptive isotopes for both cores are the same but in a slightly different order. U-238 is by far the biggest neutron sink within both cores. In the ZPPR-19B, U-235 is ranked much higher since there is much more of it within the core. This displaces the ranking of many of the other isotopes down by one. The most absorptive nonactinides are Iron-56, Magnesium-55, Nickel-58, Cromium-52, Iron-54 and Sodium-23. Taking into consideration the large amount of U-235 in the core displacing the other isotopes to lower on the list, Magnesium-55 appears slightly higher on the list while Nickel-58 appears slightly lower than what would be expected comparing to the ZPPR-9 results. The weights lost to capture of these two isotopes is fairly similar in the ZPPR-19B core but it would be difficult to ascertain exactly why these values deviate since these cores have significant differences in material amount and distribution. This investigation showed that the ZPPR-19B is providing reasonable results in terms of neutron absorption.

Table 23: Ten Most Absorptive Isotopes in ZPPR-9

| Absorptive Rank | Material Isotope | Weight Lost to Capture | Weight Gained by Fission |
|---|---|---|---|
| 1 | U-238 | 4.74E-01 | 5.62E-02 |
| 2 | Pu-239 | 7.48E-02 | 2.66E-01 |
| 3 | Fe-56 | 2.28E-02 | 0.00E+00 |
| 4 | Pu-240 | 1.05E-02 | 7.67E-03 |
| 5 | Ni-58 | 6.36E-03 | 0.00E+00 |
| 6 | Mn-55 | 5.22E-03 | 0.00E+00 |
| 7 | Cr-52 | 4.07E-03 | 0.00E+00 |
| 8 | Fe-54 | 3.84E-03 | 0.00E+00 |
| 9 | Na-23 | 3.03E-03 | 0.00E+00 |
| 10 | U-235 | 2.78E-03 | 8.27E-03 |

Table 24: Ten Most Absorptive Isotopes in ZPPR-19B

| Absorptive Rank | Material Isotope | Weight Lost to Capture | Weight Gained by Fission | Rank in ZPPR-9 | Deviation from ZPPR-9 Rank |
|---|---|---|---|---|---|
| 1 | U-238 | 4.54E-01 | 5.39E-02 | 1 | 0 |
| 2 | Pu-239 | 6.06E-02 | 2.17E-01 | 2 | 0 |
| 3 | Fe-56 | 3.31E-02 | 0.00E+00 | 3 | 0 |
| 4 | U-235 | 2.19E-02 | 7.48E-02 | 10 | 6 |
| 5 | Pu-240 | 8.55E-03 | 6.07E-03 | 4 | -1 |
| 6 | Mn-55 | 6.96E-03 | 0.00E+00 | 6 | 0 |
| 7 | Ni-58 | 6.70E-03 | 0.00E+00 | 5 | -2 |
| 8 | Cr-52 | 4.84E-03 | 0.00E+00 | 7 | -1 |
| 9 | Fe-54 | 4.81E-03 | 0.00E+00 | 8 | -1 |
| 10 | Na-23 | 3.49E-03 | 0.00E+00 | 9 | -1 |

**4.5 Plate Stretch Simplified Model Results**

While the -$ .487 bias was not unusually large, further work was needed to verify that this result was reasonable. The ZPPR-19B benchmark document contained simplifications that were used to decrease the massive complexity of the core. The first simplification was the plate stretch assumption was applied. This meant that the plates were stretched from the bottom to the top of the lattice and any front/back/top/bottom can wall or drawer material was redistributed to the can wall to the left and right between the plates. In addition all basic drawer types, such as DUM and DUF, were reduced to one drawer. For example, DUF drawers 101 through 109 were reduced to a single DUF drawer which was used in place of these. Figure 31 shows an example of this plate stretch assumption.

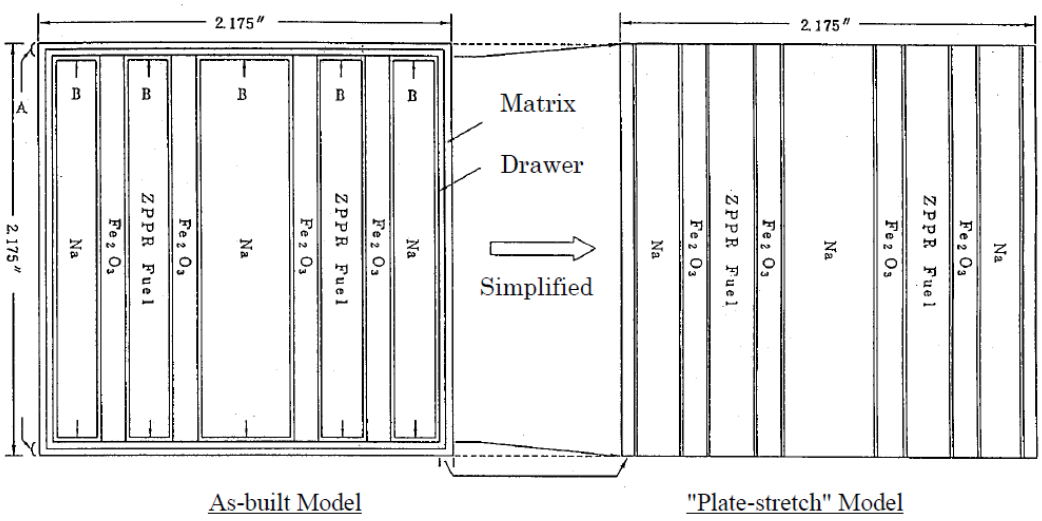


Figure 31: Plate Stretch Assumption

All counter drawers were replaced with simple drawers which had similar composition. In addition the core was reduced to a 1/8$^{th}$ core with three reflectors to take advantage of symmetry. ANL notes that these assumptions should lead to deviations in $k_{eff}$ by 0.2% at most. [7]

The advantage of this model is that through significant complexity reduction, the length of the input deck was reduced from approximately 30,000 lines to about 1,300 lines. In addition, the material properties for these assumptions were presented in a simplified manner using different material tables that were presented in terms of number density rather than mass. Thus, this model was able to be built completely independently of the complex model. Because of this, it is highly unlikely that if there were an error in the building and analysis of the complex model that it would propagate to this model. In addition, because it is a 1/8$^{th}$ core the problem converges much faster. One disadvantage of this model is that many foils placed within the core are placed below the horizontal symmetry, therefore reaction rates have not been calculated for this model. The multiplication factor for this model was:

$$k_{eff} = 0.99935 \pm 0.00011$$

Comparing to the as built model:

$$\%\, difference = \frac{.99935 - 0.99892}{0.99892} = 0.04\%$$

This is well within the 0.2% max deviation recommended by ANL.

Calculating the Bias:

$$Bias = \frac{0.99935 \ - 1.000804}{0.003866} = -\$.376$$

The question of why this model yields a slightly higher multiplication factor is complex and would require significant investigation into the previously noted assumptions. One simple observation that can account for part of this increase is that the plate stretch model displaces the material in the front of the drawer and replaces it with plate material, some of which is fissile. The front of the drawer is 30 mils thick so this assumption would be similar to decreasing the core gap by 60 mils. Calculating the increased in multiplication factor using the gap worth:

$$(0.00106 \frac{\$}{mil})(\ 60mil)(0.003866) = 0.0002458$$

Which is certainly significant since the difference in $k_{eff}$ between the as built and simplified core is 0.00043

**4.6 Reaction Rate Ratio Results**

Reaction rate ratios were measured along three transverses of the core, an axial transverse of the center drawer, a horizontal radial transverse and a radial transverse at 15°. For axial measurements the depth was measured relative to the front face of the core. Thus, smaller depths are closer to the center and deeper depths are further away from the center of the core. Radial transverse locations are referred to in sequences of numbered locations with location number one corresponding to the location closest to the center of the core and higher numbers corresponding to locations further away from the center of the core. Figures 32, 33 and 34 show the axial transverse results for the ZPPR-19B benchmark document as well as the MCNP model.

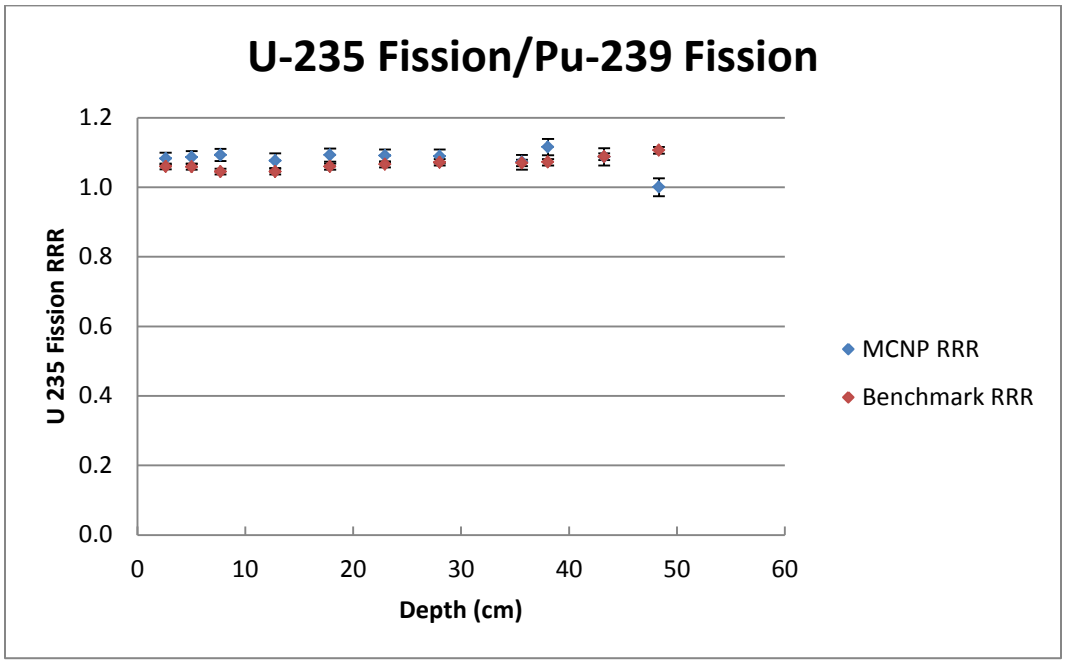


Figure 32: U-235 Fission to Pu-239 Fission Reaction Rate Ratio for Axial Transverse

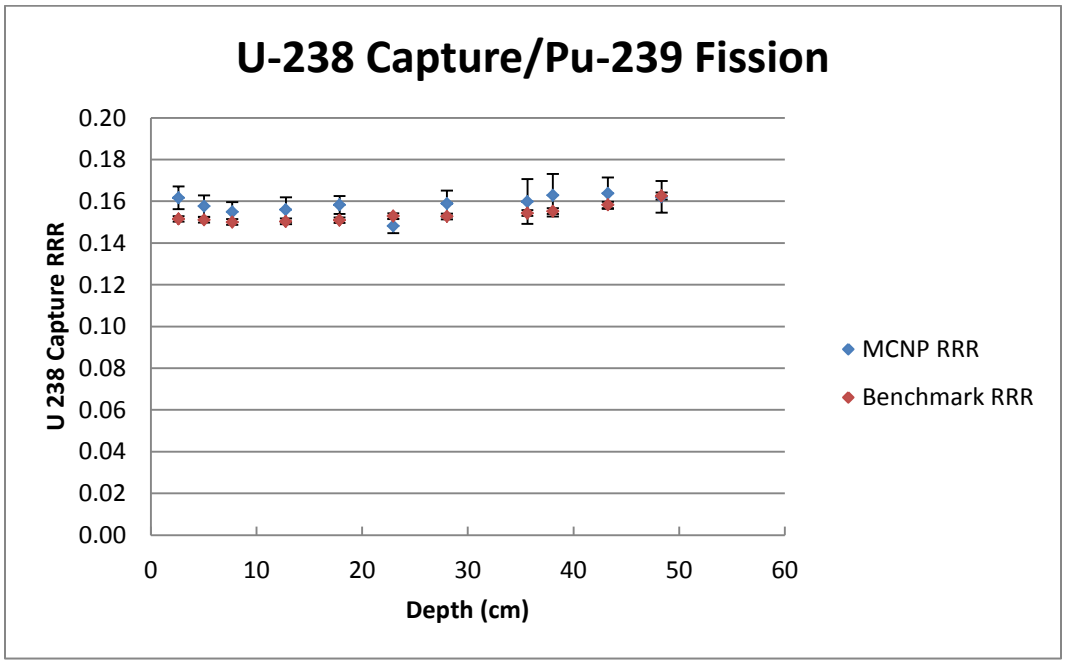


Figure 33: U-238 Capture to Pu-239 Fission Reaction Rate Ratio for Axial Transverse

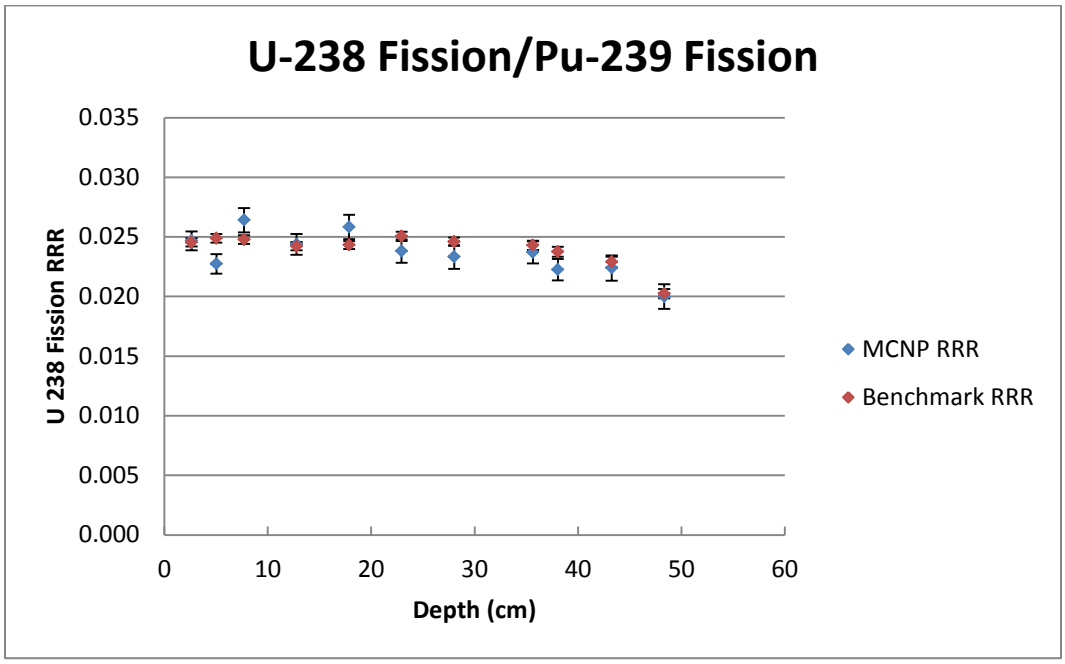


Figure 34: U-238 Capture to Pu-239 Fission Reaction Rate Ratio for Axial Transverse

Since all reaction rate ratios were taken relative to the Pu-239 fission reaction rate, these ratios will simply be referred to by the reaction rate of the material in numerator of the ratio. For example, U-235 fission reaction rate ratio means the ratio of U-235 fission to Pu-239 fission. For the U-235 fission reaction rate ratio, the MCNP model tends to slightly overpredict the ratio near the center of the core, but the measurement furthest from the front of the core underpredicts this ratio slightly. The U-238 capture reaction rate ratio is slightly overpredicted for most of the data points while the U-238 C /Pu-239 F reaction rate ratio is slightly underpredicted for most of the data points. It is important to note that because these are all measurements of ratio rate ratio and not the reaction rate itself, they do not give much information about the flux in the core. This is because the foils are placed in similar locations between the same set of plates and thus have relatively similar neutron fluxes. Thus, the reaction rate ratio gives more information about the flux spectrum than the flux itself. In addition, it can be noted that larger error bars in the MCNP results tend to indicate fewer neutrons in that particular tally location since relative uncertainty decreases as the number of particles passing through the tally increases. Therefore, larger error bars in the MCNP model tend to indicate lower fluxes. Appendix B contains calculated divided by

expected results for these transverses which is another way that these results have been presented for other computational models of the ZPPR-19B.

The reaction rate ratio results for the horizontal transverses are shown in Figures 35, 36, and 37. In these figures, location refers to a specific drawer in the transverse as shown in previously in Figure 6. For example, for this horizontal transverse, location 1 refers to the center drawer while location 2 is the drawer next to it on the right. The lowest location number is nearest to the center of the core while the highest is furthest from the center.

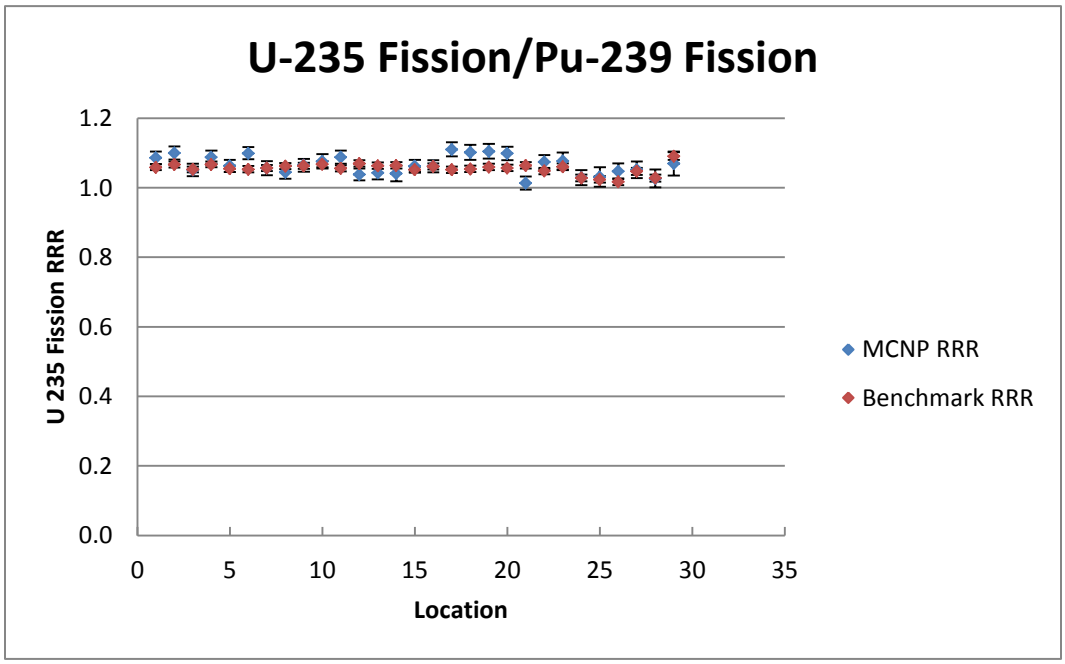


Figure 35: U-235 Fission to Pu-239 Fission Reaction Rate Ratio for Horizontal Transverse

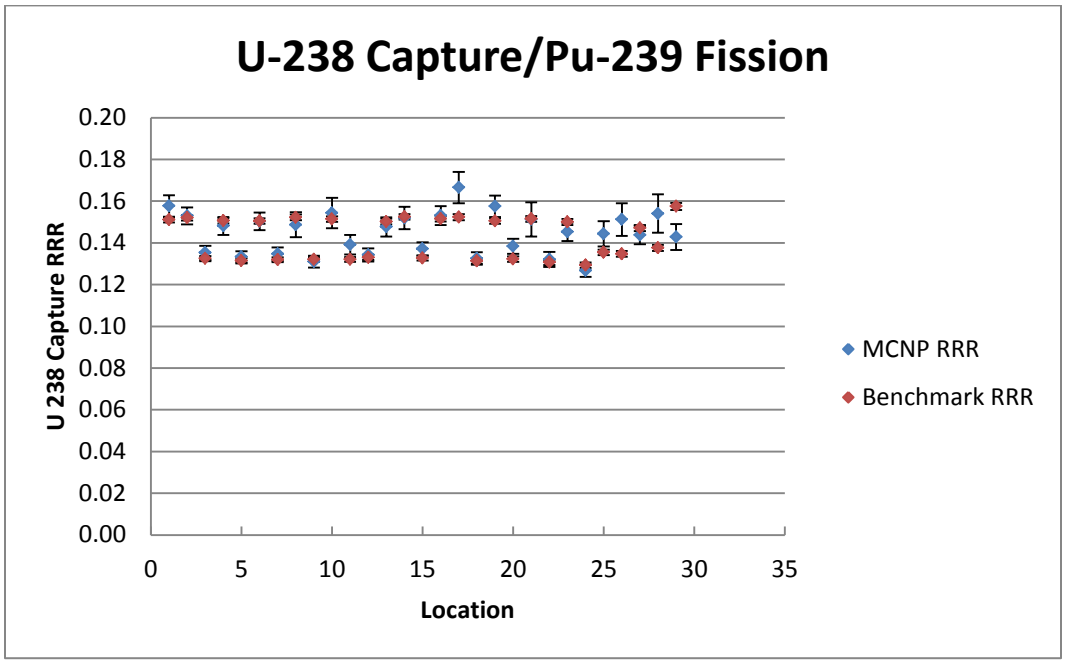


Figure 36: U-238 Capture to Pu-239 Fission Reaction Rate Ratio for Horizontal Transverse

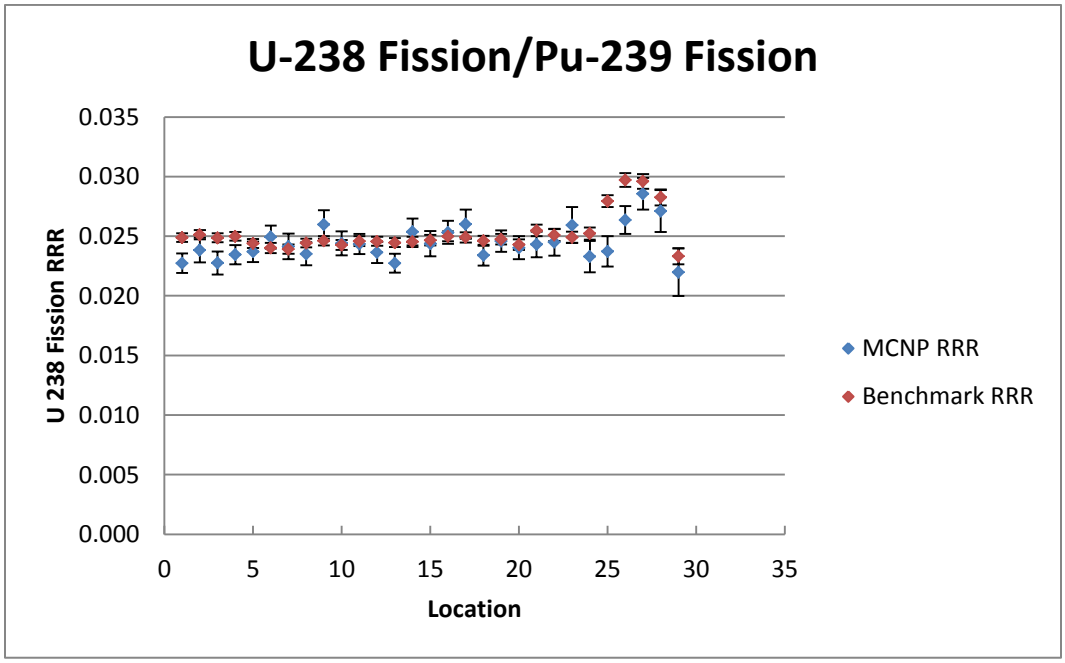


Figure 37: U-238 Fission to Pu-239 Fission Reaction Rate Ratio for Horizontal Transverse

Overall, for the U-235 fission reaction rate ratio, the MCNP results follow the experimental results fairly well but do underpredict and overproduce in certain parts of the core. For the U-238 capture reaction rate ratio, the values that are differing significantly also tend to have larger error bars than the values that have better agreement. This indicates

that the uncertainty is larger in these locations and running the calculation over more neutron histories may decrease these inconsistencies. In addition, for the U-238 capture results, step phenomenon is observed between drawer locations. This is because there is significant shielding in the DUM drawers that is not present in the DUF drawers. In the DUM drawers the U-238 foil is placed next to a plate of U-238 metal which significantly shields the exact spectrum of neutrons that U-238 readily captures since it is the same material and has the same resonance capture cross section. This phenomenon is not present in the U-238 fission reaction rate ratio results since only fast neutrons can fission U-238 and these neutrons are above the energy of the resonance capture region.

The increase in reaction rate ratio of U-238 fission for the last five locations is due to these five locations being located in the outer core. Many drawers in the outer core have twice the mass of fissile material as drawers in the inner core. This results in an increased source of "new" neutrons which results in a higher energy spectrum in this area of the core. Because of this higher energy spectrum, more neutrons are of sufficient energy to cause fission in U-238. In addition, lower energy neutrons that have undergone many collisions in the center of the core experience a 1/r decrease as they stream to the outer core.

The results for the 15° radial transverse are shown in Figures 38, 39 and 40. These results are similar to the results of the horizontal radial transverse.

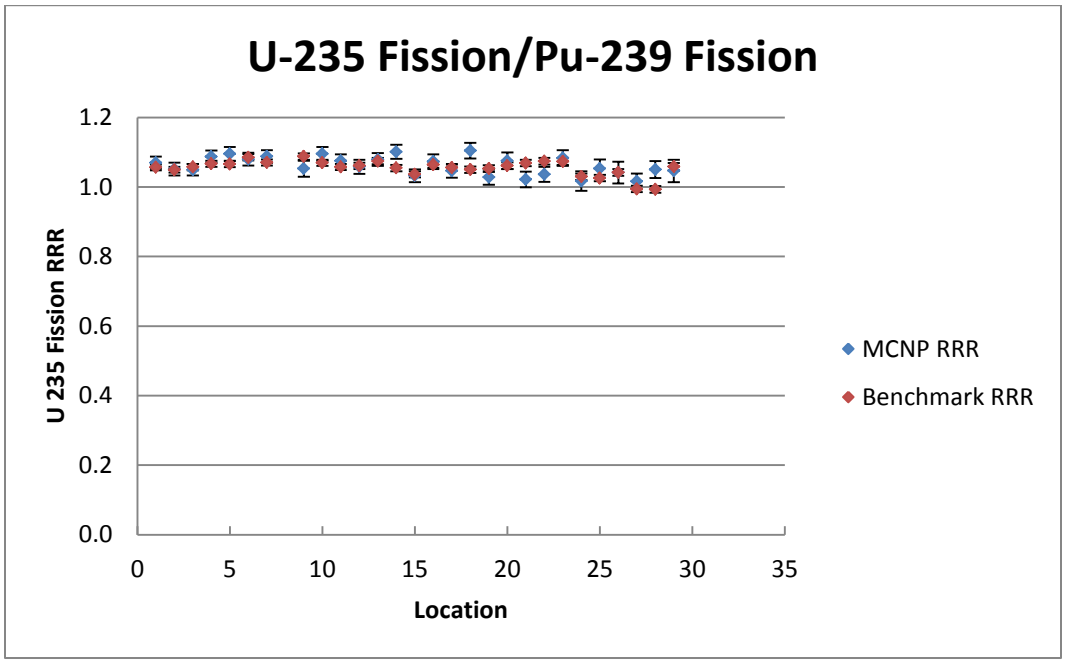


Figure 38: U-235 Fission to Pu-239 Fission Reaction Rate Ratio for 15° Transverse

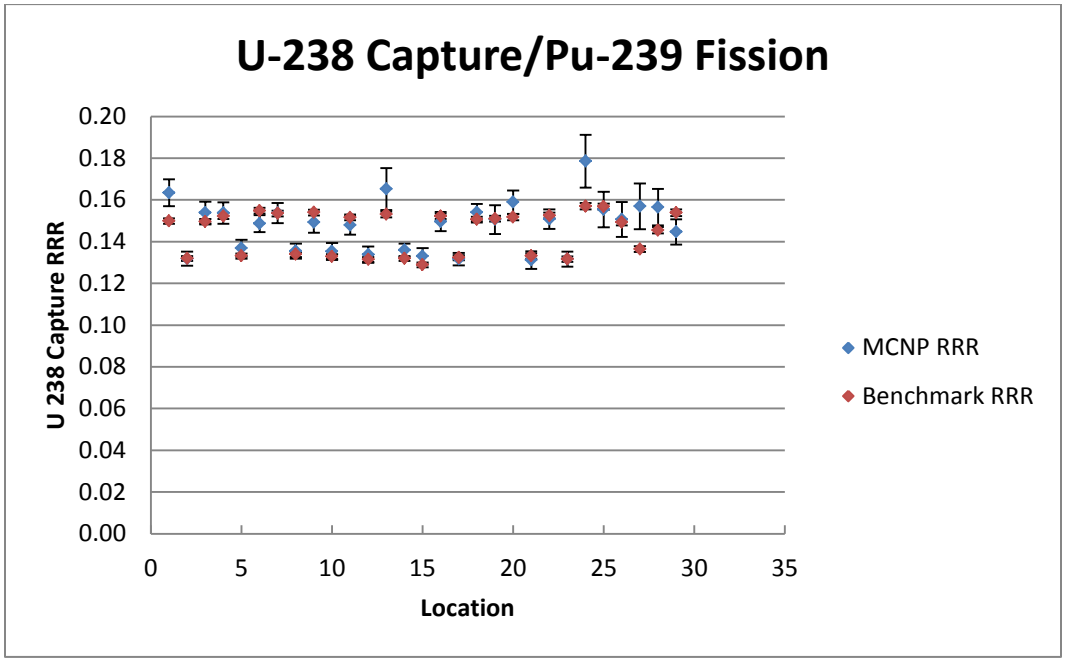


Figure 39: U-238 Capture to Pu-239 Fission Reaction Rate Ratio for 15° Transverse

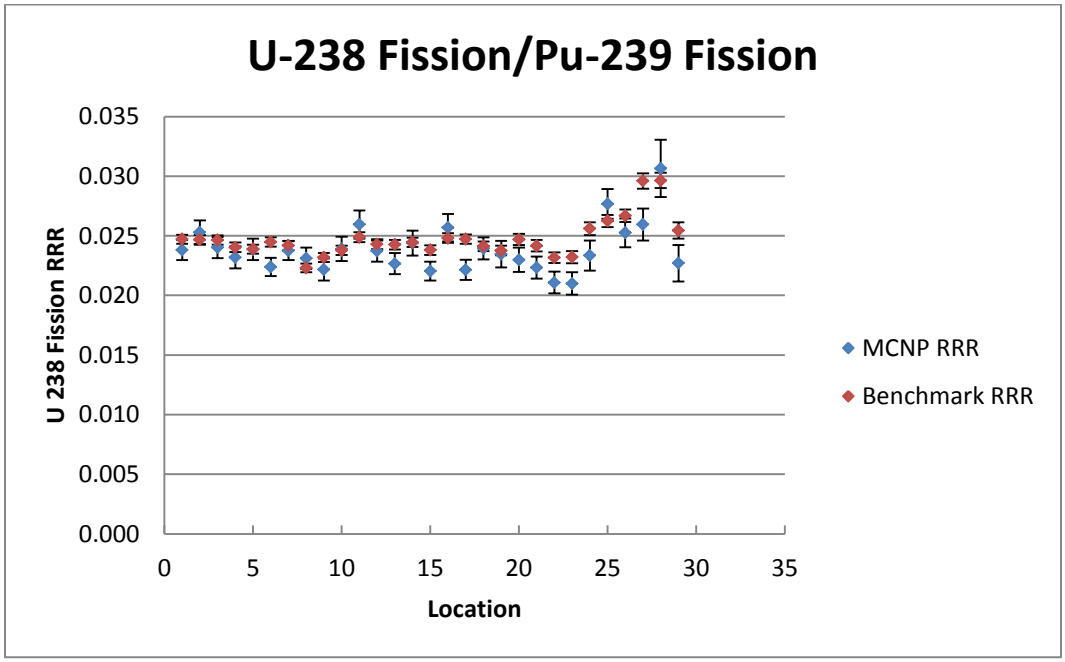


Figure 40: U-238 Fission to Pu-239 Fission Reaction Rate Ratio for 15° Transverse

It can be helpful to observe the average deviation of the MCNP results from the ZPPR-19B facility results to attain an understanding of how well these reaction rates are

predicted over the whole core. Table 25 shows calculated divided by expected results for these three transverses:

Table 25: Calculated/Expected of Transverse Reaction Rate Ratios

| | Axial Transverse | stdv | Horizontal Transverse | stdv | 15° Transverse | stdv |
|---|---|---|---|---|---|---|
| U-235 Fission | 1.0127 | 0.0117 | 1.0099 | 0.0046 | 1.0061 | 0.0046 |
| U-238 Capture | 1.0323 | 0.0081 | 1.0175 | 0.0084 | 1.0197 | 0.0090 |
| U-238 Fission | 0.9845 | 0.0146 | 0.9708 | 0.0091 | 0.9653 | 0.0095 |

The U-235 fission reaction rate ratio is fairly well predicted over all transverses. This ratio is slightly overpredicted in all cases but only in the horizontal transverse is it greater than two standard deviations from the average. The U-238 capture reaction rate ratio is overpredicted in all cases and most highly overpredicted in the axial transverse. The other two transverses are slightly greater than two standard deviations from the expected value. This shows that this overproduction of capture is most prevalent further from the center of the core. Finally, the U-238 fission reaction rate ratio is underpredicted in all transverses but most significantly in the radial transverses. The axial transverse is slightly further than one standard deviation below the expected value. Of these results the overprediction of U-238 capture and underprediction of U-238 fission are most important. Both of these deviations would have the effect of reduction in neutron multiplication factor since U-238 would capture more neutrons and produce fewer neutrons from fission creating a larger than expected neutron sink. Calculated divided by expected values for all locations are shown in Appendix B. For comparison, Table 26 shows calculated divided by expected analytical results in the inner core for a sample calculation within the benchmark document using the Japanese Evaluated Nuclear Data Library. These results show a similar bias to the MCNP results.

Table 26: Calculated/Expected for Analytical Results in Inner Core [7]

| | JENDL-3.2 | JENDL-3.3 |
|---|---|---|
| U-235 Fission | 1.011 | 1.020 |
| U-238 Capture | 1.022 | 1.032 |
| U-238 Fission | 0.987 | 0.979 |

It should be noted that in an earlier iteration of the MCNP model, the foils were not present. Table 27 shows the results of this earlier iteration.

Table 27: Calculated/Expected of Reaction Rate Ratios without Foils Modeled

| | Axial Transverse | stdv | Horizontal Transverse | stdv | 15° Transverse | stdv |
|---|---|---|---|---|---|---|
| U-235 fission | 1.0208 | 0.0062 | 1.0145 | 0.0025 | 1.0151 | 0.0037 |
| U-238 Capture | 1.1238 | 0.0240 | 1.0681 | 0.0151 | 1.0477 | 0.0126 |
| U-238 Fission | 0.9895 | 0.0084 | 0.9745 | 0.0071 | 0.9821 | 0.0074 |

These results show that for the U-238 capture reaction rate ratio, neglecting the actual foil material can result in up to a 12% overprediction in this ratio. This is due to self-shielding. Because of the resonance behavior of capture in U-238, certain neutron energies have an extremely high probability to be captured. If the foil material is not modeled, these neutrons will pass entirely through the tallied volume without being absorbed causing a much higher than expected reaction rate ratio. Even though the foils are thin, it is unlikely that at these resonance energies the neutron will reach the other side of the foil. This was remedied simply by modeling all foil material. In addition, modeling foil material leads to improved results in U-235 fission but slightly worse results in U-238 fission. Reaction rate ratios and calculated divided by expected plots for the foils not being modeled are shown in Appendix C.

# 5 CONCLUSIONS

## 5.1 Concluding Remarks

This work has shown that the ZPPR-19B has been successfully modeled with MCNP resulting in a bias of -188 pcm in the multiplication factor. Significant effort was expended to ensure that the individual drawers were model correctly. Additionally, other behaviors of the reactor such as gap worth response and primary absorption mechanisms were investigated to confirm that the model was behaving reasonably. The multiplication factor was also compared to the results of a simplified model with good agreement. Considering the significant amount of effort to verify that the actual configuration of the ZPPR-19B facility was modeled as closely as possible and the considerable agreement between the as built model and the simplified model, there is a rather high degree of confidence in the results. Recalling that the ZPPR-15B, a metallic fueled but similar facility, has been shown to have a -203 pcm bias using MCNP and the same ENDF-VII library provides further credibility to this work since the bias is of similar magnitude and direction. [16]

In addition to successfully investigating the multiplication factor, reaction rate ratios were also examined. It was determined, with a rather high degree of confidence, that for the neutron spectrum present in the ZPPR-19B, U-238 captures were overestimated while U-238 fissions were underestimated. Since capture in uranium is the primary neutron loss mechanism for such a large reactor, it is highly probable that this discrepancy significantly contributes to the underestimation of the multiplication factor. It should also be noted that it was of high importance to model the foil material within the reactor. In past iterations of the model, when it was assumed that the foil would not have a significant impact on reactivity and reaction rates, there were significant inaccuracies especially with U-238 capture. This can be attributed to the resonance absorption behavior of U-238. If the actual material is not modeled, neutron path lengths are much longer than they would have been due to the extremely high absorption cross section at certain energies. Even though the foils are extremely thin, at these high cross section energies the neutron is not likely to make it to the other side of the foil. This results in an overprediction of the U-238 capture reaction rate since the neutron path length was much longer if the foil material itself was not modeled. Once the foil material was modeled this inconsistency was resolved.

Thus, the recommendation of this thesis is that any future design work for a reactor similar to the ZPPR-19B should be aware that MCNP, using the ENDF V-II library, tends to

slightly underestimate the neutron multiplication factor. It is also hypothesized that the primary reason for this underestimation is an overestimation of the U-238 capture cross section for the neutron spectrum present in this model. These results can be taken into when designing Sodium Fast Reactors in the future.

**5.2 Future Work**

While the foils in all the drawers of the ZPPR-19B facility that contained plutonium foils were modeled, time constraints dictated that other transverses, where only uranium foils were present, were not modeled or investigated. These transverses included two additional axial transverses as well as a 30° radial transverse and a vertical radial transverse. Additional efforts could be conducted to model these transverses although it would likely increase the length and complexity of the MCNP input significantly. In addition, cell factors, which are used to correct the measured reaction rate in the foil to the average reaction rate in the drawer, could be examined in any future evaluations.

The subcritical configuration of the ZPPR-19B core could also be investigated. This was not of primary importance to this work since most of the results were for the critical configuration. The current input file contains all necessary universes for modeling the subcritical configuration, thus it is a matter of rearranging the lattice rather than having to model any new drawers. It should also be noted that many all of the drawers within the ZPPR-18 and ZPPR-19 were the same. Thus, if there was interest in modeling a different configuration of the ZPPR-19 or modeling the ZPPR-18 only rearrangement of the drawers within the lattice would be needed rather than having to completely rebuild the individual drawers.

It should be reemphasized that the only uncertainties accounted for in this work were due to the non-deterministic nature of MCNP. It was assumed that the material and geometry were exact. Considering that material masses were provided to the nearest thousandth of a gram there is significant confidence in this modeling. Nevertheless, it would be sensible to complete a sensitivity study, especially for the materials that highly effect reactivity such as the actinides.

Finally, of highest importance to the results of this thesis, other nuclear data libraries could be investigated for the current model. It is possible that other nuclear data libraries could model the reactor more closely. The Japanese Evaluated Nuclear Data Library

(JENDL) library is recommended since it was the nuclear data library used for much of the other modeling work done for the ZPPR-19B. The TALYS-based Evaluated Nuclear Data Library (TNDL) library was also recommended by TerraPower. Of primary significance in these results would be the U-238 capture reaction rate and the multiplication factor. After investigating additional libraries, it could be determined whether the U-238 capture cross section is the primary cause of the observed bias in the multiplication factor.

**6 BIBLIOGRAPHY**

[1] Waltar, Alan E., and Albert B. Reynolds. *Fast Breeder Reactors*. New York: Pergamon, 1981. Print.

[2] Baum, Edward M., Mary C. Ernesti, Harold D. Knox, Thomas R. Miller, and Aaron M. Watson. *Nuclides and Isotopes: Chart of the Nuclides*. [s. L.]: Bechtel Marine Propulsion Corporation, 2010. Print.

[3] Hannum, William H., Gerald E. Marsh, and George S. Stanford. "Smarter use of nuclear waste." *Scientific American* 293.6 (2005): 84-91.

[4] "Reactors Designed by Argonne National Laboratory." *Fast Reactor Technology*. Argonne National Laboratory, 25 Sept. 2013. Web. 20 Nov. 2013. <http://www.ne.anl.gov/About/reactors/frt.shtml>.

[5] Cochran, Thomas B., et al. "Fast breeder reactor programs: History and status." *International Panel on Fissile Materials Research Report* 8 (2010).

[6] LeSage, L. G. *AN OVERVIEW OF THE ARGONNE NATIONAL LABORATORY FAST CRITICAL EXPERIMENTS 1963-1990*. Tech. no. ANL-NT-175. N.p.: n.p., 2001. Print.

[7] Sanda, Toshio, Makoto Ishikawa, and James W. Sterbentz. *ZPPR-19B Experiment: A 1,000 MWe-Class Sodium-Cooled MOX-Fueled FBR Core Mock-Up Critical Experiment with Two-Homogeneous Zones and Control-Rod Withdrawal, Where Plutonium and Enriched Uranium Are Used Mixing in the Outer Core*. Tech. no. ZPPR-LMFR-EXP-004-CRIT-SPEC-REAC-RRATE. N.p.: International Reactor Physics Benchmark Experiments, 2006.

[8] DoE, U. S. "A technology roadmap for generation IV nuclear energy systems." *Nuclear Energy Research Advisory Committee and the Generation IV International Forum*. 2002.

[9] *TerraPower and the Traveling Wave Reactor*. TerraPower, 21 Mar. 2013. Web. <http://ansidaho.org/wp-content/uploads/2013/03/TerraPower-Mar-2013.pdf>.

[10] Beynon, T. D. "The nuclear physics of fast reactors." *Reports on Progress in Physics* 37.8 (1974): 951.

[11] Shultis, J. Kenneth, and R. E. Faw. "An MCNP primer." *Dept. of Mechanical and Nuclear Engineering, Kansas State University* (2006).

[12] Brewer, Roger. "Criticality Calculations with MCNP5: A Primer." *Los Alamos National Laboratory, LA-UR-09-00380* (2009).

[13] Team, Monte Carlo. *MCNP—A General Monte Carlo N-Particle Transport Code, Version 5, vol. I: Overview and Theory*. LANL Report LA-UR-03-1987. Los Alamos National Laboratory, Los Alamos, NM, 2003.

[14] Team, Monte Carlo. "MCNP–A General Monte Carlo N-Particle Transport Code, Version 5." *Book MCNP-A General Monte Carlo N-Particle Transport Code Version* 5 (2003).

[15] Sargent, Robert G. "Verification, validation, and accreditation: verification, validation, and accreditation of simulation models." *Proceedings of the 32nd conference on Winter simulation*. Society for Computer Simulation International, 2000.

[16] Lell, R. M., and R. D. McKnight. *Archival of the ZPPR-15B Physics Experiment: Report for Year 2*. 28 Mar. 2012. Argonne National Laboratory.

[17]McFarlane, H. F., S. B. Brumbach, S. G. Carpenter, and P. J. Collins. *Benchmark Physics Tests in the Metallic-Fuelled Assembly ZPPR-15*. 17 Apr. 1987. Argonne National Laboratory, Idaho Falls.

[18] Yang, W. S., and S. J. Kim. *A Validation Study of Existing Neutronics Tools against ZPPR-21 and ZPPR-15 Critical Experiments*. 30 Sept. 2007. Argonne National Laboratory, Argonne.

[19] Stover, Tracy E., Jr. *Optimization of Fast Critical Experiments to Reduce Nuclear Data Uncertainties in Support of a Fast Burner Reactor Design Concept. North Carolina State University* (2011).

[20] Lell, Richard M., Robert W. Schaefer, and Richard D. McKnight. *ZPR-6 Assembly 7 High 240 Pu Core Experiments: A Fast Reactor Core with Mixed (Pu,U)-Oxide Fuel and a Central High 240 Pu Zone*. N.d. Argonne National Laboratory.

[21] LeSage, L. G. *An Overview of the Argonne National Laboratory Fast Critical Experiments 1963-1990*. Apr. 2001. Argonne National Laboratory, Argonne.

[22] Lell, Richard M., Robert W. Schaefer, Richard D. McKnight, and Amr Mohamed. *ZPPR-21 Phase A: A Cylindrical Assembly of Pu Metal Reflected by Graphite*. N.d. Argonne National Laboratory.

[23] Collins, P. J., and S. B. Brumbach. *ZPPR Progress Report: November 1987 through January 1988*. 15 Feb. 1988. Argonne National Laboratory-West, Idaho Falls.

[24] Brumbach, S. B., and P. J. Collins. *ZPPR Progress Report: February 1988 through April 1988*. 13 May 1988. Argonne National Laboratory-West, Idaho Falls.

[25] "Kel-F® PCTFE (PolyChloroTriFluoroEthylene) Specifications." Boedeker, 2013. Web. <http://boedeker.com/pctfe_p.htm?gclid=CPCY7ILCg7sCFU6VfgodFHsADw>.

[26] Sanda, Toshio, Makoto Ishikawa, and Richard D. McKnight. *ZPPR-18C EXPERIMENT: A 1,000 MWe-CLASS SODIUM-COOLED MOX-FUELED FBR HOMOGENEOUS CORE MOCK-UP CRITICAL EXPERIMENT IN THE STATE OF REMOVAL OF ONE OF EIGHTEEN HALF-INSERTED CONTROL RODS, WHERE ENRICHED URANIUM IS USED WITH THE SHAPE OF A SECTOR IN THE OUTER CORE*. Tech. no. ZPPR-LMFR-EXP-008 CRIT-SPEC-RRATE. N.p.: International Reactor Physics Benchmark Experiments, 2006.

[27] Lell, Richard M., Richard D. Mcknight, Amr Mohamed, Robert W. Schaefer, Anatoli Tsiboulia, and Yevgeniy Rozhikhin. *ZPPR-21 PHASE A: A CYLINDRICAL ASSEMBLY OF PU METAL REFLECTED BY GRAPHITE*. Tech. no. PU-MET-FAST-033. N.p.: International Criticality Safety Benchmark Evaluation Project, 1995.

# APPENDICIES

**Appendix A: 700 Series Drawer Criticality Calculation Behavior**

Table A1: 700 Series Bare Drawer Results

| Drawer # | Drawer Emulated | $k_{eff}$ | stdv | % deviation from average | stdv of % dev |
|---|---|---|---|---|---|
| 701 | DUF | 0.08374 | 0.00002 | -0.995 | 0.0267 |
| 702 | DUF | 0.08479 | 0.00002 | 0.247 | 0.0268 |
| 703 | DUF | 0.08476 | 0.00002 | 0.211 | 0.0268 |
| 704 | DUF | 0.08518 | 0.00002 | 0.708 | 0.0268 |
| 705 | DUF | 0.0841 | 0.00002 | -0.569 | 0.0267 |
| 706 | DUF | 0.08404 | 0.00002 | -0.640 | 0.0267 |
| 707 | DUF | 0.08445 | 0.00002 | -0.155 | 0.0268 |
| 708 | DUF | 0.0845 | 0.00002 | -0.096 | 0.0268 |
| 709 | DUF | 0.08444 | 0.00003 | -0.167 | 0.0376 |
| 710 | DUM | 0.10013 | 0.00002 | -0.253 | 0.0250 |
| 711 | DUM | 0.10025 | 0.00002 | -0.134 | 0.0250 |
| 712 | DUM | 0.09944 | 0.00003 | -0.941 | 0.0335 |
| 713 | DUM | 0.10091 | 0.00003 | 0.524 | 0.0336 |
| 714 | SS REF | 0.09443 | 0.00002 | -0.451 | 0.0222 |
| 715 | Soft RDB | 0.11765 | 0.00003 | -0.797 | 0.0328 |
| 716 | Hard RDB | 0.18645 | 0.00006 | -5.172 | 0.0389 |
| 717 | DCF | 0.10759 | 0.00002 | -0.292 | 0.0249 |
| 718 | DCF | 0.10759 | 0.00003 | -0.292 | 0.0324 |
| 719 | DUF | 0.08402 | 0.00002 | -0.664 | 0.0267 |
| 720 | DUF | 0.0842 | 0.00002 | -0.451 | 0.0267 |
| 721 | UAC | 0.06832 | 0.00002 | 0.079 | 0.0321 |
| 722 | UAC | 0.0681 | 0.00002 | -0.243 | 0.0321 |
| 723 | UDC | 0.07141 | 0.00002 | -0.366 | 0.0312 |
| 724 | UDC | 0.07167 | 0.00002 | -0.003 | 0.0312 |
| 725 | DUF | 0.08487 | 0.00002 | 0.341 | 0.0268 |

Table A2: 700 Series Reflected Drawer Results

| Drawer | Drawer Emulated | $k_{eff}$ | stdv | % deviation from average | stdv of % dev |
|---|---|---|---|---|---|
| 701 | DUF | 1.07973 | 0.00046 | -0.064 | 0.0454 |
| 702 | DUF | 1.08879 | 0.00045 | 0.774 | 0.044 |
| 703 | DUF | 1.08926 | 0.00050 | 0.818 | 0.048 |
| 704 | DUF | 1.09192 | 0.00050 | 1.064 | 0.04891 |
| 705 | DUF | 1.08511 | 0.00047 | 0.434 | 0.0463 |
| 706 | DUF | 1.08398 | 0.00047 | 0.329 | 0.0463 |
| 707 | DUF | 1.08462 | 0.00045 | 0.388 | 0.04452 |
| 708 | DUF | 1.08439 | 0.00048 | 0.367 | 0.04713 |
| 709 | DUF | 1.08636 | 0.00044 | 0.549 | 0.0437 |
| 710 | DUM | 0.98057 | 0.00042 | 1.068 | 0.0465 |
| 711 | DUM | 0.97888 | 0.00042 | 0.893 | 0.0465 |
| 712 | DUM | 0.97288 | 0.00045 | 0.275 | 0.0494 |
| 713 | DUM | 0.98409 | 0.00044 | 1.430 | 0.0485 |
| 714 | SS REF | 0.38218 | 0.00034 | 3.613 | 0.0965 |
| 715 | Soft RDB | 0.35372 | 0.00033 | 0.853 | 0.1138 |
| 716 | Hard RDB | 0.37585 | 0.00034 | 0.597 | 0.1349 |
| 717 | DCF | 1.43974 | 0.00056 | 3.653 | 0.0489 |
| 718 | DCF | 1.44017 | 0.00054 | 3.684 | 0.0478 |
| 719 | DUF | 1.08595 | 0.00048 | 0.511 | 0.0471 |
| 720 | DUF | 1.08021 | 0.00048 | -0.020 | 0.0471 |
| 721 | UAC | 1.02249 | 0.00044 | 0.340 | 0.0476 |
| 722 | UAC | 1.01993 | 0.00045 | 0.089 | 0.0485 |
| 723 | UDC | 1.36129 | 0.00052 | 0.773 | 0.0433 |
| 724 | UDC | 1.36352 | 0.00053 | 0.938 | 0.0440 |
| 725 | DUF | 1.07781 | 0.00046 | -0.242 | 0.0454 |

**Appendix B: Calculated/Expected Values for Core Transverses**

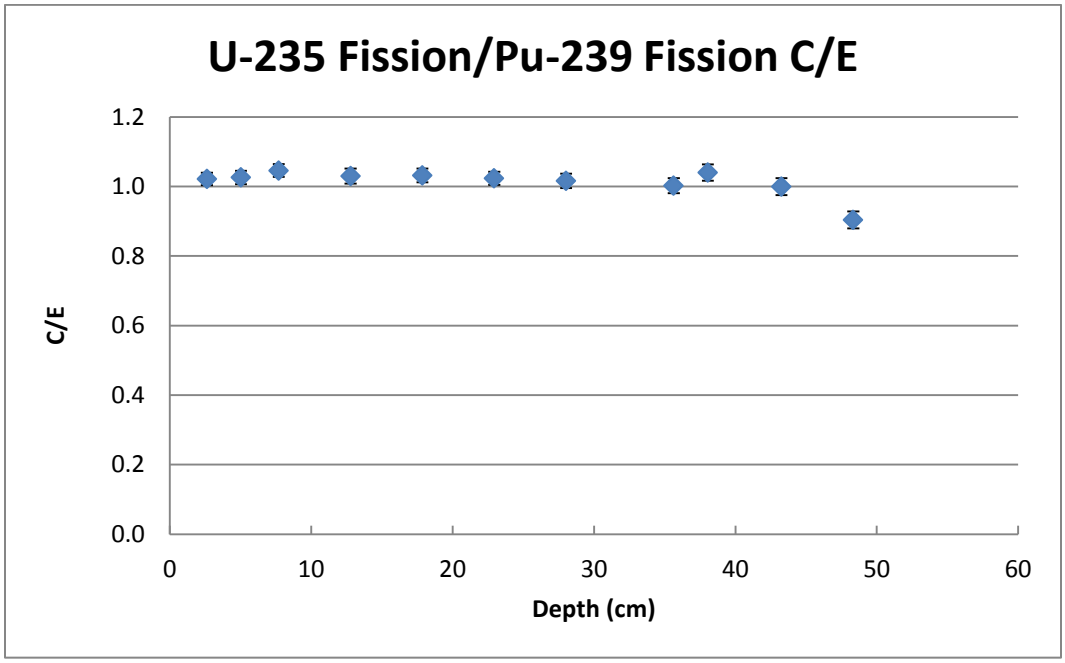


Figure B1: Calculated/Expected for U-235 Fission Reaction Rate Ratio for Axial Transverse

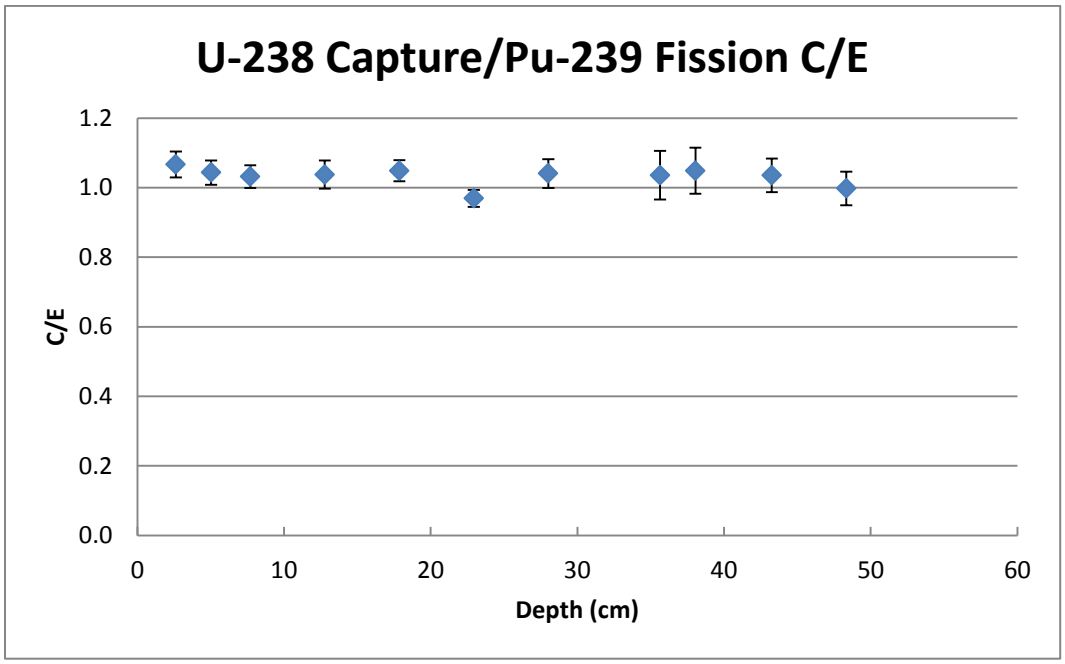


Figure B2: Calculated/Expected for U-238 Capture Reaction Rate Ratio for Axial Transverse

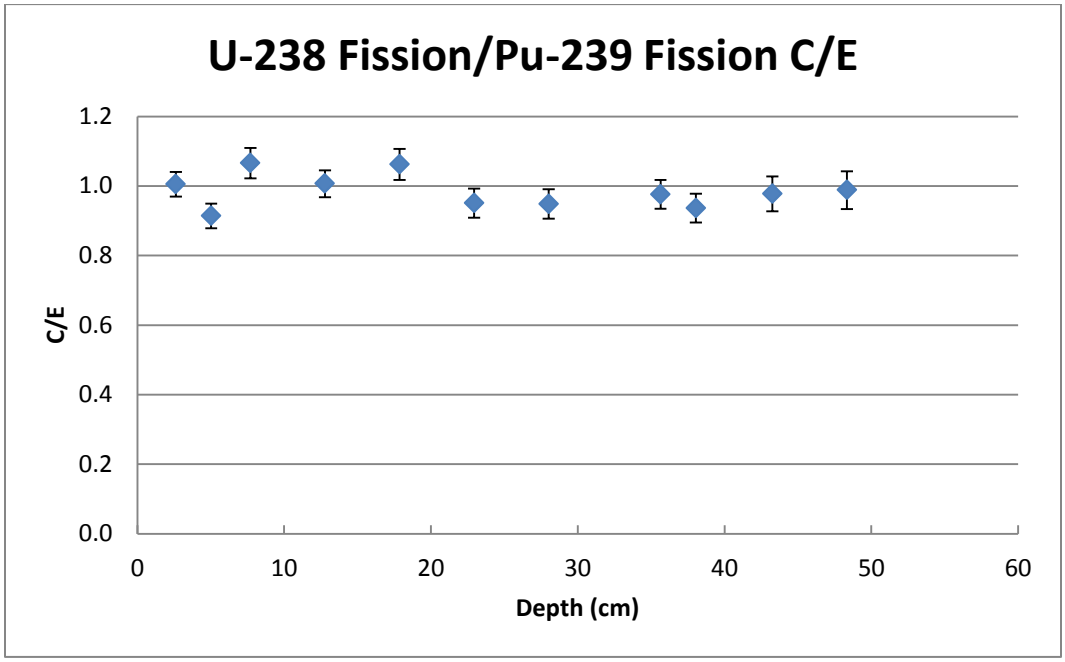


Figure B3: Calculated/Expected for U-238 Fission Reaction Rate Ratio for Axial Transverse

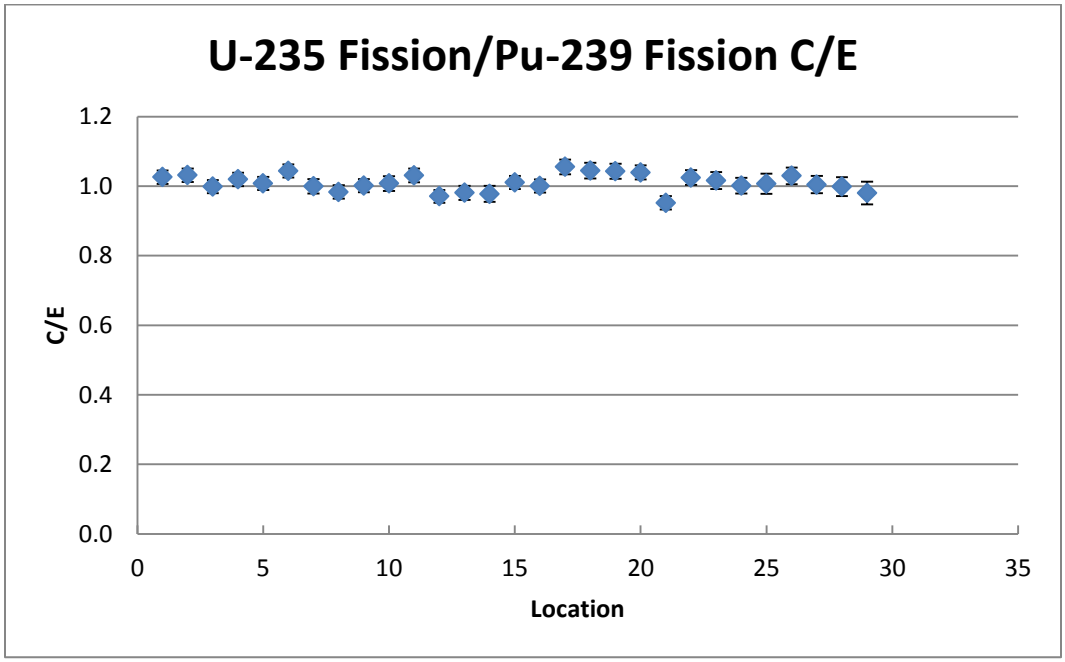


Figure B4: Calculated/Expected for U-235 Fission Reaction Rate Ratio for Horizontal Transverse

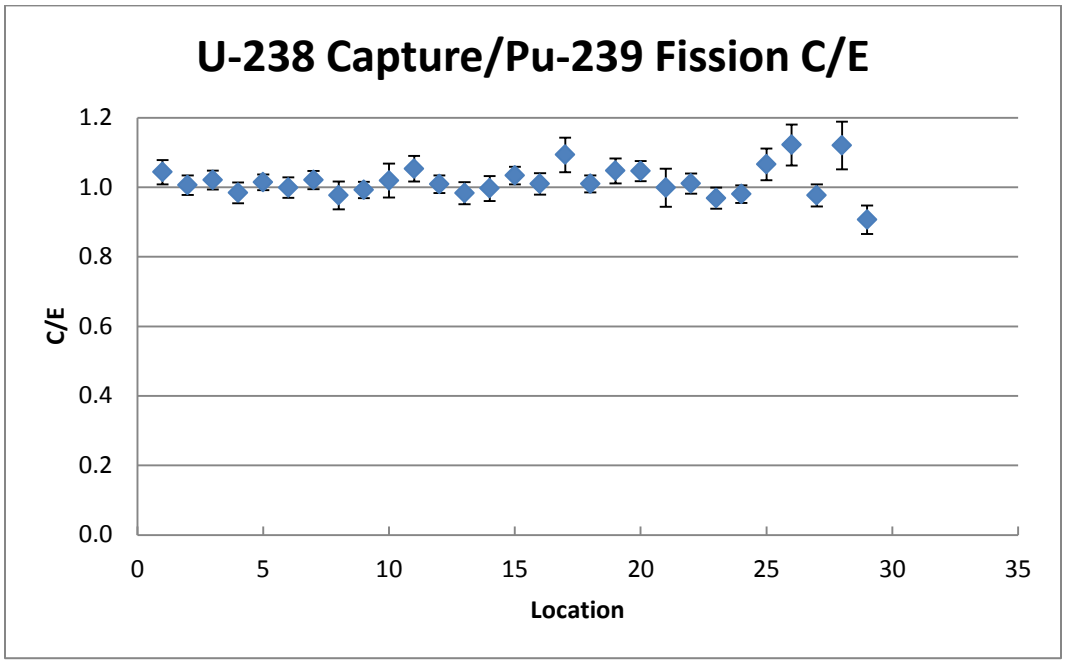


Figure B5: Calculated/Expected for U-238 Capture Reaction Rate Ratio for Horizontal Transverse

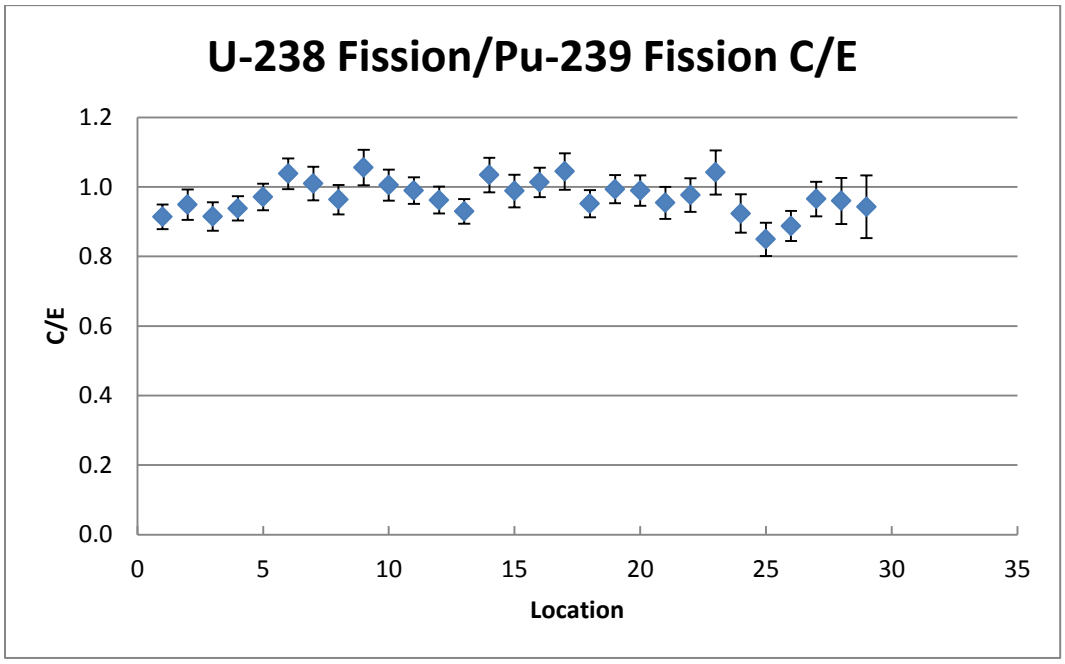


Figure B6: Calculated/Expected for U-238 Fission Reaction Rate Ratio for Horizontal Transverse

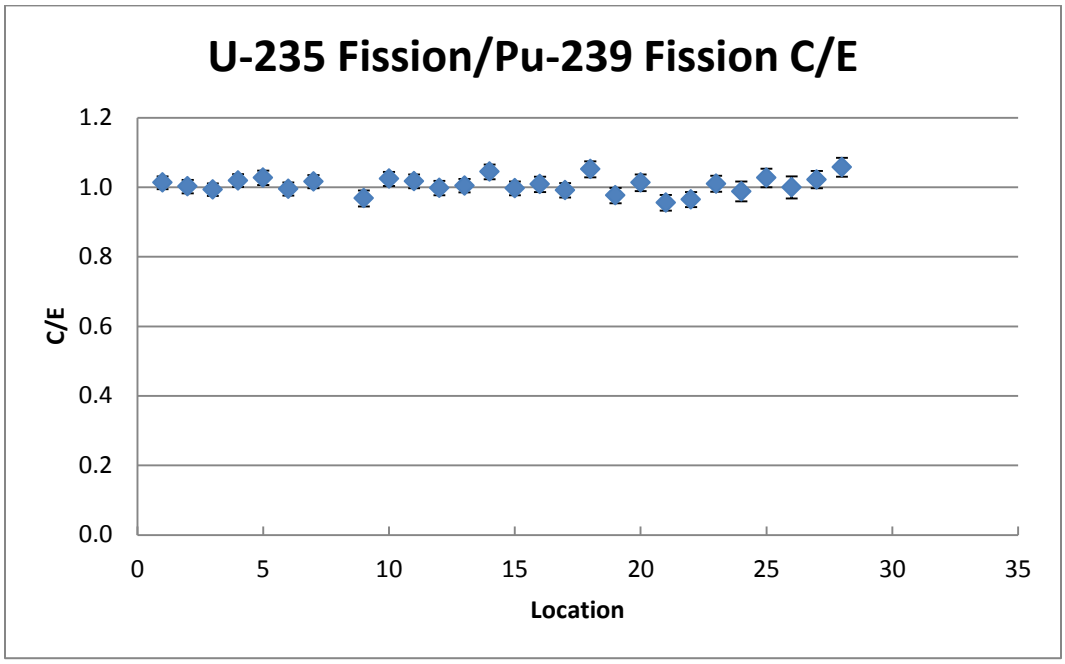


Figure B7: Calculated/Expected for U-235 Fission Reaction Rate Ratio for 15° Transverse

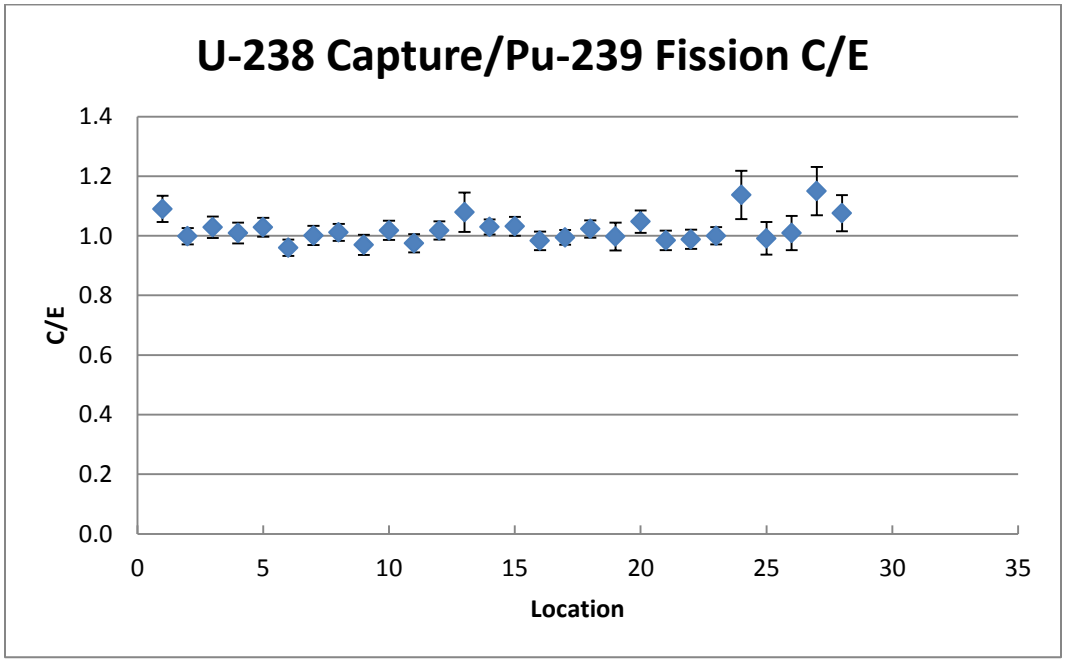


Figure B8: Calculated/Expected for U-238 Capture Reaction Rate Ratio for 15° Transverse

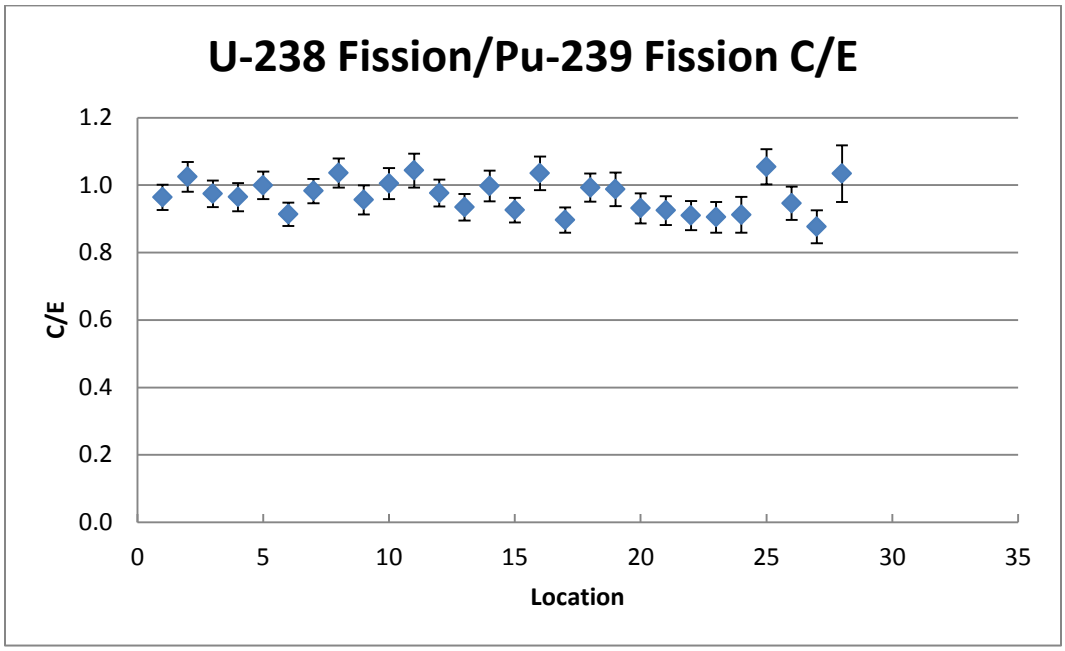


Figure B9: Calculated/Expected for U-238 Fission Reaction Rate Ratio for 15° Transverse

**Appendix C: Transverse Results without Modeled Foils**

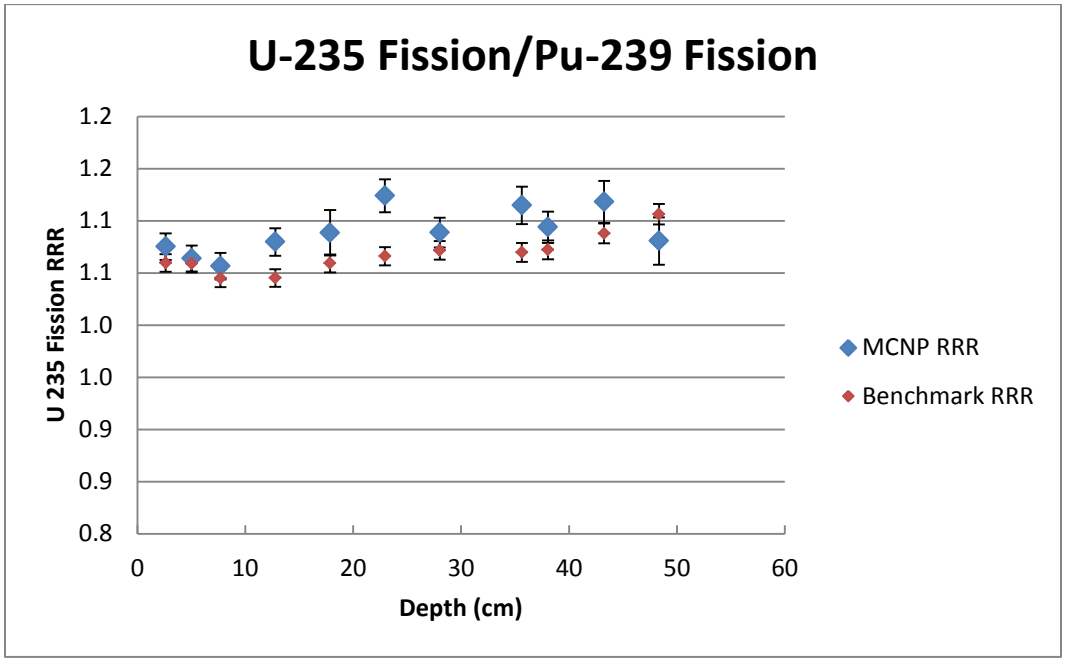


Figure C1: U-235 Fission to Pu-239 Fission Reaction Rate Ratio for Axial Transverse

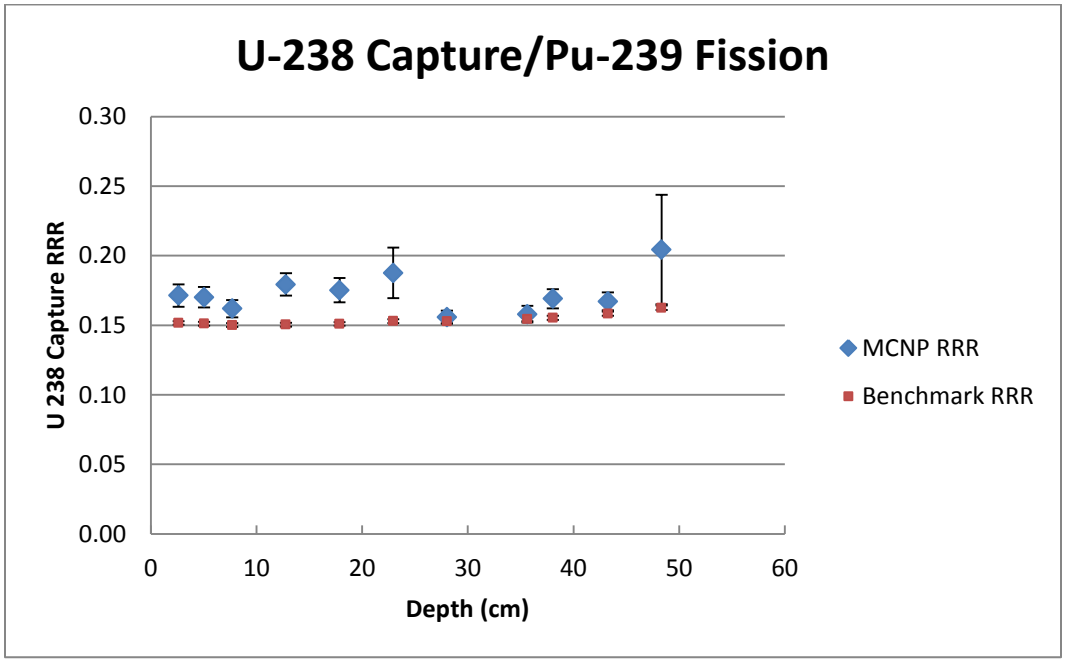


Figure C2: U-238 Capture to Pu-239 Fission Reaction Rate Ratio for Axial Transverse

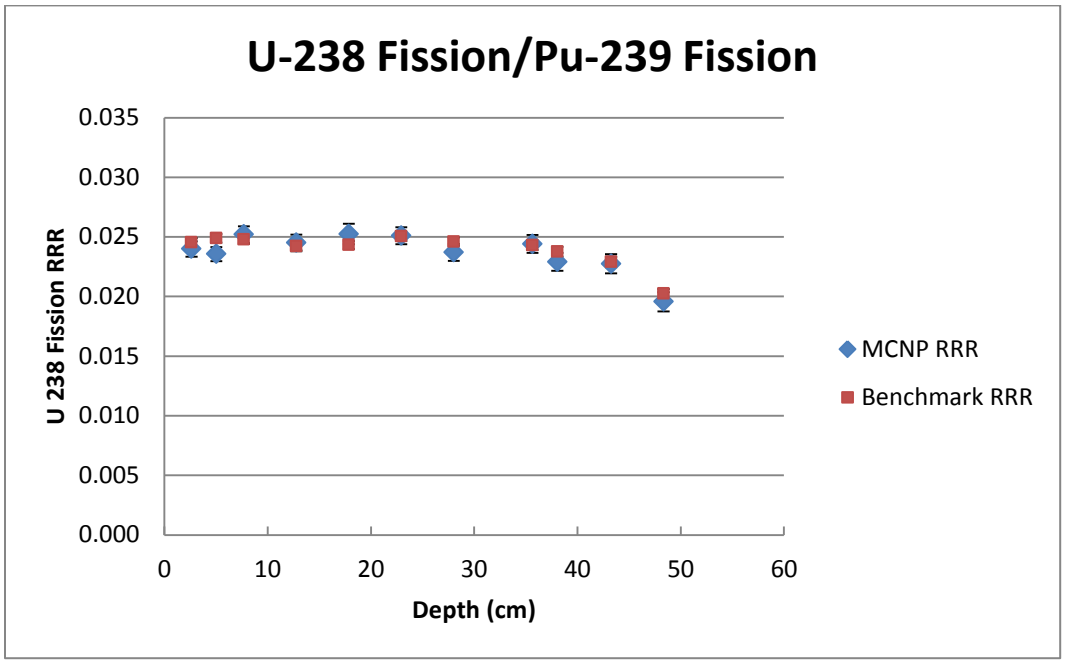


Figure C3: U-238 Fission to Pu-239 Fission Reaction Rate Ratio for Axial Transverse

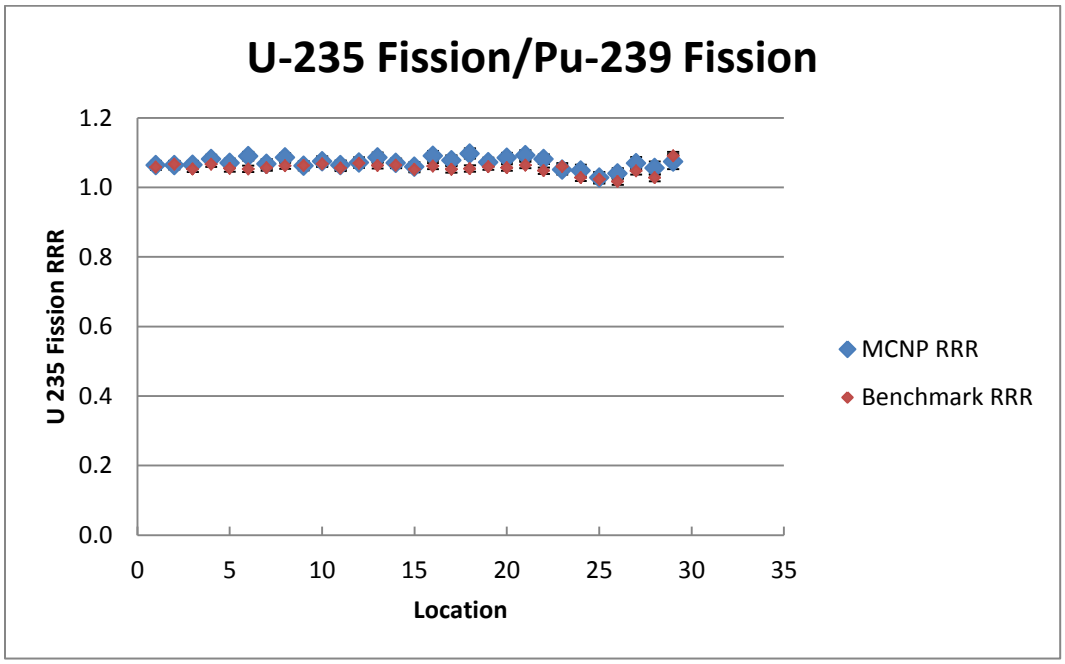


Figure C5: U-235 Fission to Pu-239 Fission Reaction Rate Ratio for Horizontal Transverse

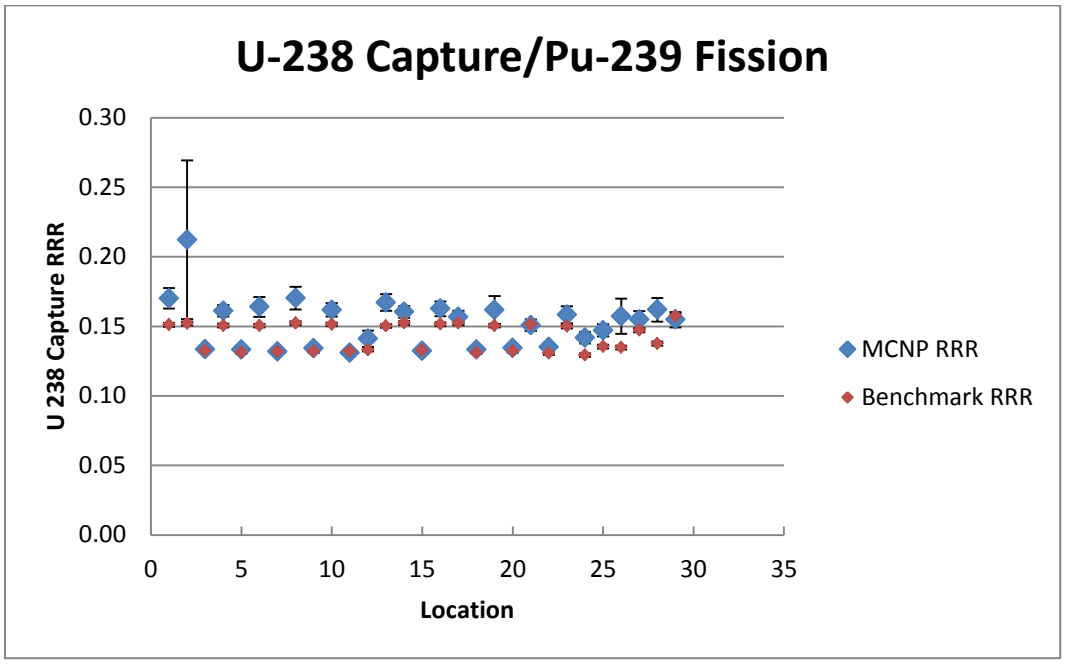


Figure C5: U-238 Capture to Pu-239 Fission Reaction Rate Ratio for Horizontal Transverse

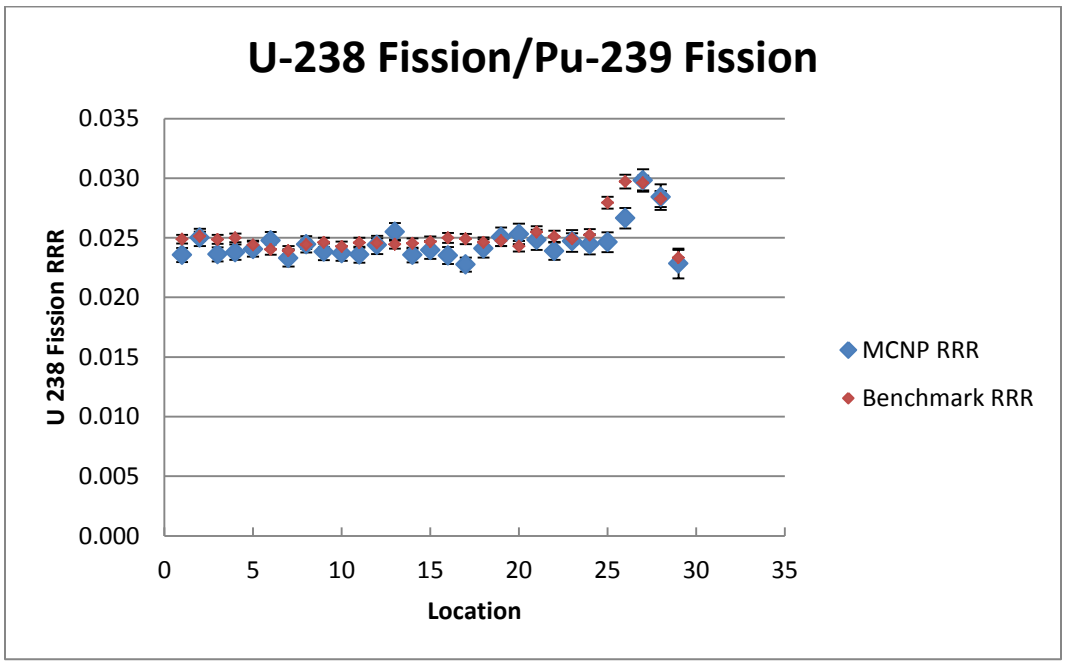


Figure C6: U-238 Fission to Pu-239 Fission Reaction Rate Ratio for Horizontal Transverse

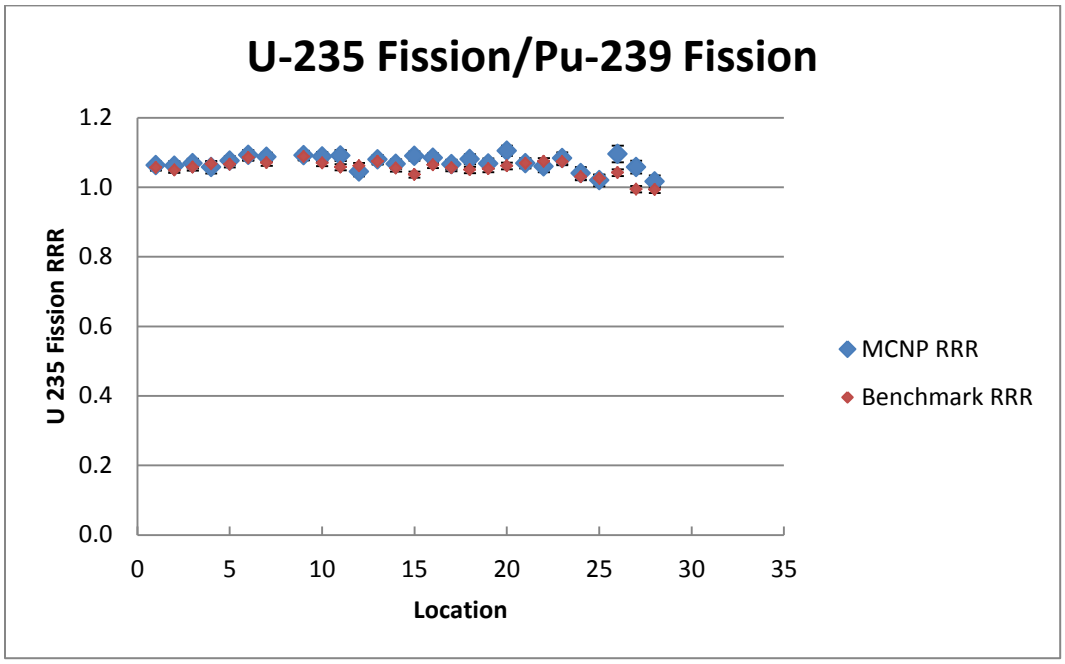


Figure C7: U-235 Fission to Pu-239 Fission Reaction Rate Ratio for 15° Transverse

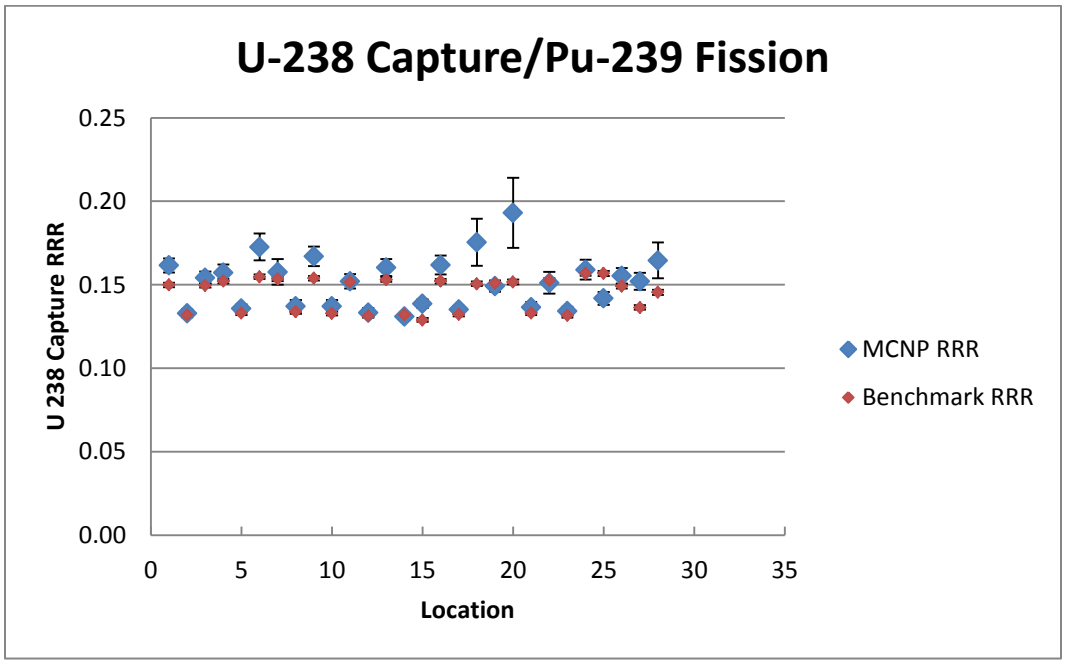


Figure C8: U-238 Capture to Pu-239 Fission Reaction Rate Ratio for 15° Transverse

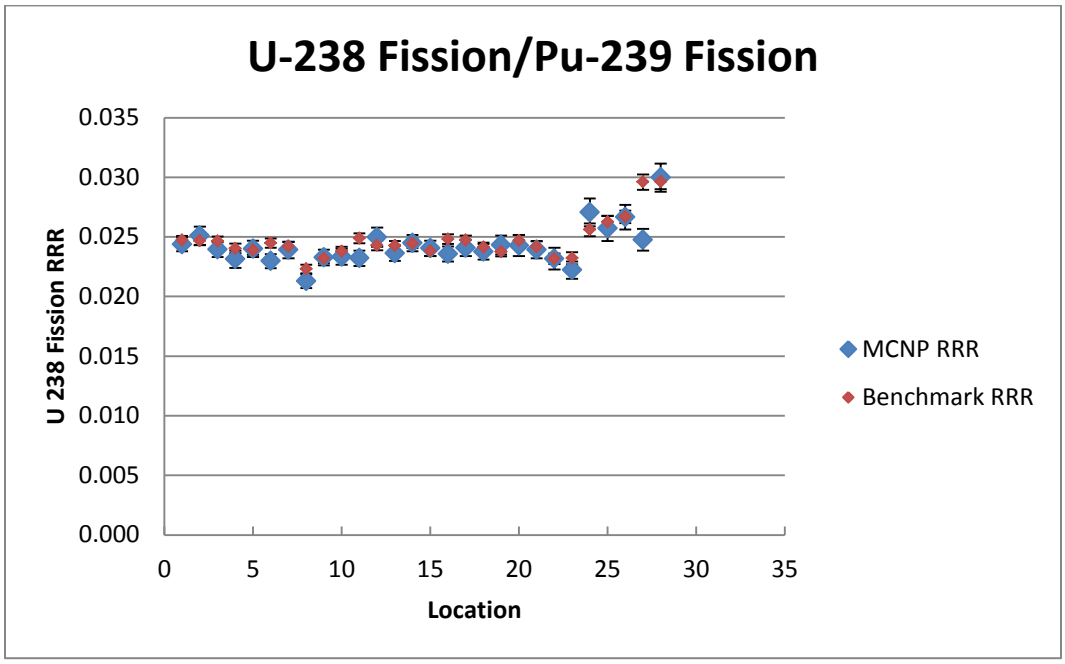


Figure C9: U-238 Fission to Pu-239 Fission Reaction Rate Ratio for 15° Transverse

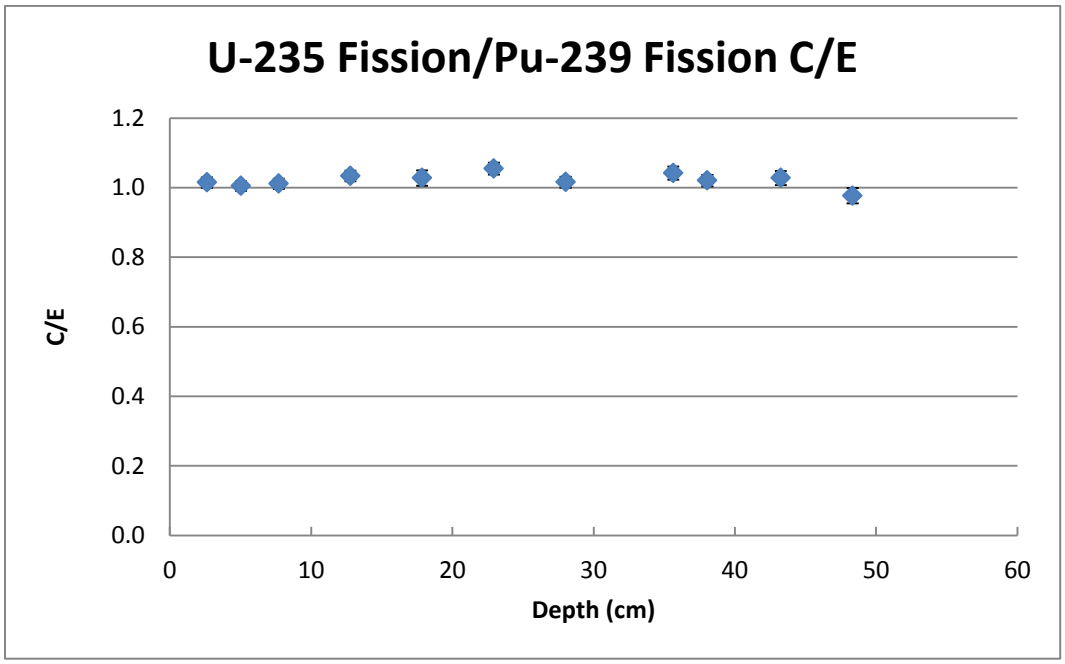


Figure C10: Calculated/Expected for U-235 Fission Reaction Rate Ratio for Axial Transverse

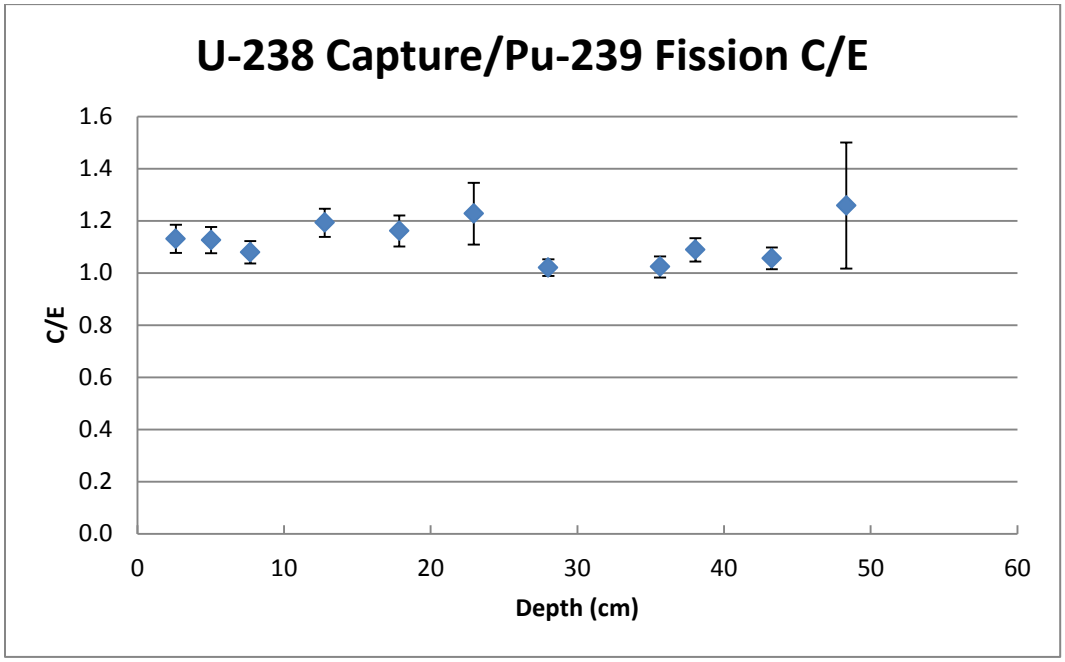


Figure C11: Calculated/Expected for U-238 Capture Reaction Rate Ratio for Axial Transverse

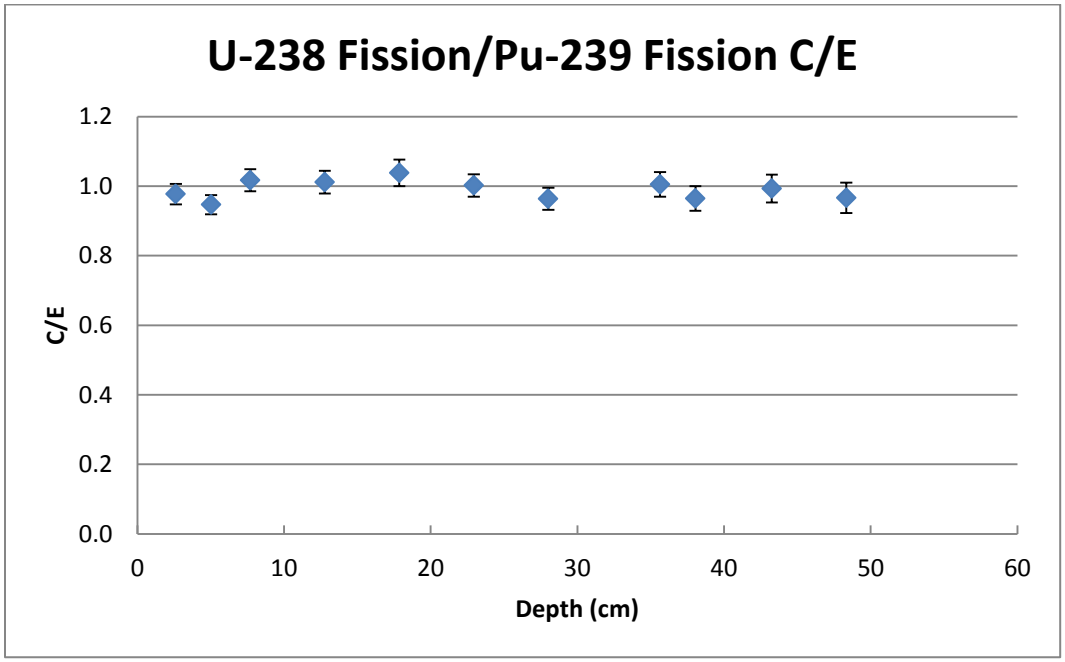


Figure C12: Calculated/Expected for U-238 Fission Reaction Rate Ratio for Axial Transverse

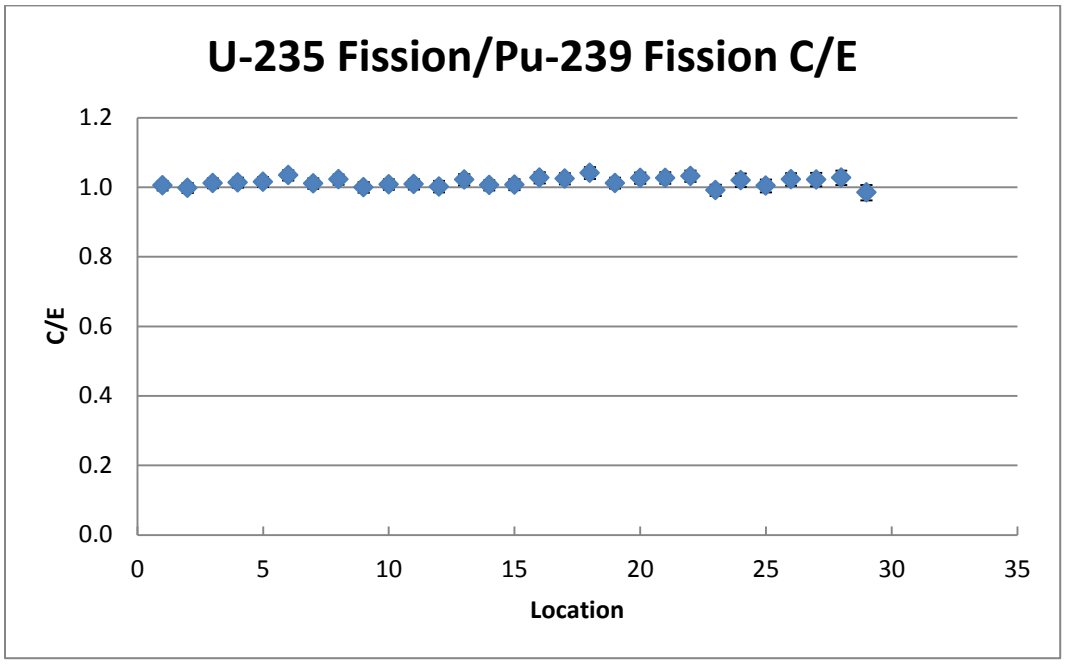


Figure C13: Calculated/Expected for U-235 Fission Reaction Rate Ratio for Horizontal Transverse

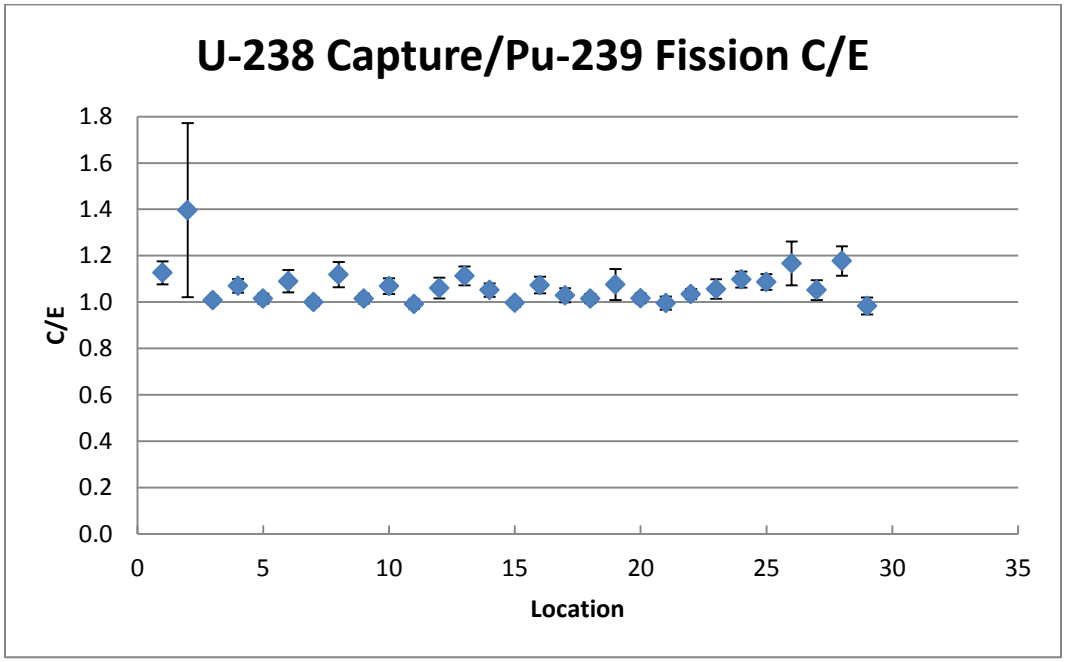


Figure C14: Calculated/Expected for U-238 Capture Reaction Rate Ratio for Horizontal Transverse

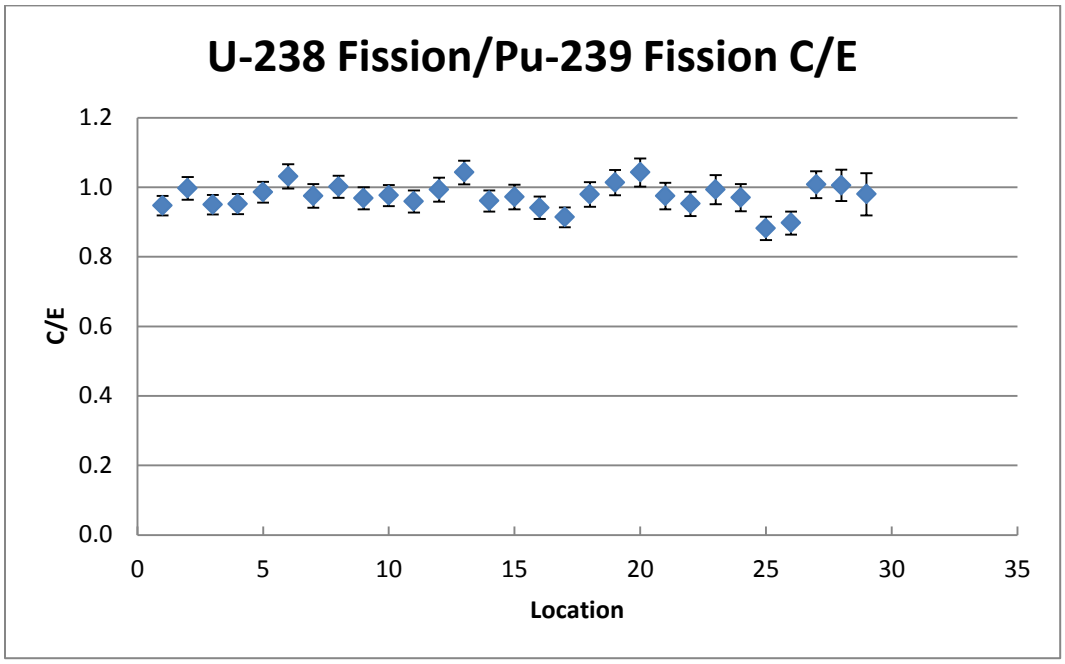


Figure C15: Calculated/Expected for U-238 Fission Reaction Rate Ratio for Horizontal Transverse

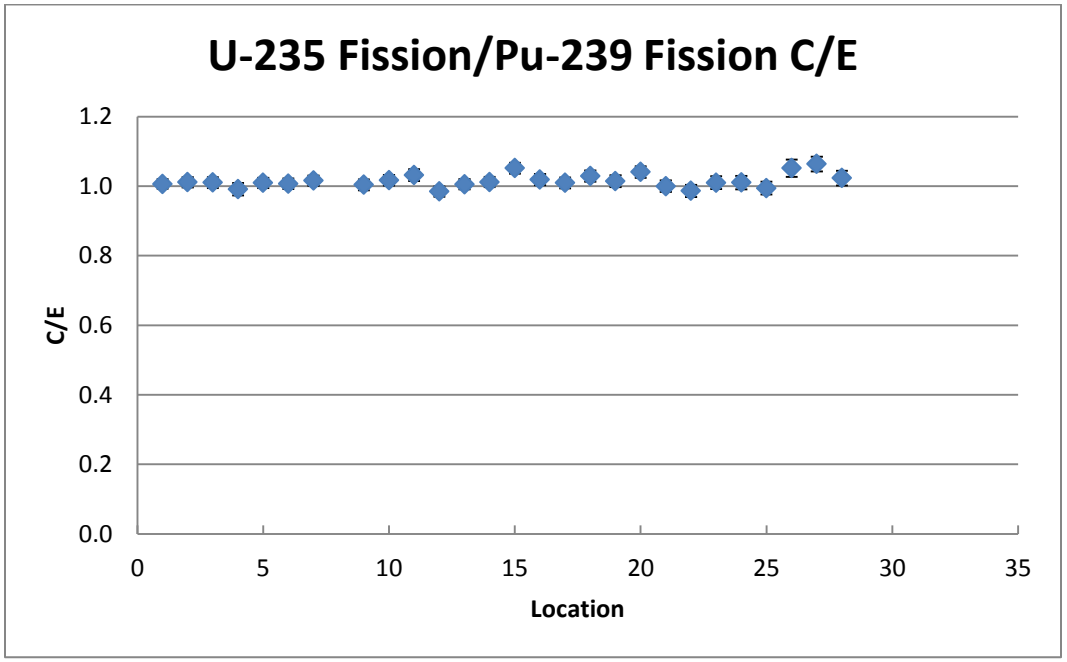


Figure C16: Calculated/Expected for U-235 Fission Reaction Rate Ratio for 15° Transverse

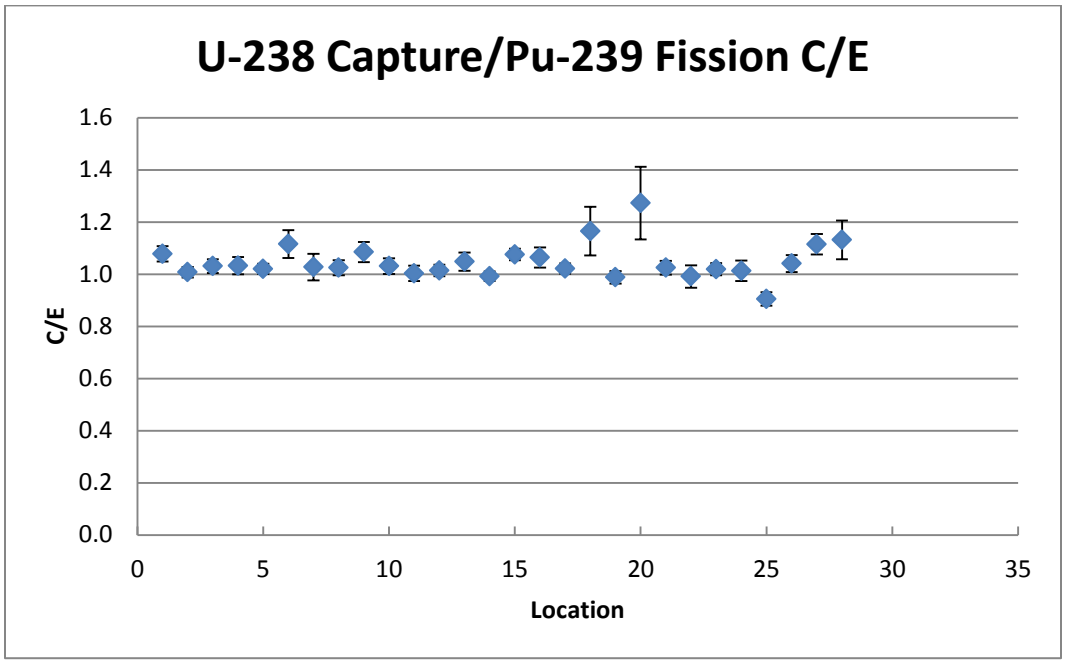


Figure C17: Calculated/Expected for U-238 Capture Reaction Rate Ratio for 15° Transverse

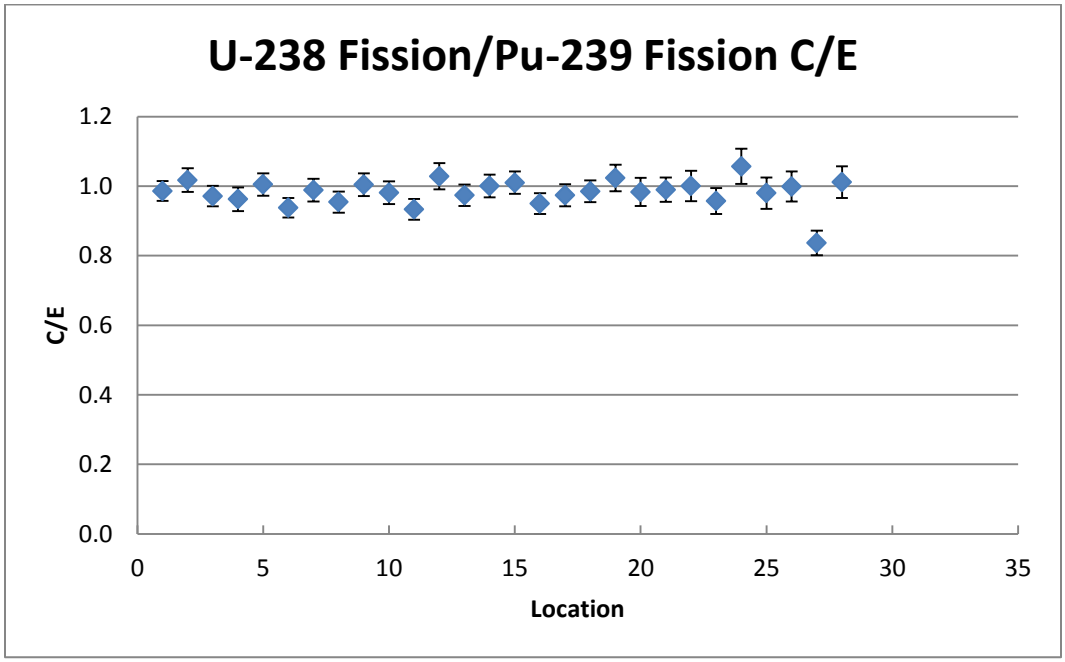


Figure C18: Calculated/Expected for U-238 Fission Reaction Rate Ratio for 15° Transverse